Action Formalism for Measurement Induced Dynamics: Topological and Thermal Aspects

Dominic Shea, MMath

Department of Physics

Lancaster University

A thesis submitted for the degree of

Doctor of Philosophy

November, 2024

Abstract

Feynman's path integral is a formulation of quantum mechanics akin to analogous formulations developed for stochastic processes and statistical physics. One process that combines quantum dynamics with stochastic features and constitutes a prevailing area of research is quantum measurement. Beyond past attempts, recent advancements, exemplified by the Chantasari-Dressel-Jordan (CDJ) method, explore measurement-induced dynamics in continuously monitored quantum systems.

This thesis utilises the CDJ path integral to explore new emerging features associated with measurement-induced dynamics. Firstly, we develop the CDJ path integral to analyse geometric phases. Focusing on self-closing trajectories from continuous measurements, we incorporate geometric phase information directly in the path integral for a single qubit and demonstrate that the geometric phase of the most likely trajectories exhibits a topological transition as a function of measurement strength. We further address the effect of Gaussian fluctuations.

Secondly, we exploit the formalism to study measurement-induced entanglement dynamics, where we combine the stochastic effect of measurements and that of local unitary noise. We identify the optimal entanglement dynamics and develop diagrammatic methods that produce a closed-form approximation of the average entanglement dynamics. The optimal trajectories and diagrammatic expansion capture the oscillations of entanglement at short times. We find by numerical investigation that long-time steady-state entanglement reveals a non-monotonic relationship between concurrence and noise strength.

Finally, we lay the basis for applying path integrals to fluctuation theorems by devising a suitable single qubit protocol to verify a recently proposed fluctuation theorem that governs the statistical behaviour of quantum systems far from equilibrium. The proposed protocol is suitable for existing quantum architectures. Our results provide a basis for extending the use of fluctuation theorems to many-body systems, where geometric phases and entanglement play crucial roles in classifying quantum order.

Acknowledgements

First and foremost, I would like to express my sincere gratitude to the inimitable Alessandro Romito for his sage guidance and seemingly inexhaustible patience throughout my time at Lancaster. I likewise want to thank the Condensed Matter Theory group for warmly welcoming me into the department, particularly my fellow PhD students Tom Simons and Chun Leung. Our regular Mahjong nights fostered my sense of belonging in the Lancaster physics community, and Chun's encouragement was instrumental in keeping me task-focused and disciplined.

I also want to express my heartfelt gratitude to my Lancaster flatmates and friends, Katie Howgate, Rachael Carver, and Amy Furney. There is no finer group of people to quarantine with during a global health crisis. Thank you to Ruben Leenders, whose weekly attendance at the LU Baking Society proved that perfection is overrated. I would also be remiss not to mention my York friends, Rahul Bageja and Asiya Campbell, with whom I enjoyed many late-night Netflix binges which never failed to uplift my spirit.

Special thanks are due to my remote collaborators, Yuval Gefen, Kater Murch, and Xiayu Linpeng, whose exhaustive expertise proved indispensable in guiding and enhancing the quality of this research.

Finally, I would like to thank my family, especially Mum. I am forever grateful for your endless support and the countless sacrifices you've made on my behalf. I couldn't have done it without you.

Declaration

I declare that the work presented in this thesis is, to the best of my knowledge and belief, original and my own work. The material has not been submitted, either in whole or in part, for a degree at this or any other university. This thesis does not exceed the maximum permitted word length of 80,000 words, including appendices and footnotes, but excluding the bibliography.

Dominic Shea

Publications

Two publications, shown below, have been created directly from the thesis, from which large portions of this published work are used within chapters 3 and 4, respectively:

Dominic Shea and Alessandro Romito. "Action formalism for geometric phases from self-closing quantum trajectories". In: *Journal of Physics A: Mathematical and Theoretical* 57.31 (July 2024), p. 315303. DOI: 10.1088/1751-8121/ad5e4b. URL: https://dx.doi.org/10.1088/1751-8121/ad5e4b

Dominic Shea and Alessandro Romito. *Stochastic action for the entanglement of a noisy monitored two-qubit system.* 2024. arXiv: 2403.08422 [quant-ph]
Submitted for publication to *Physical Review A* on the 28th of March 2024

Contents

List of Tables

List of Figures

Chapter 1

Introduction: Measurement Induced Dynamics on the Rise

The path integral formalism plays a significant role in contemporary theoretical physics. Reinvented and applied to non-relativistic quantum mechanics (QM) by Feynman in 1948 [3], it stands alongside Heisenberg's matrix operator approach [4, 5] and Schrödinger's wave mechanics [6] as an independent third formulation of QM. Feynman's formulation is most closely associated with quantum field theory and statistical mechanics [7, 8]. However, the powerful methods developed for tackling path integrals in physics proved advantageous when applied to stochastic systems more generally [9, 10]. Stochastic path integrals (SPIs), which predate the Feynman path integral, trace their origin to Wiener in 1921 [11, 12]. SPIs are utilised within diverse disciplines, from finance [13, 8] to neuroscience [10, 14]. Although significant challenges remain in adequately describing the formal mathematics of Feynman path integrals, SPIs have proven to be more tractable since it is possible to define a well-behaved measure on the space of stochastic curves in a real-valued parameter space. An example of one widely used formulation of the SPI was developed by Martin-Siggia-Rose (MSR) in 1973 [15] specifically for classical statistical dynamics.

One prominent type of stochastic process in modern physics is quantum measurement [16, 17, 18, 19], it has extraordinary practical, mathematical and

metaphysical significance [20, 21, 22] [23]. While the mathematical foundations of quantum measurement were established by Von Neumann in 1932 [24], modern research continues to elucidate further aspects of quantum measurements [21, 19], expanding the growing list of associated phenomena. Since quantum measurements are stochastic they are a natural candidate for exploiting path integral techniques. However, in contrast to quantum unitary evolution and (classical) statistical mechanics processes, measurement-induced stochasticity is state-dependent, adding further complexity. To address monitored systems, Mensky adapted Feynman's integral [25, 26, 27], constraining which trajectories are summed over in keeping with the recorded measurements. A different approach is considered in contemporary work by Chantasari-Dressel-Jordan (CDJ) [28], where they apply the MSR path integral to a continuously monitored quantum system, treating the measurement-induced dynamics analogous to a classical walk through the systems state space. This has led to a spate of research that uses the CDJ action formalism to investigate both finite and infinite dimensional systems [29, 30, 31, 32, 33].

The path-integral approach to quantum measurement has gained significance with the advent of the experimental ability to track measurement-induced quantum trajectories [34, 28, 35, 36] and the associated technological applications, including quantum feedback [37, 38]. A new wave in the development of measurement-induced quantum dynamics is ongoing, spanning from technological applications to information processing via error correction codes [39], to the engineering of exotic states of many-body systems via engineered dissipation protocols [40], to fundamental questions about many-body quantum order and entanglement along quantum trajectories [41, 42, 43, 44]. Much of the original research described in this thesis is based on applying the CDJ path integral as a tool adapted to investigate new phenomena that emerge from measurement-induced dynamics.

The first phenomenon of interest is the geometric phase, aka the Berry phase, which is discussed in Chapter 3. Introduced by Michael Berry in 1984 [45], the geometric phase is highly significant in both quantum information theory and

condensed matter physics. In quantum computation, geometric phases offer a promising route for implementing quantum gates on qubits [46]. These gates have the potential to be more resistant to errors, overcoming a major hurdle in the race to unlock the benefits of quantum computation [47, 48, 46, 18]. In condensed matter physics, the Berry phase and its concomitant quantities are critical to understanding topological phases of matter [49, 50] and their classification by topological invariants.

Geometric phases can be generated by measurements, a concept first discussed by J. Samuel and R. Bhandari in 1988 [51] and subsequently confirmed through experimental observations [52, 53]. Recent findings reveal that measurement-induced dynamics feature a topological phenomenon involving the post-selected geometric phase [54]. The critical independent variable delineating two distinct topological regimes is the strength of the quasi-continuous[1] measurement process (or some equivalent dynamics). This intriguing phenomenon has been explored in subsequent work [55, 56, 57, 58, 59, 60] and has been corroborated by experimental findings [61]. In Chapter 3, we examine the properties of these geometric phases under continuous quantum measurements using the CDJ path integral. This approach enables us to probe measurement-induced geometric phases at the level of individual trajectories, allowing us to identify a subset of self-closing quantum trajectories that exhibit a new type of topological transition within their geometric phase.

In Chapter 4, we drastically expand the scope of our investigations to include a system consisting of two monitored qubits, the most straightforward system for which we can investigate entanglement properties. The phenomenon of quantum entanglement distinguishes quantum systems from their classical counterparts: it is a central resource in quantum information processing [18, 62] and is vital to understanding some properties of many-body systems, such as thermalisation,

[1]The limiting process that defines this measurement protocol is described in Section 2.2.4. In contrast to continuous Gaussian measurements, which produce a continuous stream of readouts, the resulting measurement readouts are a countable infinity of 0's and 1's.

information scrambling and many-body localization [63, 64, 65, 66, 67, 68, 69, 62]. Recently, entanglement has been exploited to identify out-of-equilibrium many-body states resulting from the stochastic dynamics of many body systems subject to random unitary evolution and quantum monitoring [70, 71, 72, 73, 74]. This has witnessed the emergence of entanglement scaling transitions from a volume to an area law in a many-body Zeno effect along with a broader set of textcolorblackmeasurement-induced phase transitions (MiPTs) [41]. These transitions appear when tracking the entanglement along individual quantum trajectories correlated with the measurement readout (as opposed to measurement-averaged dynamics) and have been reported in recent pioneering experiments [42, 43, 44].

We investigate measurement-induced entanglement transitions, for this purpose our monitored two-qubit system is the most simplified setting wherein an entanglement transition effect may arise. An external environmental influence is modelled by Gaussian noises which buffet each qubit. Individual quantum trajectories are analysed by incorporating the additional noise terms into the associated CDJ path integral. In particular, we examine the most likely entanglement dynamics and utilise diagrammatic methods to derive a closed-form approximation for the average entanglement. Our analysis is supported by numerical simulations that benchmark the performance of our closed-form expressions. These numerical simulations also reveal the existence of a non-monotonic dependence of the entanglement on the noise strength.

Finally, in Chapter 5, we examine the thermal properties of a monitored single qubit system and study possible implementation protocols of a fluctuation theorem along measurement-induced trajectories. Fluctuation theorems (FTs) are exact relations for the statistical properties of thermodynamic quantities such as work or entropy production in nonequilibrium processes [75, 76, 77]. They can be viewed as an extension of the second law of thermodynamics to microscopic processes where stochastic fluctuations become relevant, defining the field of

stochastic thermodynamics [78, 79, 80]. Generalising thermodynamics to include stochastic quantum fluctuations is a current extensive research effort, and fluctuation theorems have been successfully extended to the quantum case utilising a two-point measurement scheme [81, 82, 83] which enables meaningful definitions of thermodynamic variables. Exploring the role of coherence [84, 85, 86], and entanglement [87, 88] is at the frontier of this effort. Fluctuation theorems have been further extended to nonequilibrium quantum jump trajectories [89, 90] and to unitary dynamics that are interrupted by a sequence of unital quantum channels [91, 92, 93]. They have also been derived for quantum systems' work, energy and entropy under unital dynamics [94, 95]. Quantum tomography may be used to investigate the statistics of individual quantum trajectories and validate the aforementioned FTs [96, 97, 98], with some of these experimental tests having already been carried out [99, 100].

We focus here on a new fluctuation theorem valid for a generalised thermodynamic description of quantum systems, including small systems undergoing open system dynamics such as measurement, decoherence and thermal relaxation, which has been developed by Manzano et al. [101, 102]. We develop a direct test of Manzano's fluctuation theorem (MFT) for a single qubit system. This turns out to be possible through a generalised measurement scheme. We propose a feasible experimental protocol suitable for available quantum architectures. Our analysis of fluctuation theorems and the definition of a protocol provide a necessary step toward the formulation of out-of-equilibrium fluctuation theorems within the CDJ path-integral.

Chapter 2

Background: Quantum Measurements, Path Integrals, Geometric Phases and Fluctuation Theorems

Introducing key background material built upon throughout the rest of this thesis, we provide a basic overview of the most salient aspects of quantum measurement, geometric phases, functional integrals and fluctuation theorems. We are beginning with a discussion of quantum measurements with a particular emphasis on continuous quantum measurement before summarising quantum channels and the Lindblad equation. We then describe various approaches to geometric phases before narrowing the focus to phases arising from measurement dynamics. Path integrals of multiple types are examined, an essential tool in our research. Additionally, three modern, highly relevant results are introduced, upon which much of the work in this thesis is built directly: A topological transition in the post-selected geometric phase, the path integral formulation of quantum measurements with emphasis on the CDJ formulation, and a nonequilibrium fluctuation theorem applicable to general quantum trajectories. Preceding the discussion of the nonequilibrium fluctuation

theorem, we review Crooks fluctuation theorem in its original formulation.

2.1 Measurement Induced Dynamics

Quantum systems evolve according to two distinct types of dynamics: unitary evolutions and non-unitary measurement back action. The unitary part of the dynamics is specified by a Hamiltonian operator, H, that drives the system continuously according to Schrödinger's equation,

$$H|\psi\rangle = i\hbar\frac{d}{dt}|\psi\rangle. \tag{2.1}$$

Quantum measurements cause the non-unitary backaction and may be described by a set of Kraus (or measurement) operators $\{M_i\}$ that update the system state vector, $|\psi\rangle \mapsto |\psi'\rangle$, according to the rule,

$$|\psi'\rangle = \frac{M_i|\psi\rangle}{\sqrt{\langle\psi|M_i^\dagger M_i|\psi\rangle}}. \tag{2.2}$$

Each possible measurement readout has an associated Kraus operator. These operators can be projection operators (satisfying $M_i^2 = M_i$) representing familiar von Neumann-type measurements [24]. However, Kraus operators belong to a broader class of operators obeying the restriction,

$$\sum_i M_i^\dagger M_i = \mathbb{I}, \tag{2.3}$$

which defines a generalized positive operator-valued measure (POVM) on a finite dimensional space [17, 16, 18]. This accounts for the greater flexibility available to experimenters who typically do not collapse system states onto an orthogonal eigenstate of some target observable; the post-measurement state is usually a more complex superposition. Generalized measurements were first delineated by Neumark (1943) [23], who modelled them using an extended Hilbert space. Let $\mathfrak{H}_S$ be the Hilbert space for the system and let $\mathfrak{H}_A$ be an ancillary space, we may then form a combined state space $\mathfrak{H}_S \otimes \mathfrak{H}_A$. The system and ancilla interact, producing an

entangled state in $\mathfrak{H}_S \otimes \mathfrak{H}_A$, a projective measurement of only the ancillary system results in the backaction given by Eq. (2.2) on the system in $\mathfrak{H}_S$ where M_i may belong to any POVM. We illustrate this with an example in Section 2.1.2.

2.1.1 Continuous Measurement

A measurement's influence on a system's state is typically treated as an instantaneous effect. However, sometimes this instantaneous treatment is inadequate [17]. Any experimental measurement collects information over a non-zero duration; in cases where the system's unitary evolution would produce a significant change in the system state within the duration of measurement, a more detailed description of the dynamics is required. Additionally, where a measurement continuously reports results (e.g. a measurement of current strength), it is necessary to know the system's state during the measurement process. Such *continuous quantum measurements* are crucial in feedback control, quantum information, metrology and computing [18, 19] and are utilised heavily throughout this thesis.

In concordance with the regular principles of quantum mechanics, we describe continuous measurement using measurement operators. For continuous measurements, these Kraus operators do not, in general, collapse the post-measurement state onto eigenstates $|a\rangle$, with associated eigenvalues a, for some target observable A on the system's Hilbert space $\mathfrak{H}_S$. A continuous measurement corresponds to an experimental procedure that extracts information (concomitantly produces backaction) in proportion to the measurement's duration. Thus an ephemeral measurement has a minuscule effect on the system's state. To model this, we must define a Kraus operator, $M(\delta t)$, that depends on the duration of measurement δt and satisfies the limit, $\lim_{\delta t \to 0} M(\delta t) \to \mathbb{I}$. For simplicity, we disregard the case where M has an explicit time dependence t, assuming that the details of the measurement process are time-independent. To continuously measure the target observable A, we assume the ancillary system is large enough to support operators with a continuous spectrum. The continuous measurement then consists of a family of Kraus operators

that have a Gaussian form,

$$M_{\delta t}(r) = \sqrt[4]{\frac{4k\delta t}{\pi}} \sum_a e^{-2k\delta t(a-r)^2} |a\rangle\langle a|, \tag{2.4}$$

believed to be the only kind of continuous measurement featuring a continuous stream of measurement results [1] [16, 103]. The index r corresponds to the possible measurement readout, which is an unbounded real number. Accordingly, we require a continuous infinity of Kraus operators to represent the measurement, with the normalisation in Eq. (2.1) converted to integral form,

$$\int M^\dagger M dr = \mathbb{I}. \tag{2.5}$$

The parameter k appearing in Eq. (2.4) controls the magnitude of the measurement back action for some fixed δt. The complete process is defined by taking the limit of a sequence of N such measurements with $\delta t \to 0$ whilst imposing the condition $N\delta t \to T$, where T is the period of the entire process. Considering the dynamics in the $\delta t \to 0$ limit calls for the toolkit of stochastic calculus, leading to the stochastic Schrödinger equation. In the following Section, we sketch the explicit construction of a continuous measurement characterised by the backaction of the form in Eq. (2.4).

2.1.2 Gaussian Qubit Measurement

An implementation of continuous Gaussian measurement has been achieved for qubit systems in a double quantum dot setup [104, 105, 106]. Recapitulating the results of Ref. [107] as adapted in Refs. [108, 28]: A charged qubit is capacitively coupled to a Quantum Point Contact (QPC), a nanoscale semiconductor with a tunable quantised conductance. The particle is subject to a double-well potential with localised ground

[1] For measurements with independent readout increments (Lèvy processes) the two recognized types of continuous measurements are Gaussian and point processes. Point processes arise from a series of discrete detector clicks occurring at random intervals, rather than producing a genuinely continuous stream of readouts. Ref. [103] presents evidence that the only type of Lèvy process that can realize a truly continuous measurement is of the Gaussian variety.

states, $|0\rangle$ and $|1\rangle$. This gives rise to an effective qubit Hamiltonian with the form $H = \frac{\epsilon}{2}\sigma_z + \frac{\Delta}{2}\sigma_x$, where ϵ is the energy splitting and Δ is the tunnelling rate.

The current flow through the QPC depends on the qubit's position. Assume the value of current, I, within the time interval, t and $t + \delta t$, for the particle at site's $|0\rangle$ or $|1\rangle$ will be Gaussian distributed according to the functions $P_{\text{current}}(I||0\rangle)$ and $P_{\text{current}}(I||1\rangle)$ with means $\bar{I}_0$ and $\bar{I}_1$ and a common standard deviation σ. For convenience, we rewrite these distributions, using the dimensionless measurement readout $r = \frac{(I-\bar{I})}{\Delta\bar{I}}$ where $\bar{I} = \frac{(\bar{I}_0+\bar{I}_1)}{2}$ and $\Delta\bar{I} = \frac{(\bar{I}_0-\bar{I}_1)}{2}$. In this transformed variable, the readout distributions for the charged particle in state's $|0\rangle$ and $|1\rangle$ are given by,

$$P(r|0) = \frac{1}{2\pi\tau\delta t}\exp\left\{-\frac{(r-1)^2}{\delta t}\frac{1}{2\tau}\right\}, \tag{2.6}$$

$$P(r|1) = \frac{1}{2\pi\tau\delta t}\exp\left\{-\frac{(r+1)^2}{\delta t}\frac{1}{2\tau}\right\}. \tag{2.7}$$

In Eqs. (2.6) and (2.7), we characterised the distributions using, τ, instead of σ. We introduce the parameter τ to represent the timescale necessary to differentiate between the $|0\rangle$ and $|1\rangle$ qubit states. For n measurements of duration δt, the $\langle I\rangle$ standard deviation scales as $\sigma/\sqrt{n}$. We define $\tau := \delta t n_0$, where n_0 is the value of n for which twice the current standard deviation separates the states $|0\rangle$ and $|1\rangle$. So $2\sigma/\sqrt{n_0} = |\overline{I_1} - \overline{I_0}|$, hence,

$$\tau = \frac{4\sigma^2\delta t}{|\overline{I_1} - \overline{I_0}|^2}. \tag{2.8}$$

From Eqs. (2.6) and (2.7) we reverse engineer the Kraus operators that model this experimental set up using Bayes rule[2],

$$P(A|B) = \frac{P(B|A)P(A)}{P(B)}, \tag{2.9}$$

we construct Kraus operators for our r measurements. Let the particle's state be given by the generic density operator,

$$\rho = \begin{pmatrix} \rho_{00} & \rho_{01} \\ \rho_{10} & \rho_{11} \end{pmatrix}, \tag{2.10}$$

[2]In Eq. (2.9), A and B are generic events, and $P(A|B)$ is the conditional probability of A given B.

expressed in the $|0\rangle$, $|1\rangle$ basis. This ensures that, $\rho_{00} = P(0)$, and $\rho_{11} = P(1)$. A conditional post-measurement state ρ_r then has elements,

$$\rho_{00|r} = P(0|r) = \frac{P(r|0)\rho_{00}}{P(r|0)\rho_{00} + P(r|1)\rho_{11}}, \tag{2.11}$$

$$\rho_{11|r} = P(1|r) = \frac{P(r|1)\rho_{11}}{P(r|0)\rho_{00} + P(r|1)\rho_{11}}. \tag{2.12}$$

After a measurement, any pure state ($\mathrm{Tr}[\rho^2] = 1$) will remain pure if there is no extra source of decoherence; this fact is used to determine the off-diagonal elements $\rho_{01|r}$ and $\rho_{10|r}$. From Eqs. (2.11) and (2.12) , and the action of a Kraus operator on a density operator ($\rho_r = \frac{M\rho M^\dagger}{\mathrm{Tr}[M\rho M^\dagger]}$), we can deduce the required measurement operator,

$$\begin{aligned} M_{\delta t}(r) &= \sqrt{P(r|0)}|0\rangle\langle 0| + \sqrt{P(r|1)}|1\rangle\langle 1| \\ &= \left(\frac{\delta t}{2\pi\tau_m}\right)^{1/4} \exp\Big(-\frac{\delta t}{4\tau_m}(r-\sigma_z)^2\Big). \end{aligned} \tag{2.13}$$

We highlight that Eq. (2.13) has the form specified in Eq. (2.4).

2.1.3 Quantum Channels

A description of open quantum systems necessitates using the density operator formalism, mentioned in Section 2.1.2, wherein a probabilistic mixture of pure quantum states is combined into a single positive-definite, hermitian, trace one operator. The tensor product structure of the underlying Hilbert spaces, $\mathfrak{H} = \mathfrak{H}_S \otimes \mathfrak{H}_E$ is inherited by the density state formalism, so for the bipartite product state, $\rho = \rho_S \otimes \rho_E$, the matrix ρ_S is associated with degrees of freedom from $\mathfrak{H}_S$ and the matrix ρ_E is likewise for subsystem E.

A density operator associated with one subsystem may always be recovered by employing the partial trace operation [3]. Independently, a unitary transformation

[3]This is the mapping, $\rho \mapsto \rho'$, which is defined by, $\mathrm{Tr}[A\rho'] = \mathrm{Tr}[(A \otimes \mathbb{I})\rho]$. Where $\mathbb{I}$ corresponds to the degrees of freedom we discard (aka trace over) and the arbitrary operator A is an observable on the system's degrees of freedom. So $\mathrm{Tr}_E[\rho] := \rho'$.

$U = e^{-i\hbar Ht}$, directed by the Hamiltonian H, maps density operators as $\rho \to \sigma$ through the relationship $\sigma = U\rho U^\dagger$. A mapping from the reduced state ρ_S to $\mathcal{E}(\rho_S)$ for some initially uncorrelated system and environment product state is given by $\mathcal{E}(\rho_S) = \mathrm{Tr}_E[U(\rho_S \otimes \rho_E)U^\dagger]$ where Tr_E is a partial trace over the environmental degrees of freedom. The transformation $\mathcal{E}$ always has the following properties:

- **Trace-preserving**: $\mathrm{Tr}[\mathcal{E}(\rho_S)] = \mathrm{Tr}[\rho_S]$.
- **Convex Linearity**: $\mathcal{E}(\sum_i p_i\rho_i) = \sum_i p_i\mathcal{E}(\rho_i)$ where $p_i \in \mathbb{R}$ and $\sum_i p_i = 1$.
- **Completely Positivity**: When the map is extended to act on some arbitrary non-interacting ancillary system ($\mathcal{E} \otimes \mathbb{I}$), the resulting state must be positive.

A map with these properties is a *quantum channel* or CPTP (completely positive trace-preserving) map, and the Kraus operator sum representation theorem [18] states that any CPTP map admits a (non-unique) Kraus operator representation

$$\mathcal{E}(\rho) = \sum_i M_i \rho M_i^\dagger. \tag{2.14}$$

The set of Kraus operators $\{M_i\}$ satisfies the completeness relation Eq. (2.15), guaranteeing the map is trace-preserving,

$$\sum_i M_i^\dagger M_i = \mathbb{I}. \tag{2.15}$$

The Kraus operator decomposition immediately suggests an interpretation. Each term in Eq. (2.14) corresponds to the generalised measurement outcome realised with probability $p_i = \mathrm{Tr}[M_i\rho M_i]$. Therefore, when applying $\mathcal{E}$ we may construe the result as a convex combination of the outcomes from this measurement process weighted by their probability. Thus, the dynamics of an open system can be framed in terms of an affiliated generalised measurement. We make use of this property in Section 5.1.

2.1.4 The Lindblad Equation

Following the heuristic derivation in Ref. [109], we describe how to obtain and understand the *Lindblad Equation* from infinitesimally short-duration quantum

channels. The Schrodinger equation, generating a closed system's unitary dynamics, is specified for a density operator in the time infinitesimal form,

$$\rho(t+\delta t) = \rho(t) - i\delta t[H, \rho(t)]. \tag{2.16}$$

As discussed in Section 2.1.3, any Markovian evolution for an open system may be specified by a quantum channel, in an infinitesimal interval δt this channel is generically expressed as,

$$\rho(t+\delta t) = \mathcal{E}_{\delta t}(\rho(t)) = (\mathbb{I} + \delta t\mathcal{L})\rho(t). \tag{2.17}$$

Eq. (2.17) entails an unentangled system and environment at each step in the evolution. The infinitesimal expansion of Eq. (2.17) implies $\dot{\rho} = \mathcal{L}(\rho)$. $\mathcal{L}$, which generates the open system evolution, is named the Lindbladian. Invariably, the channel $\mathcal{E}$ admits a Kraus operator decomposition

$$\mathcal{E}_{\delta t}(\rho(t)) = \sum_i M_i \rho(t) M_i^\dagger = \rho(t) + O(\delta t). \tag{2.18}$$

Keeping terms up to order δt, we assume M_1 takes the form $\mathbb{I} + Z\delta t$, and M_j is of the form $\sqrt{\delta t}L_j$ for $j > 1$, where the operators L_i are called Lindblad jump operators. With these assumptions M_1 in Eq. (2.18) describes the state evolution in the absence of Lindblad jumps. The collection of operators $\{M_j\}$ describes transformations that probabilistically occur during the interval δt. A time-ordered list of transformations realized during the average dynamics comprise a quantum trajectory. The operator, Z, may be written as the sum of two hermitian operators $Z = -(iH + K)$. The completeness relation Eq. (2.15) then ensures that $K = -\frac{1}{2}\sum_{i>0} L_j^\dagger L_j$. Using these transformed form of the Kraus operators in Eq. (2.18) implies the Lindblad equation,

$$\dot{\rho} = \mathcal{L}(\rho) = -i[H, \rho] + \sum_{j>1} \left(L_j \rho L_j^\dagger - \frac{1}{2} L_j^\dagger L_j \rho - \frac{1}{2} \rho L_j^\dagger L_j \right). \tag{2.19}$$

Here $\mathcal{L}$ is a linear mapping. Juxtaposing $\mathcal{L}$ with Eq. (2.16) we clearly see the leading term in $\mathcal{L}(\rho)$ captures the unitary component of the dynamics. The jump operations correspond to stochastic processes like dissipation or continuous

measurement backaction. In the latter case, the Lindblad dynamics is the expected dynamics of a measured system where the measurement record has been discarded (i.e. the non-selective dynamics). Each $L_i\rho L_i^\dagger$ term induces measurement backaction, while the term $-\frac{1}{2}L_j^\dagger L_j\rho - \frac{1}{2}\rho L_j^\dagger L_j$ provides state normalization. These effects combine in a dissipator notation defined as $D[L_j](\rho) = L_i\rho L_i^\dagger - \frac{1}{2}L_j^\dagger L_j\rho - \frac{1}{2}\rho L_j^\dagger L_j$. A more comprehensive discussion is available in Ref. [110].

2.2 Geometric Phases

Anytime a pure state of a system undergoes a closed evolution, it may accumulate an overall phase factor relative to its initial state. A measurable part of this acquired phase, the geometric phase, results from parallel transport through the systems's curved state space. These geometric phases are ubiquitous across the various subdisciplines of theoretical physics [111]. Despite their pervasiveness, it was not until S. Pancharatnam in 1956 that the influence of geometric phases was first reported; materialising in classical optics [112]. It took the introduction of the Berry Phase in 1984 for the notion of geometric phases to be appreciated in quantum mechanics. This was soon followed by the introduction of the Hannay angle in 1985 for classical dynamics [113]. Empirical investigations quickly access these geometric phases. In 1986 A. Tomita and R.Y. Chiao observed linearly polarised photons will change polarisation angle when crossing a twisted optical fibre, this rotation corresponded to an acquired geometric phase [114].

2.2.1 Berry-Simon Approach to the Geometric Phase

Berry's original conceptualization of the QM geometric phase was devised for a parameterised Hamiltonian system. This elementary formulation relies on only the Schrödinger equation and the adiabatic approximation. B. Simon would later

discover the essence of the Berry phase, identifying the presence of a vector bundle[4] over the parameter space and pinpointing the geometric phase as an element of this bundle's holonomy group[5] [115]. Geometric phases are crucial to identifying topological phases of matter like quantum Hall phases, topological insulators and superconductors [111, 49, 50, 116], and have been exploited in the design of high-fidelity quantum gates that are more resilient to the effect or random noise than dynamic gates [117, 46].

Consider a generic Hamiltonian $H(\mathbf{X}(t))$, where $\mathbf{X}(t)$ are time-dependent parameters. The instantaneous energy eigenbasis, is a solution to the energy eigenvalue problem at a particular time t,

$$H(\mathbf{X}(t))|n(\mathbf{X}(t))\rangle = E_n(\mathbf{X}(t))|n(\mathbf{X}(t))\rangle. \tag{2.20}$$

A global gauge for the mapping $\mathbf{X} \to |n(\mathbf{X})\rangle$ may not be available: so a smooth one-to-one mapping from $\mathbf{X}$ to $|n(\mathbf{X})\rangle$ may be unobtainable. This difficulty arises when the continuity of the mapping forces the phase of at least one eigenstate to be ambiguous. Nevertheless, local gauges still exist, so multiple gauges defined on non-identical overlapping domains, specifies a relationship between the two spaces.

We now make use of the adiabatic approximation [118], provided that $\mathbf{X}(t)$ is changing slowly enough, then the solution to the TDSE

$$i|\dot{\psi}\rangle = H(\mathbf{X})|\psi\rangle, \tag{2.21}$$

is well approximated by a wave function that takes the form

$$|\psi\rangle \approx e^{i\beta}|n(\mathbf{X})\rangle, \tag{2.22}$$

[4] A *fibre bundle* is formed of a continuous mapping between two topological spaces. A base space and a total space. The total space locally resembles a product of the base space and an additional typical fibre space. The defining property of a *vector bundle* is that its typical fibre is a vector space.

[5] The *holonomy group* of a vector bundle are the group of linear transformations that result from parallel transporting a vector along closed paths based in the bundle. Consult Ref. [111] or an equivalent resource for the full exposition.

where, arbitrarily, $\beta(0) = 0$. Now, substituting Eq. (2.22) into Eq. (2.21) we find

$$H(\mathbf{X})|\psi\rangle = -\dot{\beta}|\psi\rangle + ie^{i\beta}|\dot{n}\rangle. \tag{2.23}$$

Multiplying from the left by $\langle\psi(t)|$, and reorganising terms, results in the equation

$$\langle\psi|\dot{\beta}|\psi\rangle = -\langle\psi|H|\psi\rangle + i\langle n|\dot{n}\rangle. \tag{2.24}$$

The state normalisation $\langle\psi(t)|\psi(t)\rangle = 1$ simplifies the left hand side of Eq. (2.24), then integrating over time from 0 to T we obtain

$$\beta(T) = -\int_0^T \langle\psi|H(\mathbf{X})|\psi\rangle dt + i\int_0^T \langle n(\mathbf{X})|\frac{d}{dt}|n(\mathbf{X})\rangle dt. \tag{2.25}$$

This accrued global phase of a system's quantum state is an unmeasurable $U(1)$ gauge freedom (i.e. belongs to the space of phases $e^{i\alpha}$). When a system is driven adiabatically in a closed cycle, the accumulated phase is given by Eq. (2.25) and $\beta(T)$ is gauge invariant and, therefore, experimentally accessible [119, 120]. The first term of Eq. (2.25) is the dynamical phase and depends on the duration of the evolution. The second term is the Berry phase, which depends exclusively on the path taken through the Hamiltonian's parameter space. This integral over time converts into an integral over the Hamiltonian parameters

$$i\int_0^T \langle n(\mathbf{X})|\frac{d}{dt}|n(\mathbf{X})\rangle dt = i\oint_{\mathbf{X}(0)}^{\mathbf{X}(T)} \langle n(\mathbf{X}|\nabla_{\mathbf{X}}|n(\mathbf{X}\rangle \cdot d\mathbf{X}. \tag{2.26}$$

The result of Eq. (2.26) is time independent. The quantity, $\mathbf{A} = i\langle n(\mathbf{X}(t))|\nabla_{\mathbf{X}}|n(\mathbf{X}(t))\rangle$, is known as the *Berry vector potential* (or *Berry connection*). Using Stokes theorem, we transform Eq. (2.26) into an integral over the surface enclosed by the loop,

$$i\oint_{\mathbf{X}(0)}^{\mathbf{X}(T)} \mathbf{A}\cdot d\mathbf{X} = \int_\Gamma \nabla_{\mathbf{X}}\times\mathbf{A}\; dS. \tag{2.27}$$

Here Γ is the surface in parameters space enclosed by the cycle, and dS is a surface element. We may then identify the integrand of the resulting expression, the gauge-independent quantity $\nabla_{\mathbf{X}}\times\mathbf{A}$, as the *Berry curvature*.

2.2.2 Aharonov-Anandan Approach to the Geometric Phase

In 1987, Aharonov and Anandan generalised Berry's phase to generic continuous evolutions introducing a new flavour of geometric phase, the *Aharonov-Anandan phase*. Similar to the Berry-Simon approach, the Aharnovo-Anandan phase is defined as a holonomy element of a fibre bundle; however, the base space of the bundle is built from the system's state space [111, 121, 122]. This enables a general treatment of geometric phases in quantum systems at the expense of being more recondite. The approach dispenses with the need for a Hamiltonian parameter space, and where the Hamiltonian is present, the need for an adiabatic evolution is obviated. The assortment of dynamics subject to the Aharonov-Anandan approach is so diverse a geometric phase can even be associated with continuous measurement back-action [16, 17]. A compact discussion of this approach is presented here, with further details available in Refs. [54, 111].

The Aharonov-Anandan approach proceeds as follows: A ray in Hilbert space is an equivalence class of vectors that differ by, at most, a phase, $|\psi\rangle \sim e^{i\alpha}|\psi\rangle$. The appropriate base space of the Aharonov-Anandan bundle is the system's projective Hilbert space, denoted $\mathcal{P}(\mathfrak{h})$,[6] it is equivalent to the space of rank one projections $|\psi\rangle\langle\psi|$). This is assembled by endowing the set of rays with the quotient topology and metric inherited from the original Hilbert space[7]. One example of a projective Hilbert space is the Bloch sphere, where a two-dimensional space of complex vectors encodes a real two-dimensional sphere. A many-to-one map from each normalised state vector into its associated ray serves as the canonical projection in a principal $U(1)$-fibre bundle, where each typical fibre is diffeomorphic[8] to the smooth (Lie) group $U(1)$ [111, 54]. A Hamiltonian and an initial state specifies a curve, $\gamma(t)$, through the projective space. An arbitrary choice of gauge, $|n\rangle$, smoothly maps

[6]Here the Hilbert space $\mathfrak{h}$ consists of only normalised vectors.

[7]The *quotient topology* is the topology on a quotient space where a subset is open if and only if its preimage under the quotient map is open in the original space.

[8]Two manifolds are *diffeomorphic* if there exists a smooth, bijective map with a smooth inverse between them.

some open region of the projective space into its linked fibre elements, so the map

$$|n(q)\rangle : \mathcal{P}(\mathfrak{h}) \ \mapsto \mathfrak{h} \tag{2.28}$$

can promote curves in projective space into a family of wavefunctions $\gamma(t) \mapsto |n(\gamma(t))\rangle$. An evolution which is closed in the projective space may be open in the normalised Hilbert space [$\gamma(T) = \gamma(0) \implies |\gamma(T)\rangle = |\gamma(0)\rangle$][9]. Since these peripheral states are equivalent a gauge-invariant comparison may be made between them.

This accumulated phase difference may be decomposed into a dynamical and a geometric phase. The geometric phase shift is gained by parallel transporting the arbitrary initial phase along the system's path in the projective space; it is a consequence of Berry curvature (see Eq. (2.36)) and depends exclusively on the chosen path. The necessary condition for parallel transport of a normalised state is [46],

$$\langle\psi(t)|\dot{\psi(t)}\rangle = 0. \tag{2.29}$$

The dynamical phase is the remainder and depends on the average energy and cycle duration. Take the example from Sjoqvist's discussion of geometric phases in Ref. [46]. An arbitrary superposition of two energy eigenstates $|E_1\rangle$ and $|E_2\rangle$ undergoes some unitary evolution,

$$|\psi(t)\rangle = \alpha \exp(-iE_1 t)\,|E_1\rangle + \beta \exp(-iE_2 t)\,|E_2\rangle. \tag{2.30}$$

This state cycles with a period $T = \frac{2\pi}{E_2 - E_1}$, and corresponds to the curve $\lambda(t)$ in $\mathcal{P}(\mathfrak{h})$. After one cycle this system has accumulated a global phase,

$$|\psi(T)\rangle = \exp\left(-i\frac{2\pi E_1}{E_2 - E_1}\right)|\psi(0)\rangle. \tag{2.31}$$

The accrued phase factor, $\exp\left(-i\frac{2\pi E_1}{E_2 - E_1}\right)$[10], may be split into a geometric and

[9]Here $|\gamma(0)\rangle$ is any vector such that $|\gamma(0)\rangle\langle\gamma(0)|$ corresponds to the point $\gamma(0)$ and similarly for $|\gamma(T)\rangle$. We have that $|\gamma(0)\rangle \sim |\gamma(T)\rangle$.

[10]Which could equivalently be calculated as $\exp\left(-i\frac{2\pi E_2}{E_2 - E_1}\right)$. This choice leads to $\chi_{\text{geom}} = 2\pi|\alpha|^2$, which differs by exactly 2π from the equation derived in the text.

dynamical component[11] as

$$\begin{aligned}\chi_{\text{geom}} &= 2\pi|\beta|^2, \\ \chi_{\text{dyn}} &= -\frac{2\pi}{\underbrace{E_2 - E_1}_{T}}\left(\underbrace{|\alpha|^2 E_1 + |\beta|^2 E_2}_{\langle E\rangle}\right).\end{aligned} \tag{2.32}$$

Similar to the Eq. (2.25) these two contributions can be calculated from the formula,

$$\chi_{\text{global}} = -\int_0^T \langle\psi(t)|H|\psi(t)\rangle dt + i\int_0^T \langle n(\lambda(t))|\frac{d}{dt}|n(\lambda(t))\rangle dt. \tag{2.33}$$

Where in place of a mapping from a Hamiltonian parameter space X, we use the gauge defined by $|n(\lambda(t))\rangle = e^{-i\text{arg}[\langle\psi(0)|\psi(t)\rangle]}|\psi(t)\rangle$. The derivation of Eq. (2.33) proceeds in the same manner as demonstrated for Eq. (2.25). We may again identify the integrand of Eq. (2.33)

$$A = i\langle n(\gamma(t))|\frac{d}{dt}|n(\gamma(t))\rangle dt, \tag{2.34}$$

with the Berry potential, which is a gauge-dependent one-form. The geometric component of the phase is again the contribution from the Berry potential

$$\chi_{\text{geom}} = \int_\gamma A dt. \tag{2.35}$$

The exterior derivative[12] of the Berry potential dA gives the related gauge-independent Berry curvature. The geometric phase is then given, again employing Stokes theorem, by

$$\chi_{\text{geom}} = \int_\Gamma dA, \tag{2.36}$$

where Γ is the surface in projective space enclosed by γ. This component of the global phase depends entirely on the path through projective space. We further draw the reader's attention to the fact that Eq. (2.35) can apply to open paths in configuration space. In these cases, the resulting phase contributes towards the *open*

[11] We note that when calculated for $E_1 \to E_2$ and $E_2 \to E_1$ the period and average energy both change value, and the equation for the geometric phase changes sign, $\chi_{\text{geom}} = -2\pi|\beta|^2$.

[12] See e.g. Ref. [111].

geometric phase. When the associated path is closed, we refer to the phase as the *closed geometric phase*. We discuss the geometric significance of the open geometric phase in Section 2.2.3. The two separate but interrelated approaches to describing geometric phases are completely reconciled by a bundle-morphism structure [123].

2.2.3 Measurement Induced Geometric Phases

It is clear how the Aharonov-Anandan formalism applies to continuous dynamics but its administration is more abstruse for a discontinuous time-ordered sequence of pure states; such as those that would arise from a course of measurements. We further observe that for measurement-induced effects, the dynamics (and, therefore, the associated phases) acquire stochastic properties. This issue of how exactly to treat geometric phases for discontinuous dynamics was elucidated by J. Samuel and R. Bandhari [51] in 1988.

The strategy employed adapted the Pancharnatnam phase to quantum systems. The *relative phase* between two non-orthogonal state vectors is defined as the phase angle of their inner product,

$$\chi_{A,B} = \arg\Big[\langle\psi_A|\psi_B\rangle\Big]. \tag{2.37}$$

Consider a collection of points $\{q_i\}$ for $i \in 1, ..., N$ in projective space, and an arbitrary choice of gauge $|\tilde{n}\rangle$ which maps that points into corresponding normalised elements of the Hilbert space $\{q_i\} \mapsto \mathfrak{h}$. For the post-selected back action of a single projective measurement

$$|\phi\rangle = \underbrace{|\tilde{n}(q_2)\rangle\langle\tilde{n}(q_2)|}_{\text{measurement}}\,\tilde{n}(q_1)\rangle = \underbrace{\langle\tilde{n}(q_2)|\tilde{n}(q_1)\rangle}_{\text{phase factor}}\,|\tilde{n}(q_2)\rangle, \tag{2.38}$$

the induced global phase is the relative phase $\arg\Big[\langle\tilde{n}(q_2)|\tilde{n}(q_1)\rangle\Big]$ and is inherently gauge dependent. For a chronological cycle of N states, with $q_1 = q_N$, generated by a sequence of projective measurements, the global Pancharatnam phase χ_p is accumulated by multiplying together successive relative phase factors,

$$|\psi_{\mathrm{f}}\rangle = |\tilde{n}(q_N)\rangle\langle\tilde{n}(q_N)|...|\tilde{n}(q_2)\rangle\langle\tilde{n}(q_2)|\tilde{n}(q_1)\rangle, \tag{2.39}$$

$$\chi_p = \arg\Big[\langle\tilde{n}(q_N)|...|\tilde{n}(q_2)\rangle\langle\tilde{n}(q_2)|\tilde{n}(q_1)\rangle\Big]. \tag{2.40}$$

Since the initial and final states belong to the same ray, $|\tilde{\psi}_\mathrm{i}\rangle = |\tilde{N}\rangle \propto |\psi_\mathrm{f}\rangle$, the phase difference in Eq. (2.39) is therefore a gauge invariant quantity.

We now establish the geometric character of χ_p. We utilise the following essential theorem[13]: *There exists a certain gauge* $|n^*\rangle$ *such that the relative phase between* $|n^*(q_i)\rangle$ *and* $|n^*(q_{i+1})\rangle$ *vanishes for all* i. *Suppose* $\gamma_i(t)$ *specifies a length minimizing geodesic between* q_i *and* q_{i+1}, *from* $t = t_i$ *to* $t = t_{i+1}$. *The gauge* $|n^*\rangle$ *is constructed from the parallel transport of* $|\tilde{n}(q_0)\rangle$ *along* γ_i. We track the phase difference between the parallel transport gauge and our arbitrary gauge, so $|n^*(\gamma(t))\rangle = e^{i\beta(t)}|\tilde{n}(\gamma(t))\rangle$ with $\beta(0) = 0$. The phase accumulated in Eq. (2.38), corresponding to one projective measurement, is found from

$$\begin{aligned}\langle\tilde{n}(q_2)|\tilde{n}(q_1)\rangle &= \frac{\langle\tilde{n}(q_2)|\tilde{n}(q_1)\rangle}{|\langle\tilde{n}(q_2)|\tilde{n}(q_1)\rangle|} \\ &= \frac{\langle n^*(q_2)|e^{-i\beta(t_2)}|n^*(q_1)\rangle}{|\langle\tilde{n}(q_2)|\tilde{n}(q_1)\rangle|} \\ &= e^{-i\beta(t_2)}\end{aligned} \tag{2.41}$$

Where we have used the fact that successive $|n^*(q_i)\rangle$ are in phase. The gauge invariant accumulated phase in Eq. (2.39) is given by the sum

$$\chi_p = -\sum_i(\beta(t_{i+1}) - \beta(t_i)) = -\beta(T). \tag{2.42}$$

Since $\beta(T)$ gives the phase difference between the parallel transport of $|\tilde{n}(t_1)\rangle$ along γ, χ_p is similarly endowed with this geometric meaning. The phase accumulated may be computed through the geometric component of Eq. (2.33),

$$\chi_p = -i\int_0^T \langle\tilde{n}(\gamma(t))|\frac{d}{dt}|\tilde{n}(\gamma(t))\rangle dt. \tag{2.43}$$

The Pancharatnam phase in Eq. (2.39) is equivalent to consecutive parallel transports along a concatenated path of shortest geodesics. This phase has the unmistakable character of a geometric phase, being determined by the enclosed

[13]Proved in Ref. [111]

Berry curvature Eq. (2.36). For a qubit, the geometric phase for a closed loop on the Bloch sphere is proportional to the solid angle enclosed by the loop. Hence, the geometric phase for a cyclical discrete set of post-measurement states is proportional to the solid angle enclosed by the length-minimising geodesics connecting the states [111].

The above applies, *mutatis mutandis*, to generalised measurements. The caveat is the potential for a dynamic phase contribution during the measurement protocol. This potentiality arises because nonprojective measurements invariably involve the influence of an interaction Hamiltonian between the system and detector. Nevertheless, non-projective measurements without a dynamical phase are possible. Any measurement back action, M, satisfying the parallel transport condition

$$\langle\psi|M^\dagger|\psi\rangle > 0, \tag{2.44}$$

which demands $\langle\psi|M^\dagger|\psi\rangle$ is real and positive, cannot induce a dynamical phase. Satisfying this condition allows the measurement-induced geometric phase to be directly observed in an interferometer setup [54]. We further note that a similar argument applies to the case of open geometric phases. The phase contribution from the continuous but open trajectory, given by Eq. (2.35) may be added to the relative phase $\arg[\langle\psi(0)|\psi(T)\rangle]$, this sum then becomes a gauge invariant quantity. The value of the induced, gauge invariant phase is then equal to the result of concatenating the path $|\psi(t)\rangle\langle\psi(t)|$ with a self-closing shortest geodesic and feeding this modified path into Eq. (2.35).

Research into measurement-induced geometric phases has often concentrated on associating a version of the geometric phase to the averaged (mixed) state described by a density matrix, either via the Uhlmann phase [124, 125, 126] or through the interferometric geometric phase [127, 128, 129]. It is only recently that the statistical properties of the geometric phase along individual stochastic realisations (aka quantum trajectories) have begun to be investigated [54, 55, 130, 55, 56, 57]. One feature that emerges upon such a detailed investigation is a new type of topological transition.

2.2.4 Topological Features of Measurement Induced Geometric Phases

Recently, it has been shown that geometric phases arising from a particular measurement protocol and post-selection exhibit a topological transition as a function of the measurement strength [54, 130, 72]. We will recapitulate the main features of this transition here, basing the discussion on the model used in the first prediction of this topological effect. This original model consists of a qubit subject to a sequence of cyclically rotating measurements. Further work has shown that the topological nature of the transition is a more generic feature of single qubit measurement-induced dynamics, including different measurement procedures and protocols, as well as Hamiltonian dynamics and dephasing [55, 56, 57]. The phenomenon is robust against several perturbations, including additional adiabatic dynamics and dephasing [131, 61]. This, in turn, has facilitated the experimental observation in superconducting and optical architectures [61, 60]. We note that this transition is distinct from the topological order transition induced by measurements in many-body systems [132, 133, 134, 135, 136].

Gebhart et al. [54] consider the measurement-induced geometric phase subject to a quasi-continuous sequence of weak measurements of the observable σ_z on a qubit system. Take the Bloch sphere representation of the projective Hilbert space in conventional spherical coordinates. The back action for each of the two possible measurement outcomes, when the basis of the Hilbert space coincides with the weak measurements target eigenstates, is specified by the Kraus operators[14],

$$M_1 = \begin{pmatrix} 1 & 0 \\ 0 & \sqrt{1-\eta} \end{pmatrix}, \tag{2.45}$$

$$M_0 = \begin{pmatrix} 0 & 0 \\ 0 & \sqrt{\eta} \end{pmatrix}. \tag{2.46}$$

[14] In Ref. [131] it is demonstrated that a range of binary Kraus operators may be chosen which all go on to exhibit a topological transition within their post-selected geometric phases.

The dimensionless parameter η characterises the strength of the measurement. This measurement is applied along the measurement axis

$$\mathbf{n}_k = (\sin(\Theta_k)\cos(\Phi_k), \sin(\Theta_k)\sin(\Phi_k), \cos(\Theta_k), \tag{2.47}$$

where $\Phi_k = \frac{2\pi k}{N}$ and N is the total number of measurements read off and Θ_k is chosen to be some fixed value Θ_0 for the entire sequence. This specifies some cyclical measurement sequence at a fixed latitude on the qubit system's Bloch sphere. The qubit rotation matrix

$$R(\Theta_k, \Phi_k) = e^{-\frac{1}{2}i\Phi_k}\exp\left[\frac{1}{2}i(\Theta_k\sigma_2 + \Phi_k\sigma_3)\right] \tag{2.48}$$

may be used to determine the exact form of the Kraus operators Eq. (2.45) and (2.46) at each step in the process via the transformation $E_k^{1/0} = RM_{1/0}R$. The entire measurement protocol is defined by taking the limit $N \to \infty$ and $\eta \to 0$, where η is chosen to depend on N to produce non-trivial dynamics via $\eta = \frac{4c}{N}$. The parameter c, defined through the limiting procedure, serves as a measurement strength parameter of the entire sequence of measurements since single measurements have a vanishing measurement strength.

Post-selecting the ensuing dynamics for a sequence of readouts associated solely with M_1 results in a quantum trajectory that depends on both the measurement latitude and measurement strength (Fig. 2.1). The quantum trajectory generally remains open, except in the strong measurement limit where the state scrupulously follows the measurement axis. An open geometric phase may be associated with the post-selected trajectory. This phase can be directly generated using a final von Neumann measurement that projects the system's state back onto its original position in projective space, following another post-selection that discards the unwanted outcomes from the final projection.

This sequence of measurements (in addition to the final post-selection) may be implemented along the equator of the Bloch sphere; in this case, a state with an initialisation, $(\phi(0) = \Phi(0), \theta(0) = \frac{\pi}{2})$, must remain on the equator of the Bloch sphere simplifying the dynamics to be one-dimensional. A sharp transition in

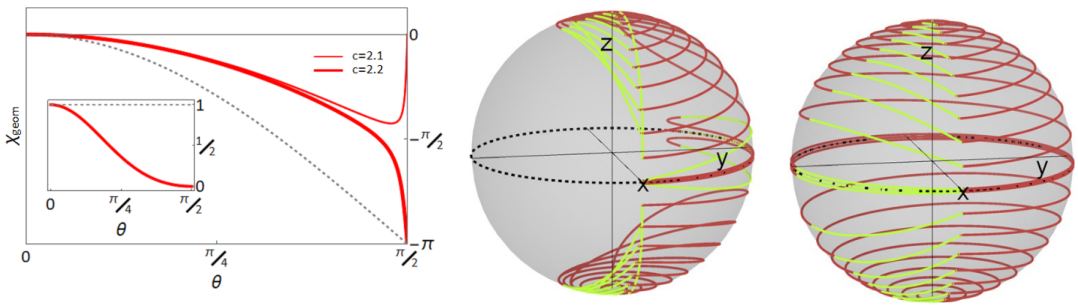

Figure 2.1: (Reproduced directly from Ref. [54]) [Left] Measurement-induced geometric phase against Θ (labeled as θ in the figure). Red lines are the phase accrued by all M_1 quantum trajectories plotted for two different measurement strengths c. [Center & Right] The Θ-dependent family of M_1 quantum trajectories illustrated on the Bloch sphere for $c = 2.1$ (center) and $c = 2.2$ (right). The yellow portion of each trajectory corresponds to the length-minimizing geodesic.

the value of the geometric phase then occurs. No phase is accrued in the weak measurement regime with $c \leq 2.1$. In the strong regime with $c \geq 2.2$, a phase of $-\pi$ is produced. This may be understood as originating from the topology of the Bloch sphere equator (which is just S^1). When the state has not been driven more than halfway around the equator, the final strong measurement returns the system to its initial configuration via a length-minimising geodesic that doubles back along the state's trajectory, enclosing no area on the Bloch sphere. States driven more than halfway around the Bloch sphere must be concatenated with a final length-minimising geodesic that encircles the entire upper half of the Bloch sphere. This effect will serve as a signature of a transition across the entire Bloch sphere.

Gebhart et al. investigated this procedure for state preparations, across the Bloch sphere. The spaces topology enforces a sharp transition of geometric phase as a function of measurement strength. Choosing a family of trajectories specified by the initial conditions and measurement protocols with $\Theta(0) = \theta(0) \in [0, \pi]$, and $\phi(0) = \Phi(0)$, establishes a mapping between the sphere spanned by the direction of measurement operators, $\mathbf{n}(t)$, and the Bloch sphere through the Kraus operator M_1.

It is then demonstrated that this mapping undergoes a topological transition [54] as a function of the measurement strength c from a phase in which the image of the trajectories covers the Bloch sphere to one in which it fails to cover the entire sphere. A Chern number,

$$C \equiv \frac{1}{2\pi}\int_0^{\pi} d\Theta \int_0^1 B dt = \frac{1}{2\pi}(\chi(\pi) - \chi(0)), \tag{2.49}$$

with $B(\Theta, t) = \mathrm{Im}\{\partial_t\langle\psi|\partial_\Theta|\psi\rangle - \partial_\Theta\langle\psi|\partial_t|\psi\rangle\}$, distinguishes these two topological regimes. The Chern number can take discrete values, $C = -1$ or $C = 0$, which are directly related to the dependence of the geometric phase as shown in the last step of Eq. (2.49). The topological transition of this mapping is then manifest in the measurement-induced geometric phase as a function of measurement latitude, $\chi(\Theta)$, bifurcating the function into monotonic and non-monotonic regimes. The critical value of c for which this transition occurs is determined at the Bloch sphere equator. The mapping $[0, \pi] \ni \Theta \to \chi \in [0, 2\pi]$ is in fact a mapping $S_1 \to S_1$ with winding number $w = 0, 1$.The latter is equivalently determined by $w = [\chi(\pi/2) - \chi(0)]/\pi \in \{0, 1\}$.

2.3 Action Formalism for Measurement Induced Dynamics

Here, we concisely introduce the Feynman path integral, the type of functional integral with which physicists are typically most familiar. We use the prototypical example of a nonrelativistic one-dimensional single-particle to illustrate the main idea. We also acquaint the reader with the earliest approach, due to M.B. Mensky [26], to use path integral methods to treat quantum measurement. We illustrate how Mensky's approach operates for Gaussian monitoring and draw a connection to non-Hermitian quantum mechanics.

Work by Chantasri-Dressel-Jordan [28, 29, 34] has led to the development of a new approach to investigate continuous Gaussian quantum measurements using

astochastic path integral (SPI). The version of SPI they develop calculates state transition probabilities as a weighted summation of all possible quantum trajectories that enact the transition. It shares in common with the Martin-Siggia-Rose (MSR) approach to classical stochastic systems, the introduction of conjugate momenta variables that enforce dynamical constraints that apply to the system. This enables the assignment of a stochastic action, a generalisation of the usual probability density, to each trajectory. The CDJ method's predictions have been experimentally validated in qubit systems [32, 33, 31] and have been applied to other systems, including the harmonic oscillator [137]. We review the main features of both these SPI formulations in Sections 2.3.2.1 and 2.3.2.2.

2.3.1 Path Integrals for Amplitudes

2.3.1.1 Feynman Path Integral

The original, approximately coeval formulations of quantum mechanics were Schrödinger's wave mechanics and Heisenberg's matrix mechanics. These approaches describe the evolution of a quantum system in terms of partial differential equations describing the evolution of wave functions or via the application of unitary matrices $U = e^{-iHt}$ applied to vectors in Hilbert space. Feynman introduced a third equivalent formulation, based upon a functional integral, in the 1940s. This approach has the virtue of explicitly connecting a system's dynamics to some associated classical trajectories, offering a more intuitive perspective.

The main idea of the Feynman path integral is to consider all possible paths that a classical particle could take between two points in configuration space within a specified time interval. Each path contributes to the overall probability **amplitude** of the particle's motion. The probability amplitude for a particle to move from an initial state to a final state is obtained by summing the contributions of all possible paths. This is accomplished by assigning a phase to each path and then summing over all possible paths in state space. We emphasise these paths do not need to satisfy the classical principle of least action: any path satisfying the necessary

boundary conditions is sufficient.

The Feynman path integral is expressed mathematically as

$$K(x_f, t_f; x_i, t_i) = \int \mathcal{D}[x(t)] e^{iS[x(t)]}. \tag{2.50}$$

Here, K is interpreted as the probability amplitude for the particle to move from (x_i, t_i) to (x_f, t_f), $\mathcal{D}[x(t)]$ represents a path integral over all possible paths, and $S[x(t)]$ is the action of the classical system that has been quantised. To demonstrate, we consider the quintessential example of a time-independent Hamiltonian $H = \frac{p^2}{2m} + V(x)$ driving a system over time T divided into N time steps,

$$\begin{aligned} K(x_f, t_f; x_i, t_i) &= \langle x_f | \left(e^{-iH\Delta t} \right)^N | x_i \rangle \\ &= \int \prod_{j=1}^{N-1} dx_j \langle x_f | U(\Delta t) | x_{N-1} \rangle \langle x_{N-1} | U(\Delta t) | x_{N-2} \rangle ... \langle x_1 | U(\Delta t) | x_i \rangle. \end{aligned} \tag{2.51}$$

In Eq. (2.51), $\Delta t = \frac{T}{N}$ and $U(\Delta t) = e^{-iH(\frac{T}{N})}$. Inserting the resolution of the identity for the momentum eigenstates $\mathcal{I} = \int |p\rangle\langle p| dp$ and $\langle x|p\rangle = \frac{1}{\sqrt{2\pi}} e^{ipx}$ and using $e^{AB} \approx \left(e^{\frac{A}{N}} e^{\frac{B}{N}} \right)^N$ for arbitrary operators[15], we obtain

$$\begin{aligned} &K(x_f, t_f; x_i, t_i) = \\ &= \int \prod_{j=1}^{N-1} dx_j \int \prod_{j=0}^{N-1} dp_j \frac{1}{\sqrt{2\pi}} e^{ip_{N-1}x_f} \langle P_{N-1} | e^{i\frac{p^2}{2m}\Delta t} e^{iV(x)\Delta t} | x_{N-1} \rangle \langle x_{N-1} | p_{N-2} \rangle \dots \\ &= \int \prod_{j=1}^{N-1} dx_j \int \prod_{j=0}^{N-1} dp_j \frac{1}{\sqrt{2\pi}} e^{ip_{N-1}(x_f - x_{N-1})} e^{i\frac{p^2}{2m}\Delta t} e^{iV(x)\Delta t} \times \dots \times \ . \end{aligned} \tag{2.52}$$

Letting $T = -i\tau$ and $\Delta\tau = \frac{\tau}{N} = i\Delta t$ then applying a sequence of algebraic manipulations we find,

$$\begin{aligned} &K(x_f, t_f; x_i, t_i) \approx \\ &\int \prod_{j=1}^{N-1} dx_j \int \prod_{k=0}^{N-1} dp_k \left(e^{-\frac{\Delta t}{2m}(p_{N-1} - \frac{im}{\Delta t}(x_f - x_{N-1}))^2 - \frac{m}{2\Delta t}(x_f - x_{N-1})^2} e^{iV(x)\frac{T}{N}} \dots \times \dots \right) \\ &= \int \prod_{j=1}^{N-1} dx_j \int \prod_{k=0}^{N-1} dp_k \left(\sqrt{\frac{m}{2\pi\Delta\tau}} e^{-\frac{m}{2}\frac{(x_f - x_{N-1})^2}{\Delta\tau}} e^{iV(x)\frac{T}{N}} \dots \times \dots \right) \\ &= \int \prod_{j=1}^{N-1} dx_j \sqrt{\frac{m}{2\pi\Delta\tau}}^N \left(e^{-\frac{m}{2}\frac{(x_f - x_{N-1})^2}{\Delta\tau} + \Delta\tau V(x_{N-1})} \dots \times \dots \right) \end{aligned} \tag{2.53}$$

[15]The error of this approximation decreases for large N.

The approximation becomes exact once the limit $N \to \infty$ is taken so

$$K(x_f, t_f; x_i, t_i) = \lim_{N\to\infty} \sqrt{\frac{m}{2\pi\Delta\tau}}^N \int \prod_{j=1}^{N-1} e^{-i\Delta t\left(\left(\frac{x_{j+1}-x_j}{\Delta t}\right)^2 - V(x_j)\right)} dx_j. \tag{2.54}$$

This limit defines the Feynman path integral for the one-dimensional spinless particle governed by a time-independent Hamiltonian. This is usually written in the shortened form presented in Eq. (2.50). It is also typical to encounter path integrals that are defined in phase space; in this case, the action functional takes the form $S[q,p] = \int_0^T (p\dot{q} - H(p,q,t))dt$ and there is an additional functional integration over the momentum variable with no specified boundary conditions. While path integrals of this type deal exclusively with the unitary dynamics of a system, later work [26, 27, 138] has succeeded in incorporating measurement-induced dynamics into the path integral formulation.

2.3.1.2 Restricted Path Integral

In the usual formulations of quantum mechanics, the influence of measurements, discrete or continuous, are straightforwardly described using Kraus operators, as discussed in Section 2.1. Assimilating the effect of measurements in the path integral formulation of quantum mechanics may be achieved by effectively restricting the paths through phase space that are integrated over. This encodes the backaction of the measurement on the system into the calculated probability amplitudes. This leads to the restricted path integral (RPI), which was developed by M.B. Mensky [26] and C.M. Caves [27] and foreseen by Feynman [3]. We follow the introduction to RPIs given by Mensky in Ref. [138].

The 'restriction' in the restricted path integral is determined by the information the measurement supplies about the system. Consider the Feynman path integral, as described in 2.3.1.1, given by

$$\langle q_f|U|q_i\rangle = \int \mathcal{D}[p]\mathcal{D}[q] e^{i\int_0^T (p\dot{q} - H(p,q,t))dt}. \tag{2.55}$$

In cases where a classical particle would be excluded from an entire portion of its phase space, such as in the case of a particle in a box with impenetrable

walls, the integration in Eq. (2.55) may proceed over phase space paths that are compatible with this restriction- paths that wander outside the confines of the box are extraneous to the calculation. In this sense, even regular Feynman path integrals may have implicit restrictions on their functional domain.

If some generic quantum system is then subject to continuous measurement, a combination of the Kraus operators from Section 2.1.1 and the usual unitary driving combine to produce a new readout dependent propagator, $U_{r(t)}$, where the readout $r(t)$ is a continuous stochastic function. The set of U_r is subject to the completeness relation, $\int dr (U_r)^\dagger U_r = 1$, ensuring conservation of probability. A new path integral may then be used to express these propagators,

$$\langle q_f | U_r | q_i \rangle = \int \mathcal{D}[p]\mathcal{D}[q] w_r[p,q] e^{i\int_0^T (p\dot{q} - H(p,q,t))dt}. \tag{2.56}$$

Eq. (2.56) is identical to Eq. (2.55) except for the addition of a supplementary functional $w_r[p,q]$ that takes into account the information gleaned from the readout $r(t)$ by assigning a probability density $w_r[p,q]$ to every possible path. Heuristically, this function expresses how likely a phase space path $(p(t), q(t))$ is expected to be realised given that the readout $r(t)$ is observed - imposing a penalty for classical paths that would be unlikely to coincide with the readout $r(t)$. The probability density associated with $r(t)$ during a measurement readout is given by

$$P(r \in A) = \int_A dr \mathrm{Tr}\, U_r \rho_i (U_r)^\dagger. \tag{2.57}$$

For example, consider continuously monitoring the observable $A(t)$ with some known classical form $A(p,q,t)$. The measurement $r(t)$ then characterises the values of this observable at t. Take the square average deflection $\frac{1}{T}\int_0^T [A(t) - r(t)]^2 dt$ as a measure of the deviation of $A(p,q,t)$ from the value of the output $r(t)$. In this case $w_r[p,q]$ may be described by assigning a gaussian distribution,

$$w_r[p,q] = e^{-\frac{1}{T(\Delta r_T)^2}\int_0^T [A(t)-r(t)]^2\, dt}. \tag{2.58}$$

Here, Δr specifies the measurement error, and T is the period of the monitoring process overall. The correct choice of functional in Eq. (2.58) depends on the nature

of the monitoring the system is subjected to. With Eq. (2.58) the path integral in Eq. (2.56) becomes

$$U_r(q_f, q_i, T) = \int \mathcal{D}[p]\mathcal{D}[q] e^{i\int_0^T (p\dot{q}-H)dt - \frac{1}{T(\Delta a_T)^2}\int_0^T [A(p,q,t)-r(t)]^2\,dt}, \tag{2.59}$$

which may be evaluated or, if necessary, approximated using assorted methods.

The dynamics implied by Eq. (2.59) are driven by an effective non-Hermitian Hamiltonian,

$$H_r(p, q, t) = H(p, q, t) - \frac{i}{T(\Delta a_T)^2}[A(p, q, t) - r(t)]^2. \tag{2.60}$$

This links the RPI with an alternative strategy for a continuously monitored or open system: non-Hermitian theory solves the Schrödinger equation with an effective non-Hermitian Hamiltonian

$$\frac{\partial}{\partial t}|\psi\rangle = \left(-iH - \frac{1}{T(\Delta r_T)^2}(A - r(t))^2\right)|\psi\rangle. \tag{2.61}$$

Normalising the solution gives the post-measurement state; the unnormalised magnitude of the state vectors corresponds to the probability of obtaining $r(t)$. The average density matrix associated with the resultant post-measurement ensemble is specified by

$$\dot{\rho} = -i[H, \rho] - \left(\frac{1}{T(\Delta r_T)^2}\right)^2 [A, [A, \rho]]. \tag{2.62}$$

2.3.2 Stochastic Path Integrals

Although physicists are most familiar with path integrals of the kind introduced by Feynman, historically, the sum over trajectories approach was introduced by Wiener in the early 20th century specifically to deal with classically stochastic systems [11, 12]. This approach involves expressing a transition probability as a summation of all the stochastic trajectories that might facilitate the state transition weighted by their respective likelihoods (depending on the context, the log of the path probability is sometimes called the stochastic action, the Onsanger-Malchup functional, or the MSR action [139, 140]). Stochastic systems may be modelled by stochastic

differential equations (SDEs), which can rarely be solved in closed form. This then necessitates the use of approximate methods. By expressing stochastic systems as path integrals, approximations such as WKB expansions, variational approaches and perturbative expansions [9, 8] may be applied systematically [141]. Onsager and Machlup applied stochastic path integrals to analyse out-of-equilibrium stochastic processes, providing insights into diffusion-like phenomena [142]. Advancing theory and experimental techniques highlight the importance of SPI as an investigative tool. They are being employed to investigate novel phenomena triggered by noise, such as noise-induced phase transitions and stochastic resonance [143, 144, 145, 146].

2.3.2.1 Martin-Siggia-Rose Path Integral

An example of an advantageous variant of the stochastic path integral method is the Martin-Siggia-Rose approach developed for classical statistical dynamics [147, 148]. Consider a simple stochastic system described by the SDE, $\dot{q} = -q(t) + \eta(t)$, with some gaussian white noise satisfying $\langle \eta(t)\eta(t') \rangle = \delta(t-t')$. Any arbitrary functional $\mathcal{F}[q]$ may be expressed in the form of a SPI

$$\langle \mathcal{F}[q] \rangle = \Big\langle \int \mathcal{D}q \mathcal{F}[q] \delta(\dot{q} + q - \eta) \Big\rangle. \tag{2.63}$$

The functional integration is over all paths in configuration space. However, the Dirac-delta function enforces the constraints imposed by the SDE governing the system dynamics -since not all paths in configuration space will be accessible during the stochastic dynamics.

Making use of the defnition, $\mathcal{D}p = \lim_{n\to\infty} \prod_i dp_i$, and rewriting the delta function using the formula

$$\delta(t) \propto \int_{-\infty}^{\infty} e^{ipq} dp \tag{2.64}$$

which introduces the response field p. Eq. (2.65) becomes

$$\langle \mathcal{F}[q] \rangle = \Big\langle \int \mathcal{D}q \mathcal{D}p \mathcal{F}[q] e^{-i \int p(\dot{q}+q-\eta) dt} \Big\rangle. \tag{2.65}$$

Separating out the term that depends on η and performing the averaging over this stochastic variable we find $\langle e^{i \int (p\eta) dt} \rangle = e^{\int p^2 dt}$ and so Eq. (2.65) is then expressed

as a path integral directly[16]

$$\langle \mathcal{F}[q] \rangle = \int \mathcal{D}q\mathcal{D}p\mathcal{F}[q]e^{-i\int p(\dot{q}+q)+p^2 dt}. \tag{2.66}$$

This exact procedure may be followed to construct a path integral for a system governed by any SDE, including systems with coloured noise. In general the MSR path integral takes the form

$$\langle \mathcal{F}[x(t)] \rangle = \int \mathcal{D}q\mathcal{D}p]\, \mathcal{F}[x(t)]\, e^{-S[x,\tilde{x}]}, \tag{2.67}$$

where for an SDE with

$$\dot{q}(t) = M(q) + H(q)\xi(t)$$

and the following noise correlator $\langle \xi(q,t)\xi(q',t') \rangle = H(q,t,q',t')$ the action functional becomes

$$S[q,p] = \int ip[\dot{q} - M(q)] + \frac{\sigma}{2}H(q)^2 p^2 dt. \tag{2.68}$$

Although the example chosen above admits a closed-form solution, for Eq. (2.67) such a solution will not generically be available. Fortunately, various approximate methods can be systematically employed to produce approximate solutions for the original dynamics.

One such approach uses Generating functions, a mathematical tool that encodes all moments of the stochastic process in its functional derivatives with respect to some extra variables $\lambda(t_i), \tilde{\lambda}(t_j)$. We may use Eq. (2.66) to produce a moment-generating function, choosing $\mathcal{F}[q] = e^{\int \lambda(t_i)q(t_i)+\tilde{\lambda}(t_J)p(t_j)dt_i dt_j}$.This moment-generating function may be approximated by separating the action into a solvable Gaussian part dubbed the free action S_f and then Expanding the remaining part of the integrand S_I as

$$\mathcal{G}(J,\tilde{J}) = \int \mathcal{D}x(t)\mathcal{D}\tilde{x}(t)e^{-S_f}\sum_{n=0}^{\infty}(-1)^n\frac{S_I^n}{n!}. \tag{2.69}$$

Provided there is some reason that the error introduced by terminating the expansion at some finite order will be small, then Eq. (2.69) will be useful. The resulting

[16]Here we ignore the overall normalisation constant.

functional $\langle \mathcal{F}[q] \rangle = \mathcal{G}(\lambda, \tilde{\lambda})$ may then be used to generate approximations of the moments and moment generating functions via the successive application of variational derivatives i.e.

$$\left\langle \prod_m^i \prod_n^j q(t_i) p(t_j) \right\rangle = \frac{1}{\mathcal{G}(0,0)} \prod_m^i \prod_n^j \frac{\delta}{\delta J(t_i)} \frac{\delta}{\delta \tilde{J}(t_j)} \mathcal{G} \Big|_{J=\tilde{J}=0}. \tag{2.70}$$

Note that in addition to moments $\langle q^n \rangle$, we may readily generate two-point correlation functions $\langle q(t_1)q(t_2) \rangle$, which provide information about the statistical correlations between different points in space and time, defined to be the average of the product of two state parameters over all possible configurations of the system. The two-point correlator of electron spin might indicate whether spins tend to align or anti-align at different spatial positions. Furthermore, the decay of correlations with distance or time can provide insights into a system's characteristic length scales or time scales.

The MSR path integral method is beneficial for studying nonequilibrium thermodynamics systems, where traditional equilibrium statistical mechanics methods are not directly applicable. The MSR path integral Eq. (2.67) makes it especially easy to calculate linear response functions $\langle q(t_i)p(t_j) \rangle$, which describe the relationship between a system's response and an external stimulus or perturbation. Specifically, it quantifies how the system reacts to minute disturbances which slightly perturb it from thermodynamic equilibrium.

2.3.2.2 Chantasari-Dressel-Jordan Path Integral

As a central tool used in this thesis, we review the CDJ path integral more closely than the preceding path integral formulations. The density operator of a quantum state may be generically parameterised by real coordinates q_i, using an orthogonal operator basis $\{\hat{\sigma}_i\}$,

$$\hat{\rho} = \sum_{j=1}^{D^2-1} q_j \hat{\sigma_j}, \tag{2.71}$$

where D is the dimension of the Hilbert space associated with the system. Now, suppose we subject our parameterised state to some unitary evolution and measure

the state at regular intervals δt; for each time interval, we have the general state update equation,

$$\hat{\rho}(t+\delta t) = \frac{U_{\delta t}\hat{\rho}(t)U_{\delta t}^{\dagger}}{\mathrm{Tr}[U_{\delta t}\hat{\rho}(t)U_{\delta t}^{\dagger}]}, \tag{2.72}$$

where $U_{\delta t} = \exp(-\frac{i}{\hbar}\hat{H}\delta t)M_{\delta_t}$ is the product of the unitary evolution operator and a Kraus operator associated with some generalised measurement performed on the system. The joint probability density function for the state parameters $\{\mathbf{q}\}$ (which are vectors with dimension D^2-1) and measurement readouts $\{r\}$ at the end of each time interval is

$$P[\{\mathbf{q}\},\{r\}] = \mathcal{F}_{0,N}\prod_{i=0}^{n-1} P(\mathbf{q}_{i+1}, r_{i-1}|\mathbf{q}_i), \tag{2.73}$$

given some generic initial and final conditions $(\mathbf{q}_{\mathrm{in}}, \mathbf{q}_f)$ encoded in the Dirac-delta functions $\mathcal{F}_{0,n} = \delta(\mathbf{q}_{-1}-\mathbf{q}_{\mathrm{in}})\delta(\mathbf{q}_n-\mathbf{q}_f)$. Each factor in the product may itself be written as the product of a Dirac-delta function and some readout probability $P(r|q)$. The delta function can then be written in exponential form at the cost of introducing a new set of conjugate coordinates $\{\mathbf{p}\}$, obtaining the equation

$$P[\{\mathbf{q}\},\{r\}] = \mathcal{F}_{0,N}\prod_{i=0}^{n-1}\frac{1}{2\pi i}\int_{-i\infty}^{i\infty}\exp(-\mathbf{p}_i\cdot(\mathbf{q}_{i+1}-\mathbf{q}_i-\delta t\mathcal{L}[\mathbf{q}_i,r_i]))P(r_i|\mathbf{q}_i)d\mathbf{p}_i. \tag{2.74}$$

Here these delta functions are integrated along contours with endpoints at $\pm i\infty$. Following convention [147] we have applied a wick rotation ($p_k \to -ip_k$) to the integral representation of the Dirac-delta function (Eq. (2.64))[17].Taking this expression into the continuum limit, with measurements whose strength is proportional to δt, the joint probability function is expressible as a path integral

$$P(\mathbf{q}(t), r(t), \mathbf{q_f}|\mathbf{q_i}) = \int \mathcal{D}\mathbf{p}(t)e^{\mathcal{S}[\mathbf{q},\mathbf{p},r]}, \tag{2.75}$$

$$\mathcal{S} = \int -\mathbf{p}\cdot\dot{\mathbf{q}} + \underbrace{\mathbf{p}\cdot\mathcal{L}[\mathbf{q},r]+\mathcal{F}[\mathbf{q},r]}_{Stochastic\ Hamiltonian} - \mathbf{p}\cdot(\mathbf{q}-\mathbf{q_i})\delta(t) - \mathbf{p}\cdot(\mathbf{q}-\mathbf{q_f})\delta(t-T)dt. \tag{2.76}$$

[17]This avoids the appearance of a mixture of real and imaginary terms in the exponent. This is especially convenient since every CDJ stochastic action will evaluate to a real number when fed an accessible quantum trajectory and readout pair.

Here, the functional $\mathcal{S}$ is the stochastic action. The functional $\mathcal{L}[\mathbf{q}, r]$ is the derivative of the state parameters for a given (continuous) measurement readout. It may be determined by finding the linear expansion in δt of the right-hand side of Eq. (2.72) given the parameterisation in Eq. (2.71). The second functional $\mathcal{F}[\mathbf{q}, r]$, can be found in the linear expansion of

$$\ln P(r|\mathbf{q}) = \ln(\mathrm{Tr}[U_{\delta t}\hat{\rho}(t)U_{\delta t}^{\dagger}]). \tag{2.77}$$

The nonphysical conjugate variable $\mathbf{p}$, essentially a continuum version of a Lagrangian multiplier, can give useful insights into the physics of continuously measured systems. The sum of stochastic action for each of these nonphysical paths around a single quantum trajectory will reproduce the probability density of that path

$$P(\mathbf{q}(t)|\mathbf{q_i}) = \int \mathcal{D}\mathbf{p}(t) e^{\mathcal{S}[\mathbf{q},\mathbf{p},r]}. \tag{2.78}$$

The probability density function for a final state given an initial state is given by

$$P(\mathbf{q_f}|\mathbf{q_i}) = \int \mathcal{D}\mathbf{p}(t)\mathcal{D}\mathbf{q}(t)\mathcal{D}r(t) e^{\mathcal{S}[\mathbf{q},\mathbf{p},r]}. \tag{2.79}$$

Treating the conjugate momenta as real and the extremizing the stochastic action produces a system of ordinary differential equations equivalent to the continuum limit of a Lagrange multiplier optimisation of the function $P(r|q)$. Hence, solutions to the system of ordinary differential equations solved for some given boundary conditions are significant because they give the paths most likely to be followed between any two states. Specifying initial conditions instead gives optimum paths for a series of post selections at different times.

An example of explicitly calculating a CDJ path integral is provided for the trivial, one-dimensional, stochastic action $p\dot{q}$. The CDJ SPI is then,

$$P(q(T)|q(0) = \int \mathcal{D}p\mathcal{D}q\mathcal{D}r e^{\int_0^T dtp\dot{q}} = \int \mathcal{D}p\mathcal{D}q e^{\int_0^T dtp\dot{q}}. \tag{2.80}$$

In principle, we may always transform back and forth between the continuous limit

and discrete time; this transformation is encoded in the rules,

$$\begin{aligned}\int dt \to \delta t \sum_j^n, \quad q(t) \to p_i, \quad p(t) \to p_i, \quad \delta(p(0) - q_{\text{in}}) \to \delta(q_{-1} - q_{\text{in}}),\\ \delta(p(T) - q_f) \to \delta(q_n - q_f), \quad \int \mathcal{D}p\mathcal{D}q \to \int\int \lim_{\substack{n\to\infty,\delta t\to 0\\ \delta t n = T}} \prod_{j=1}^n \frac{dq_j}{2\pi}\frac{dp_j}{2\pi i}.\end{aligned} \tag{2.81}$$

Eq. (2.80) then becomes,

$$P(q|q_0) = \mathcal{F}_{0,n} \int\int \lim_{n\to\infty} \prod_{j=1}^n \frac{dq_j}{2\pi}\frac{dp_j}{2\pi i} e^{\delta t \Sigma_j^n p_j (\frac{q_{j+1}-q_j}{\delta t})}. \tag{2.82}$$

We proceed to explicitly calculate this by first making he substitution $p_j = ik_j$, and then cancelling the δt's, so

$$\begin{aligned}P(q_n|q_0) &= \mathcal{F}_{0,n} \int\int \lim_{n\to\infty} \prod_{j=1}^n \frac{dq_j}{2\pi}\frac{dk_j}{2\pi} e^{\delta t \Sigma_j^n i k_j (\frac{q_{j+1}-\theta_j}{\delta t})}\\ &= \mathcal{F}_{0,n} \int\int \lim_{n\to\infty} \prod_{j=1}^n \frac{dq_j}{2\pi}\frac{dk_j}{2\pi} e^{\Sigma_j^n i k_j (q_{j+1}-q_j)}.\end{aligned} \tag{2.83}$$

Changing from Fourier to Dirac-delta functions, we find,

$$P(q_n|q_0) = \int \lim_{n\to\infty} \prod_{j=1}^n \frac{dq_j}{2\pi} \prod_j^n \delta(q_{j+1} - q_j) q_i \delta_{j,1} q_f \delta_{j,n} = \delta(q_f - q_i). \tag{2.84}$$

As expected, the trivial stochastic action enforces the constraint $\dot{q} = 0$.

2.4 Fluctuation Theorems

The thermodynamic properties of systems in equilibrium, undergoing no macroscopic evolution, are well understood. The state in thermodynamic equilibrium π is known to depend on the system's Hamiltonian, H (with energy spectrum $\{E_i\}$) and the inverse temperature β as,

$$\pi = \frac{e^{-\beta H}}{\mathcal{Z}}. \tag{2.85}$$

The partition function $\mathcal{Z} = \text{Tr}[e^{-\beta H}]$ may be utilised to calculate and predict macroscopic, experimentally accessible thermodynamic properties such as the

specific heat capacity and average energy. However, understanding and quantifying the behaviour of out-of-equilibrium systems is more challenging.

Near equilibrium, the deviation of the system's properties from unperturbed values can be calculated using linear response functions [149, 150]. Fluctuation theorems (FTs), which relate forward and backward thermodynamic processes, are incredibly general statements. They put stringent conditions on the distributions of thermodynamic quantities, such as work and entropy production, even in the far-from-equilibrium regime. Perhaps the most famous of these FTs is Crook's Fluctuation Theorem (CFT) developed by Gavin E. Crooks in 1998 [151], which implies the celebrated Jarzynski equality [152, 153]. In its original formulation, CFT applies to stochastic dynamics. Using the assumption that the system's state may be considered a classical probability distribution over energy eigenstates, the CFT may be applied to quantum systems. However, this approach neglects the effects of interference. Fully quantum mechanical FTs were developed in the decades following Crooks and Jarzynski's original work [154, 155, 156]. These quantum FTs employ a two-point measurement scheme - which is a prerequisite for meaningfully discussing observable properties of a system, such as the energy, which are indeterminate in the absence of measurement [81]. One prominent example of a quantum mechanical variant of an FT is due to Manzano [101, 102].

2.4.1 Crook's Fluctuation Theorem

We follow the method described in the original research [151] to set out Crooks FT. When applying work to a system as part of some thermodynamic process, we may consider the Hamiltonian $H(\lambda(t))$ with the spectrum $E_i(\lambda(t))$. Here $\lambda(t)$ specifies how an experimenter may control the system's Hamiltonian in a form-invariant[18] manor during the time interval $t \in [0, T]$. This produces a time-dependent energy spectrum of the system. The system's statistics may be approximated as a diagonal-

[18]Form-invariant in the sense that the form of the Hamiltonian's dependence on the parameter λ is unchanged irrespective of the value of λ.

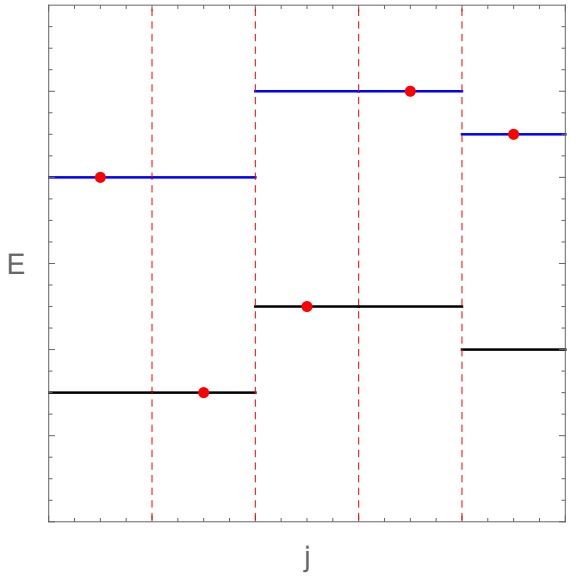

Figure 2.2: An illustration of the kind of stochastic dynamics covered by CFT. Two distinct energy levels (indicated by blue and black lines) are plotted against the step-index j. Vertical dashed lines delineate successive steps. The red dot represents the system state. For half the steps the system may jump between distinct energy levels, in the other half the state remains within a fixed energy level while the energy levels vary.

density matrix written in the instantaneous energy basis. For this section, we employ a somewhat idiosyncratic conceptualization of a quantum trajectory σ. Consider N time steps occurring between $t \in [0, T]$, at each time step $j \in (0, N)$ we let the function $x(j)$ specify which of the i energy levels the system occupies. Each step in the dynamics then consists of first a stochastic jump between energy levels from $E(t_j)_{x(j)}$ to $E(t_j)_{x(j+1)}$, and secondly a possible change in energy within a level $E(t_j)_{x(j+1)}$ to $E(t_{j+1})_{x(j+1)}$. We see that σ is an ordered list of all of these values $\sigma = (..., E(t_j)_{x(j)}, E(t_j)_{x(j+1)}, E(t_{j+1})_{x(j+1)}, ...)$. This behaviour is illustrated in Fig. (2.2). For a given trajectory σ, we may identify heat exchange with the random hops between energy levels,

$$Q[\sigma] = \sum_j (E(t_j)_{x(j+1)} - E(t_j)_{x(j)}), \tag{2.86}$$

while the work may be readily identified with energy changes associated with changes within the energy levels

$$W[\sigma] = \sum_j (E(t_{j+1})_{x(j+1)} - E(t_j)_{x(j+1)}). \tag{2.87}$$

The overall stochastic dynamics is Markovian and may be specified by a series of N transition matrices whose j-th member is specified by the elements, $M(t_j)_{p,q} = P(p; t_{j+1}|q; t_j)$, where $P(p|q)$ specifies the probability of a jump between energy level q and p at time t_j. The stochastic dynamics is assumed to satisfy the condition,

$$M(t_j)\pi(t_j) = \pi(t_j) = \frac{e^{-\beta H(t_j)}}{\mathcal{Z}}. \tag{2.88}$$

Eq. (2.88) implies that the dynamics, if applied to an equilibrium probability distribution, would leave it unchanged. If the protocol $\lambda(t)$ is replaced with $\lambda(T-t)$, the stochastic dynamics may be specified by a series of reversed Kraus operators

$$\tilde{M} = \pi M^T \pi^{-1}, \tag{2.89}$$

applied in the reverse order.

Eq. (2.89) establishes a relationship between the forward and reverse transition probabilities. The ratio of the probability between the forward and reverse probability in Eq. (2.90) may then be simplified since $\tilde{M}_{ji} = \pi_i^{-1} M_{ji} \pi_j$, revealing the distribution is controlled by the heat in σ

$$\frac{P(\sigma|x(0))}{\tilde{P}(\tilde{\sigma}|\tilde{x}(0))} = e^{\beta Q[\sigma]}. \tag{2.90}$$

When we have a system in a specific energy eigenstate that occurs with probability $\rho(x)$[19], the entropy of that state is, $s(x) = -\ln \rho(x)$, and represents how much information is required to fully describe it. For some ensemble, the total entropy is given by $S(x) - \sum_x \rho(x) \ln \rho(x)$.

Consider an evolving process, with an initial probability distribution $\rho(x(0))$ and a final distribution $\rho(x(T))$. The entropy production per trajectory is

$$\omega = \ln \rho\left(x(\tau)\right) - \ln \rho\left(x(0)\right) - \beta Q[x(t)]. \tag{2.91}$$

[19]This corresponds to diagonal elements of the system's density matrix in the energy eigenbasis, so $\rho(x) = \rho(t)_{x(t),x(t)}$.

This quantity ω combines two key elements: how the uncertainty of the system's state changes, plus entropy changes in the surrounding environment. We note that $\omega_F = -\beta Q[\sigma]$ corresponds to the change in entropy in the environment. We further observe that the entropy produced along the corresponding trajectories σ and $\tilde{\sigma}$ will be ω_f and $-\omega_f$ respectively. Using these initial probabilities and performing a summation over all trajectories σ gives an expression for the probability of producing the entropy ω, $P(\omega)$ via any stochastic trajectory,

$$P(\omega) = \sum_{x(0)} \sum_{x(T)} \left(\sum_{\sigma} \rho(x(0)) P(\sigma|x(0)) \delta_{(\omega, \omega_F(\sigma))} \right) \tag{2.92}$$

$$\tag{2.93}$$

We then insert Eq. (2.90) and the condition that $x(T) = \tilde{x}(0)$, we derive the following equation

$$\begin{aligned} P(\omega) &= \sum_{\tilde{x}(0)} \sum_{\tilde{x}(T)} \left(\sum_{\tilde{\sigma}} \rho(\tilde{x}(0)) \tilde{P}(\tilde{\sigma}|\tilde{x}(0)) e^{\omega_F(\tilde{\sigma})} \delta_{(\omega, \omega_F(\tilde{\sigma}))} \right) \\ &= e^{\omega} \tilde{P}(-\omega). \end{aligned} \tag{2.94}$$

This results in the fluctuation theorem in terms of entropy production,

$$\frac{P(\omega)}{\tilde{P}(-\omega)} = e^{\omega}, \tag{2.95}$$

which is then found to hold for a variety of thermodynamic ensembles.

2.4.2 Nonequilibrium Potential for Quantum Channels

We continue exploring thermodynamic systems governed by $H(\lambda(t))$, discussing one generalisation of fluctuation theorems which accounts for the effects of interference. Although there are a variety of such generalisations, we are particularly interested in a fluctuation theorem proposed by Manzano which applies to a wide range of dynamics. The dynamics of a subsystem interacting with its environment can be described by a CPTP map $\mathcal{E}$. We show how Manzano's theorem may be derived for open systems subject to CPTP dynamics.

In contrast to the previous case, where the dynamics are confined to diagonal density matrices, we cannot directly equate work with Eq. (2.87) and heat with Eq. (2.86). Instead, the total work done to the system is given by the energy difference between the initial and final state of the combined system and environment. For describing the thermodynamics of more general quantum dynamics, Manzano introduces a new quantity, the nonequilibrium potential ϕ_i. Every CPTP map $\mathcal{E}$ admits at least one fixed point (or invariant state) which satisfies

$$\mathcal{E}(\pi) = \pi. \tag{2.96}$$

Here, π is, in general, not an equilibrium density matrix. The nonequilibrium potentials for a given CPTP map are defined to be

$$\phi_i = -\ln(\pi_i), \tag{2.97}$$

where π_i is an eigenvalue of the map's fixed state.

If the class of CPTP maps is restricted to those that admit a Kraus operator representation of the form

$$M_k = \sum_{ij} m_{ji}^k |\pi_j\rangle\langle\pi_i|, \tag{2.98}$$

where $m_{ji} = 0$ if $\phi_i - \phi_j \neq \Delta\phi_k$, then each M_k will be unambiguously associated with some value $\Delta\phi_k$. These Kraus operators specify more general stochastic dynamics than their counterparts in Eq. (2.88) since they allow for transition into coherent superpositions of eigenstates of π. If multiple fixed states of $\mathcal{E}$ exist, the values $\{\Delta\phi_k\}$ are independent of the particular choice of fixed state. Indeed, $\{\Delta\phi_k\}$ may be considered a property of the channel as a whole, independent of a chosen Kraus representation. Knowledge of a time-ordered sequence of values for the index k_i specifies a quantum trajectory.

There is a reduced system dynamics associated with the system-bath time-reversed dynamics $\Theta H(\lambda(T-t))\Theta^\dagger$, provided we make a weak coupling approximation between the system and environment. These reduced dynamics are specified by the dual map $\tilde{\mathcal{E}}$. The Kraus representation of $\tilde{\mathcal{E}}$, with the matrices $\{\tilde{M}\}$),

determines the map. The Kraus operators of the dual map are related to the Kraus representation of the original CPTP map by

$$\tilde{M} = \mathcal{A}\pi^{\frac{1}{2}} M \pi^{-\frac{1}{2}} \mathcal{A}^{\dagger}. \tag{2.99}$$

We note that this is analogous to Eq. (2.89). Eq. (2.99) ensures the dual reverse Kraus operators, for some arbitrary choice of unitary or anti-unitary operator $\mathcal{A}$, and an invariant state of $\mathcal{E}$ satisfy the property

$$\mathrm{Tr}[M_{k_2} M_{k_1} \pi M_{k_1}^{\dagger} M_{k_2}^{\dagger}] = \mathrm{Tr}[\tilde{M}_{k_1} \tilde{M}_{k_2} \tilde{\pi} \tilde{M}_{k_2}^{\dagger} \tilde{M}_{k_1}^{\dagger}]. \tag{2.100}$$

Where $\tilde{\pi} = \mathcal{A}\pi\mathcal{A}^{\dagger}$ is the invariant state for the dual dynamics. It may be shown that for quantum channel $\mathcal{E}$ that admits a Kraus representation of the form Eq. (2.98) the forward and dual Kraus operators satisfy the detailed balance relation

$$\tilde{M} = e^{\frac{\Delta\phi}{2}} \mathcal{A} M^{\dagger} \mathcal{A}. \tag{2.101}$$

We now specify a protocol to obtain specific quantum trajectories and their dual trajectories. Consider a system with reduced dynamics $\mathcal{E}$ and let the system be initially prepared in the state $|\psi_n\rangle$. Each Kraus operator in the decomposition of $\mathcal{E}$ can be associated with a specific physical process occurring during the dynamics. Knowledge of which M_k induces back action on the state provides information about the exact quantum trajectory taken by the system. Complete this procedure with a final projective measurement onto the system state $|\phi_m\rangle$. The corresponding quantum trajectory may then be specified by the sequence (n, k, m). This trajectory has a corresponding dual trajectory. For the reverse dual dynamics initialise the system's state with $\mathcal{A}|\phi_m\rangle$. The dual Kraus operator $\tilde{M}_k$ is then considered to act on the system. Finally, a projective measurement of the state $\mathcal{A}|\psi_n\rangle$ completes the construction of the corresponding dual trajectory.

We may calculate the probabilities of the forward trajectory (given by the sequence $\gamma = (m, k_1, ..k_j, ...k_N)$) using the formula

$$p(m, k_N, \ldots, k_1|n) = |\langle\phi_m| M_{k_N}^{(N)} \cdots M_{k_1}^{(1)} |\psi_n\rangle|^2.$$

A similar formula applies for the dual trajectory $\tilde{\gamma} = (\tilde{m}, \tilde{k}_R, \ldots, \tilde{k}_1, \tilde{n})$. For a single-step trajectory we find the equation,

$$\frac{p(m,k|n)}{\tilde{p}(\tilde{n},\tilde{k}|\tilde{m})} = \frac{|\langle\phi_m|M_k|\psi_n\rangle|^2}{|\langle\psi_n|\mathcal{A}^\dagger M_k \mathcal{A}|\phi_m\rangle|^2} = e^{-\Delta\phi(k)}. \tag{2.102}$$

This may easily be generalised to quantum trajectories that involve the application of many more Kraus operators during the dynamics. This is especially important for considering a time-dependent $H(\lambda(t))$, where more insight into the reduced dynamics is achieved by a concatenation of potentially disparate CPTP maps. This generalization is given by Eq. (2.103),

$$\frac{p(m,k_1,..k_j,...k_N|n)}{\tilde{p}(\tilde{n},\tilde{k}_N,...\tilde{k}_j,...,\tilde{k}_1|\tilde{m})} = e^{\alpha(n,m)-\sum_j \Delta\phi(k_j)}. \tag{2.103}$$

Here $\alpha(n,m) = -\ln \tilde{p^i_m} + \ln p^i_n$ is a boundary term that accounts for the possibility that the initial state may be mixed, so the initial state of the forward dynamic takes the form $\rho^i = p^i_0|\phi_0\rangle\langle\phi_0| + ... + p^i_n|\phi_n\rangle\langle\phi_n| + ... + p^i_N|\phi_N\rangle\langle\phi_N|$ and the initial state of the reverse dynamics is $\tilde{\rho}^i = \tilde{p}^i_0|\phi_0\rangle\langle\phi_0| + ... + \tilde{p}^i_m|\phi_m\rangle\langle\phi_m| + ... + \tilde{p}^i_N|\phi_N\rangle\langle\phi_N|$. This ensures any probability ratio differences originating from the initial projective measurements $|n\rangle\langle n|$ and $|m\rangle\langle\tilde{m}|$ and the choice of initial and final state are accounted for. Eq. (2.103) takes the same form as Eq. (2.95) and establishes a relationship between the distribution of forward and reverse trajectories governed by the accumulation of nonequilibrium potential along those trajectories.

Chapter 3

Features of Measurement-Induced Open and Closed Geometric Phases

In this chapter, we explore in detail the dynamics of qubit systems under the kind of continuous measurement protocol described in Sections 2.1.1 and 2.1.2. We are especially interested in examining the attributes of individual quantum trajectories; we, therefore, need to interrogate the system more closely than the stochastic Schrödinger equation would typically allow. We focus our investigation on features analogous to the intriguing topological transition demonstrated by Valentin and others described in Section 2.2.4; for binary projective measurements, this topological transition arises only in the open geometric phase. Our research reveals that for continuous measurement a phenomenologically identical topological transition occurs again in the open geometric phase. Furthermore, we find that the open geometric phase transition remains topological for a variety of post-selection conditions of the readout record and state preparations.

Since the qubit system of interest exhibits a continuous stochastic evolution, we find that the CDJ path integral formulation delineated in Section 2.3.2.2 is an ideal tool to investigate individual quantum trajectories and, in particular,

the measurement-induced closed geometric phases associated with the set of self-closing quantum trajectories. By incorporating a phase variable in the CDJ action for continuous Gaussian measurements we obtain a path-integral formulation for open and closed geometric phases. Variational methods enable us to find and systematically investigate these rare self-closing trajectories and their associated phases. Our research reveals a noteworthy result: the geometric phase of the most probable trajectories undergoes a qualitatively distinct type of topological transition as a function of the measurement strength. We additionally calculate the quantitative impact of including Gaussian corrections to the path integral formalism to our result, where our calculations are shown to align with results obtained through numerical simulations of the complete set of quantum trajectories.

3.1 Geometric Phases Induced by Gaussian Measurements

3.1.1 Cyclically Rotating Gaussian measurements

First, we consider the measurement-induced time evolution of a qubit, with a generic state given by the density matrix $\rho = \frac{1}{2}(\mathbb{I} + \boldsymbol{x} \cdot \boldsymbol{\sigma})$. The vector $\boldsymbol{\sigma}$ consists of Pauli matrices $(\sigma_X, \sigma_Y, \sigma_Z)$ and $\boldsymbol{x}$ is a unit vector on the Bloch sphere of the system parameterised by latitude θ and longitude ϕ. The qubit is subject to a time-dependent sequence of weak measurements over a fixed time, T. We define a continuous process by dividing T into N time steps of length δt, where $t_k = k\delta t$ and $k \in \{n \in \mathbb{N} \cup \{0\} \mid n < N\}$. During each time interval, we measure the operator $A(k) = \boldsymbol{n}(k) \cdot \boldsymbol{\sigma}$, where $\boldsymbol{n}$ is a unit vector specified by spherical coordinates (Θ, Φ) (see Eq. 2.47). Following Section 2.2.4, we specify $\Theta(k) = \Theta$ and $\Phi(k) = 2\pi t_k/T$, so that the target observables are constrained to closed loops of constant latitude on the Bloch sphere (see Fig. 3.1a). At each time step, the measurement of the observable $A(k)$ is performed as a Gaussian measurement, with

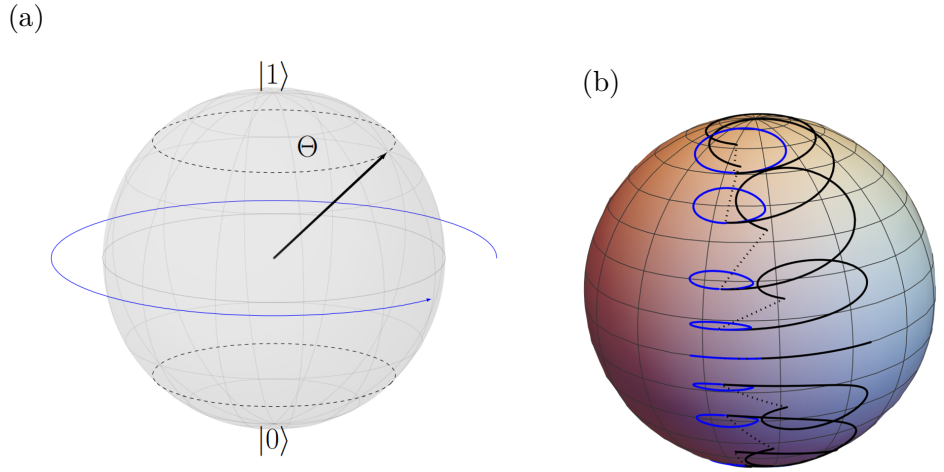

Figure 3.1: **Cyclically rotating qubit measurement protocol and corresponding quantum trajectories**. Panel a) A continuous sequence of Gaussian measurements of operators $\sigma \cdot \mathbf{n}(t)$ at constant latitude Θ, represented by $\mathbf{n}(t)$ tracing out a path on the Bloch sphere (dotted lines). Panel b) Examples of quantum Trajectories on the Bloch sphere generated by the measurement sequence in panel (a) for self-closing (blue) and open (black) boundary conditions. Dotted lines indicate the length-minimising geodesics closing the open path trajectories.

measurement outcomes distributed according to a Gaussian probability distribution (see 2.1.1) [16, 17].

For a system in the state ρ_k, the Gaussian measurement of A_k entails a measurement outcome r_k drawn from the probability distribution

$$P(r_k|\rho_k) = \mathrm{Tr}[E(r_k,k)^\dagger E(r_k,k)\rho_k], \tag{3.1}$$

and the corresponding state update ρ_{k+1} is given by

$$\rho_{k+1} = E(r_k,k)\rho_k E(r_k,k)^\dagger / P(r_k). \tag{3.2}$$

The entire process is controlled by the set of Kraus operators $E(r_k,k)$. For the specific protocol at hand, with measurements constrained at a fixed latitude, we have

$$E(r_k,k) = R(\mathbf{n}(k))^{-1} M_{\delta t}(r_k) R(\mathbf{n}(k)), \tag{3.3}$$

where

$$M_{\delta t}(r_k) = \sqrt[4]{\frac{\delta t}{2\pi\tau}} \exp\left(-\frac{\delta t}{4\tau}(r_k - \sigma_z)^2\right), \tag{3.4}$$

and $R(\boldsymbol{n}(k))$ is a rotation operator $R(\boldsymbol{n}(k)) = e^{-\frac{1}{2}i\phi_k}\exp\left[\frac{1}{2}i(\theta_k\sigma_2 + \phi_k\sigma_3)\right]$ that takes the Bloch sphere state (θ, ϕ) to $|0\rangle$. Here, $\boldsymbol{n}(k)$ denotes the measurement axis at time t_k. We note that Eq. (3.4) is exactly the kind of continuous measurement that could be implemented in a capacitively coupled double quantum dot system (see Section 2.1.2) with a target observable σ_Z. The rotational component of $E(r_k, k)$ ensures that the measured operator is $\boldsymbol{\sigma}\cdot\boldsymbol{n}$. We refer to the parameter τ as the inverse measurement strength, which has the same meaning as discussed in Section 2.1.2, although here τ is not necessarily linked to any one experimental implementation of the measurements. In the continuous limit $\delta t \to 0$, $N \to \infty$ with $\delta t N = T$ transforms the sequences of measurement readouts r_k and the corresponding qubit state variables ϕ_k and θ_k, which are parameterizations of the qubit state in the spherical Bloch sphere, into continuous functions of time, $r(t)$, $\phi(t)$, $\theta(t)$ defining a continuous stochastic process which we study throughout this chapter (see Fig. 3.1b).

This measurement protocol is akin to the one presented in Ref. [54] and described in detail in Section 2.2.4. We note again that this original protocol involves a quasi-continuous sequence of measurements with binary outcomes $r(t) = r^j = j$ for $j \in \{1, 0\}$ and corresponding Kraus operators E_j defined via Eq. (3.3) with $M_{\delta t}(r_k)$ replaced by M_j from Eq. (2.45)-(2.46). This choice of Kraus operators replaces the continuous set of Kraus operators parametrized by r in Eq. (3.3). We stress the key differences between the two protocols manifest in the ensuing distribution of quantum trajectories. Firstly, in section 2.2.4 the resulting set of trajectories included trajectories with discontinuous jumps even in the quasi-continuous limit, whereas all trajectories stemming from Gaussian measurements are continuous. Secondly, for Gaussian trajectories the set of accessible trajectories is invariant after a change in measurement strength, here the measurement strengths only modulates the trajectory likelihoods, whereas for binary measurement the set of accessible trajectories exhibits a measurement strength dependence. We also note

that different measurement setups are required for the disparate measurements. In the quasi-continuous scenario, trajectories exhibiting a topological transition had to be distilled from post-selection 'Null' type readout ($j = 1$). We go on to show that a variety of post-selection methods result in topological transitions for the Gaussian case.

3.1.2 Geometric Phase of the Monitored Qubit

Here we recapitulate some key points from Section 2.2.3 and apply the results to our Gaussian qubit measurements directly. All measurement readout sequences $r(t)$ have associated trajectories on the Bloch sphere $|\psi(t)\rangle$. Each is associated with a unique geometric phase via the functional

$$\chi^{\mathrm{g}}[\psi(t)] = \arg\langle\psi(0)|\psi(T)\rangle + i\int_0^T \langle\psi(t)|\dot{\psi}(t)\rangle dt, \tag{3.5}$$

where $|\psi(t)\rangle$ is a lift of the curve in projective space into Hilbert space that satisfies an initial condition $|\psi(0)\rangle$ written in an arbitrary gauge. While geometric phases are typically associated with closed paths in Hilbert space, we note that Eq. (3.5) is valid for paths in projective space that do not close [46]. In these cases, the geometric phase is equivalent to the geometric phase of the given curve in projective space concatenated with a length-minimizing geodesic that closes the trajectory. Recall we refer to the geometric phase as the open geometric phase, as opposed to the closed geometric phase associated with self-closing trajectories. In practical terms, the open geometric phase corresponds to the closed geometric phase of a post-selected trajectory including an additional projective measurement onto $|\psi(0)\rangle\langle\psi(0)|$.

An important feature of a Gaussian measurement is that it parallel transports the state of the system so there is no dynamical phase contribution to subtract from the global phase. Adopting a pure qubit state parameterisation in spherical coordinates ($\mathbf{q} = (\phi, \theta, \chi)$) that includes a gauge-dependent global phase χ, the systems state is

$$|\psi(\mathbf{q}(t))\rangle = e^{i\chi(t)}\begin{pmatrix} \cos\left(\frac{\theta(t)}{2}\right) \\ e^{i\phi(t)}\sin\left(\frac{\theta(t)}{2}\right) \end{pmatrix}. \tag{3.6}$$

The parallel transport condition Eq. (2.44) holds across each time step, simplifying the geometric phase from Eq. (3.5) to

$$\chi^{\mathrm{g}} = \arg\Bigg[e^{-i(\phi(0)-\chi(T))}\Big(\sin\frac{\theta(0)}{2}e^{i\phi(T)}\sin\frac{\theta(T)}{2} + e^{i\phi(0)}\cos\frac{\theta(0)}{2}\cos\frac{\theta(T)}{2}\Big)\Bigg], \tag{3.7}$$

where we have used gauge freedom to choose $\chi(0) = 0$. When $\phi(0) = \phi(T)$ and $\theta(0) = \theta(T)$ then $\chi^{\mathrm{g}} = \chi(T)$.

3.2 Path Integral: incorporating phase data

3.2.1 Chantasri-Dressel-Jordan Path Integral with Phase Tracking

To study the geometric phases associated with quantum trajectories from Gaussian measurements, we formulate a path integral for the probability distribution of the induced quantum trajectories that explicitly incorporates the phase of the monitored state. We do so by incorporating phase information in the CDJ path integral formulation for a Gaussian-monitored qubit [28], using the state parameterisation in Eq. (3.6). Since this phase is parallel transported, the global phase is directly equivalent to the geometric phase on a closed path. The path integral is constructed from the joint conditional probability of finding a state $\mathbf{q}(T)$ and readout $r(T)$, given some initialization $\mathbf{q}_i$, under the evolution in Eq. (3.2). This probability, in the continuum limit, can be expressed as a product of sequential conditional probabilities (see Eq. (2.74)) so

$$\mathcal{P}(\mathbf{q}(T), r(T)|\mathbf{q}_i) = \mathcal{K}(t_0, t_N)\times \lim_{\delta t\to 0, N\to\infty}\prod_{k=0}^{N-1} P(\mathbf{q}(k+1)|\mathbf{q}(k), r(k))P(r(k)|\mathbf{q}(k)), \tag{3.8}$$

where $\mathcal{K}(t_0, t_N) = \delta^3(\mathbf{q}(N) - \mathbf{q}_f)\delta^3(\mathbf{q}(0) - \mathbf{q}_i)$ sets the initial and final states to be $\mathbf{q}_i$ and $\mathbf{q}_f$. The readout probability distribution function, $P(r|\mathbf{q})$, can be obtained directly from Eq. (3.2) and (3.3), so within each time step

$$P(r|q) \approx \sqrt{\frac{\delta t}{2\pi\tau}} \exp\left(-\frac{\delta t}{2\tau}(r^2 - 2ra + 1)\right), \tag{3.9}$$

$$a(\Theta, \Phi, \theta, \phi) = \cos(\theta)\cos(\Theta) + \sin(\theta)\sin(\Theta)\cos(\phi - \Phi). \tag{3.10}$$

Here $\langle r \rangle = \int rP(r|\mathbf{q})dr = a$ is the mean measurement record function, which corresponds to the most probable readout within a given time interval. The remaining term in Eq. (3.8) is the state update, which is deterministic and can be expressed as a delta function

$$\begin{aligned} P(\mathbf{q}(t+\delta t)|\mathbf{q}(t), r(t)) &= \delta^d(\mathbf{q}(t+\delta t)|\mathbf{q}(t), r(t)) \\ &= \left(\frac{1}{2\pi i}\right)^d \int_{-i\infty}^{i\infty} d^d\mathbf{p} e^{-\mathbf{p}\cdot(\mathbf{q}(t+\delta t))}, \end{aligned} \tag{3.11}$$

where by expressing the Dirac-delta functions[1] in Fourier form each q gains a conjugate momentum p_q, so $\mathbf{p} = (p_\phi, p_\theta, p_\chi)$. The deterministic update associated with $\delta^d(\mathbf{q}(t+\delta t)|\mathbf{q}(t), r(t))$ is expressed in the differential equations,

$$\dot{\phi} = -\tfrac{r}{\tau} f_{\Theta,\Phi}(\theta, \phi) \tag{3.12}$$

$$\dot{\theta} = \tfrac{r}{\tau} g_{\Theta,\Phi}(\theta, \phi,) \tag{3.13}$$

$$\dot{\chi} = \tfrac{r}{2\tau} h_{\Theta,\Phi}(\theta, \phi,). \tag{3.14}$$

with $f_{\Theta,\Phi}(\theta, \phi) = \csc(\theta)\sin(\Theta)\sin(\phi - \Phi)$, $g_{\Theta,\Phi}(\theta, \phi) = (\cos(\theta)\sin(\Theta)\cos(\phi - \Phi) - \sin(\theta)\cos(\Theta))$ and $h_{\Theta,\Phi}(\theta, \phi) = \tan\left(\frac{\theta}{2}\right)\sin(\Theta)\sin(\phi - \Phi)$. Following the usual procedure for constructing path integrals [8, 147, 28, 29, 30], we express $\mathcal{P}$ in terms of an action principle,

$$\mathcal{P} \propto \int D\mathbf{q}D\mathbf{p}Dr \exp\left(-\int_0^T S[\mathbf{q}, \mathbf{p}, r]dt\right), \tag{3.15}$$

$$\begin{aligned} S[\mathbf{q}, \mathbf{p}, r] = &-p_\theta\left(\dot{\theta} - \frac{r}{\tau}g_{\Theta,\Phi}\right) - p_\phi\left(\frac{r}{\tau}f_{\Theta,\Phi} + \dot{\phi}\right) \\ &-p_\chi\left(\dot{\chi} - \frac{r}{2\tau}h_{\Theta,\Phi}\right) + \frac{r(2a - r) - 1}{2\tau}. \end{aligned} \tag{3.16}$$

[1] Once again we use the conventional relabeling $\mathbf{p} \to -i\mathbf{p}$.

The action $S[\mathbf{q}, \mathbf{p}, r]$, is a generalization of the probability density of a quantum trajectory, encoding all the statistical details of the measurement process. Compared to the CDJ action in Ref. [28], Eq. (3.16) now includes the variable χ and the time dependence of the measurement operators. This formalism allows us to identify the most probable trajectories (with a given initial and final state) by variational methods. This results in a system of differential equations for quantum trajectories that are either the most-likely path to traverse between the boundary points or a minimum/saddle point solution, given by Eq. (3.12), (3.13) and (3.14) in combination with the time derivatives of the momentum variables[2], $\dot{p_\chi} = 0$,

$$\begin{aligned}
\dot{p_\phi} &= \frac{r}{\tau} p_\phi \frac{\partial f_{\Theta,\Phi}}{\partial \phi} - \frac{r}{\tau} p_\theta \frac{\partial g_{\Theta,\Phi}}{\partial \phi} - \frac{r}{2\tau} p_\chi \frac{\partial h_{\Theta,\Phi}}{\partial \phi} - \frac{r}{\tau} \frac{\partial a}{\partial \phi}, \\
\dot{p_\theta} &= \frac{r}{\tau} p_\phi \frac{\partial f_{\Theta,\Phi}}{\partial \theta} - \frac{r}{\tau} p_\theta \frac{\partial g_{\Theta,\Phi}}{\partial \theta} - \frac{r}{2\tau} p_\chi \frac{\partial h_{\Theta,\Phi}}{\partial \theta} - \frac{r}{\tau} \frac{\partial a}{\partial \theta},
\end{aligned} \tag{3.17}$$

and a constraint on the measurement record function

$$\begin{aligned}
r = \frac{1}{2} p_\chi h(\theta, \Theta, \phi, \Phi) - p_\phi f(\theta, \Theta, \phi, \Phi) \\
+ p_\theta g(\theta, \Theta, \phi, \Phi) + a(\theta, \Theta, \phi, \Phi).
\end{aligned} \tag{3.18}$$

We observe that by introducing the variable χ, the calculation of the optimal geometric phase becomes more straightforward, as its value can be determined concurrently with the optimal quantum trajectory.

3.2.2 Optimum Dynamics of Stationary Gaussian Measurements

To illustrate the effectiveness of the variational method in the simplest possible case we apply the CDJ action formalism to time-independent Gaussian measurements aligned exactly along the z-axis of the Bloch sphere. This is readily achieved by setting $p_\gamma, \gamma, \Theta, \omega$ equal to zero in the full stochastic action Eq. (3.16). Then using

[2]Here we treat the conjugate momenta as real, exactly reproducing the Lagrange multiplier method of maximizing the functional $\int \frac{r(2a-r)-1}{2\tau} dt$ with constraints.

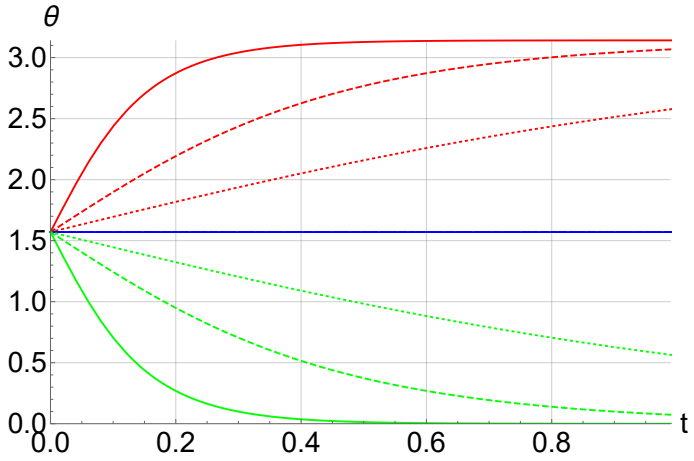

Figure 3.2: The latitude state parameter against time (in units of τ) for Gaussian σ_z measurements. Path colour indicates the initial momentum; red paths correspond to $p_\phi(0)$ =10, green paths $p_\phi(0) = -10$ and the blue trajectory corresponds to $p_\phi(0) = 0$. The type of path indicates the measurement strength: solid $\tau = 1$, dashed $\tau = 3$, dotted $\tau = 7$.

the definition of the stochastic Hamiltonian (Eq. (2.76)) we find

$$\mathcal{H} = \left(\frac{\sin^2(\theta)}{2\tau}\right) p_\theta^2 - \left(\frac{\sin(\theta)\cos(\theta)}{\tau}\right) p_\theta - \frac{\sin^2(\theta)}{2\tau}. \tag{3.19}$$

By extremizing the Hamiltonian we find the following equations of motion

$$\begin{aligned} \dot{\phi} &= 0, \\ \dot{p_\phi} &= 0, \end{aligned} \tag{3.20}$$

$$\begin{aligned} \dot{\theta} &= \frac{1}{\tau}\sin(\theta)(p_\theta \sin(\theta) - \cos(\theta)), \\ \dot{p_\theta} &= \frac{1}{\tau}\left(\cos(\theta) - p_\theta \sin(\theta)(p_\theta \cos(\theta) + \sin(\theta))\right). \end{aligned} \tag{3.21}$$

The optimum dynamics in the θ and ϕ directions are fully independent and $\phi(t)$ is necessarily trivial due to the symmetry of our chosen measurement. These equations of motion have no closed-form solutions; we proceed by finding and plotting a range of solutions numerically in Fig. 3.2. We observe the expected optimum dynamics: for states initialized on the Bloch sphere equator, any initially positive (negative) conjugate momentum drives the quantum trajectory inexorably towards the state

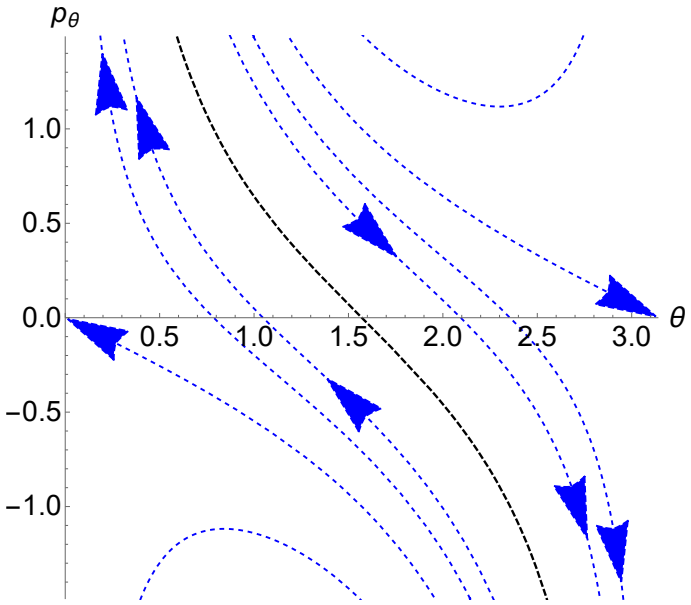

Figure 3.3: The flow in phase space for continuous Gaussian measurements directed along the z-axis of the Bloch sphere. The measurement strength is tuned to $\tau = 1$. Equilibrium solutions appear as the dashed black line.

$|0\rangle$ ($|1\rangle$). Increasing the measurement strength hastens this process. A vanishing initial momentum ensures a stationary optimum trajectory.

Further insight can be gained by plotting the CDJ phase space portrait of this system (Fig. 3.3); this is the flow of Eq. (3.21) in the phase space. We observe that the dynamics bifurcates into qualitatively distinct regions. Variation of the measurement strength leaves the flow in phase space unchanged but does affect the rate at which a path in the phase space is traversed. Eq. (3.21) has equilibrium solutions whenever $p_\theta = \cot\theta$, these are plotted in Fig. (3.3) and are associated with the 'stochastic energy'[3], $-\frac{1}{2\tau}$.

3.2.3 Co-rotating Coordinates

It will be useful to consider the action in Eq. (3.16) rewritten in a spherical coordinate system that co-rotates with the measurement axis defined by new

[3]The value of the stochastic Hamiltonian evaluated at $p_\theta = \cot\theta$, as defined in Ref. [28].

polar and azimuthal coordinates $(\tilde{\theta}, \tilde{\phi})$. Such a coordinate transformation is implemented by the change-of-basis matrix $B = \exp(i\Phi\sigma_z/2)$. In this coordinate system, the dynamics are described by the Kraus operator $\tilde{E}$ and an effective Hamiltonian $\tilde{H}$. Here $\tilde{E} = R^{-1}(\tilde{\boldsymbol{n}})M_{\delta t}R(\tilde{\boldsymbol{n}})$, and is now time-independent since $\tilde{\boldsymbol{n}} = (\sin(\Theta), 0, \cos(\Theta))$ is fixed. While $\tilde{H} = i\dot{B}B^\dagger = -\frac{1}{2}\dot{\Phi}\sigma_z$, and acts unitarily on the system state. The state update is given by

$$\rho(t+\delta t) = \frac{e^{-i\tilde{H}}\tilde{E}\rho\tilde{E}^\dagger e^{i\tilde{H}}}{\mathrm{Tr}[e^{-i\tilde{H}}\tilde{E}\rho\tilde{E}^\dagger e^{i\tilde{H}}]}. \tag{3.22}$$

In terms of the action, this point transformation acts directly on the Bloch sphere coordinates as,

$$\begin{aligned} \tilde{\phi} &= \Phi - \phi(t), \quad \tilde{\theta} = \theta, \\ \dot{\phi} &= -\dot{\tilde{\phi}} + \dot{\Phi}, \quad \dot{\tilde{\theta}} = \dot{\theta}, \end{aligned} \tag{3.23}$$

and also induces a corresponding transformation on the conjugate momentum,

$$p_\phi = -\tilde{p}_\phi, \quad p_\theta = \tilde{p_\theta}. \tag{3.24}$$

These coordinate transformations applied to Eq. (3.16) (omitting χ and p_χ), lead to the CDJ action in rotating coordinates,

$$\begin{aligned} \tilde{S}[\tilde{\theta}, \tilde{\phi}, p_{\tilde{\theta}}, p_{\tilde{\phi}}] = \frac{1}{2\tau}\Bigg[&+ 2r\tilde{a} - r^2 - 1 \\ &+ 2\tilde{p}_\theta\Big(r\cos(\tilde{\theta})\sin(\Theta)\cos(\tilde{\phi}) - r\sin(\tilde{\theta})\cos(\Theta) - \tau\dot{\tilde{\theta}}\Big) \\ &+ 2\tilde{p}_\phi\left(\tau(\dot{\Phi} - \dot{\tilde{\phi}}) - r\csc(\tilde{\theta})\sin(\Theta)\sin(\tilde{\phi})\right)\Bigg]. \end{aligned} \tag{3.25}$$

with $\tilde{a} = \sin(\tilde{\theta})\sin(\Theta)\cos(\tilde{\phi}) + \cos(\tilde{\theta})\cos(\Theta)$. From this reformulation, it is evident that the rotating measurement protocol equivalently captures the physics of the Zeno effect, i.e. the competition between measurement and unitary evolution in a qubit.

3.2.4 Lagrangian Formulation

Since the path integral in Eq. (3.16) is Gaussian in r it is possible to integrate out the measurement record. The ensuing action is quadratic in the momentum variables, which can then also be integrated out to give a configuration space path integral,

$$\begin{aligned}\mathcal{P} &\propto \int D\mathbf{q}D\mathbf{p}Dre(-S[\mathbf{q},\mathbf{p},r]) \\ &= \int D\mathbf{q}\mathfrak{p}[\mathbf{q}] = \int D\mathbf{q}\mu(\theta,\phi)e^{\int_0^T \mathcal{L}[\theta,\phi]}.\end{aligned} \tag{3.26}$$

This alternate formulation is characterized by a probability measure denoted as $\mathfrak{p}[\theta,\phi]$ which consists of two components: an everywhere singular[4] Lagrangian

$$\begin{aligned}\mathcal{L}(\theta,\phi) = &-\frac{1}{2}\tau\sin^2(\theta)\csc^2(\Theta)\dot{\phi}^2\csc^2(\phi-\Phi) - \frac{1}{2\tau} \\ &- \frac{\dot{\phi}}{2}\sin(2\theta)\cot(\Theta)\csc(\phi-\Phi) - \sin^2(\theta)\cot(\phi-\Phi)\dot{\phi},\end{aligned} \tag{3.27}$$

and a path-dependent functional measure, $\mu(\theta,\phi)$, given by

$$\mu(\theta,\phi) = \mathrm{Det}[\frac{\csc^2(\theta)\sin^2(\Theta)\sin^2(\phi-\Phi)}{2\tau}]^{-\frac{1}{2}}. \tag{3.28}$$

The path dependence of μ can be attributed to the multiplicative nature of the underlying stochastic process which acts like a curvature effect in the time axis [158]. The Lagrangian is characterised by a non-invertible Hessian matrix. This particularity results from the imposition of semi-holonomic constraints within the configuration space, as specified by the equations,

$$\dot{\theta} = \frac{\dot{\phi}}{2}\Big((2\sin^2(\theta)\cot(\theta_0)\csc(\phi-\phi_0) - \sin(2\theta)\cot(\phi-\phi_0)\Big), \tag{3.29}$$

$$\dot{\chi} = \frac{\dot{\phi}}{2}(\cos(\theta)-1). \tag{3.30}$$

These constraints naturally appear during the process of functional integration, wherein terms exhibiting, at most, linear dependence on momentum play the role of Legendre multipliers. These multipliers, in turn, enforce Eq. (3.29) and (3.30).

[4] A singular Lagrangian is defined as one where the matrix of second derivatives with respect to velocities is not invertible [157].

We find that Eq. (3.27) may be derived via an alternative method which we demonstrate for $\Theta = \frac{\pi}{2}$. Consider the probability density implied by Eq. (3.1), temporarily suppressing the discrete time index, we find

$$P(r|\phi) = \sqrt{\frac{\delta t}{2\pi\tau}} e^{-\delta t \frac{(r^2+1)}{2\tau}} \Big(\cos(\phi - \phi_0) \sinh\left(\frac{\delta t r}{\tau}\right) + \cosh\left(\frac{\delta t r}{\tau}\right)\Big). \tag{3.31}$$

Then taking the small-time approximation and exponentiating both sides we get

$$e^{\ln(P(r|\phi)} = \exp\left[\frac{1}{2}\left(\ln\left(\frac{\delta t}{2\pi\tau}\right) - \frac{(r^2 - 2r\cos(\phi+1)\,\delta t}{\tau} + O\left(\delta t^2\right)\right)\right]. \tag{3.32}$$

Next, we ignore the divergent part (in the path integral, this would be absorbed into the functional measure); this may be justified since we will typically only calculate the ratio of probabilities. Then solving Eq. (3.12) and switching to the rotating coordinate frame we find the relationship

$$r_{i+1} = \tau \csc(\tilde{\phi}_i)\Big(\omega + \frac{\tilde{\phi}_i - \tilde{\phi}_{i+1}}{\delta t}\Big). \tag{3.33}$$

Substituting this into the exponent in Eq. (3.32) we obtain to first order in time, the discreet transition probability,

$$\begin{aligned} P(\phi_{i+1}|\phi_i) \propto \exp[&\frac{\tau(\tilde{\phi}_i - \tilde{\phi}_{i+1})^2 \csc^2(\tilde{\phi}_i)}{\delta t} + 2(\tilde{\phi}_i - \tilde{\phi}_{i+1})\csc(\tilde{\phi}_i)(\tau\omega\csc(\tilde{\phi}_i) - \cos(\tilde{\phi}_i)) \\ &+ \delta t(-2i\tilde{\phi}_i + 2i\tilde{\phi}_{i+1} + \tau\omega^2\csc^2(\tilde{\phi}_i) + \frac{1}{\tau} - 2\omega\cot(\tilde{\phi}_i))]. \end{aligned} \tag{3.34}$$

The probability density (omitting boundary terms) may be determined by multiplying together an infinite series in the appropriate limit,

$$P[\phi(t)] \propto \lim_{\substack{\delta t\to 0, N\to\infty \\ \delta t N = T}} \prod_i^N P(\phi_{i+1}|\phi_i), \tag{3.35}$$

which explicitly evaluates to,

$$\begin{aligned} P[\phi(t)] \propto \exp\Bigg[-\frac{1}{2}\int_0^T \Big(&\tau\dot{\tilde{\phi}}^2\csc^2(\tilde{\phi}) - 2\dot{\tilde{\phi}}\csc(\tilde{\phi})(\tau\omega\csc(\tilde{\phi}) - \cos(\tilde{\phi})) \\ &+ \tau\omega^2\csc^2(\tilde{\phi}) - 2\omega\cot(\tilde{\phi}) + \frac{1}{\tau}\Big)dt\Bigg]. \end{aligned} \tag{3.36}$$

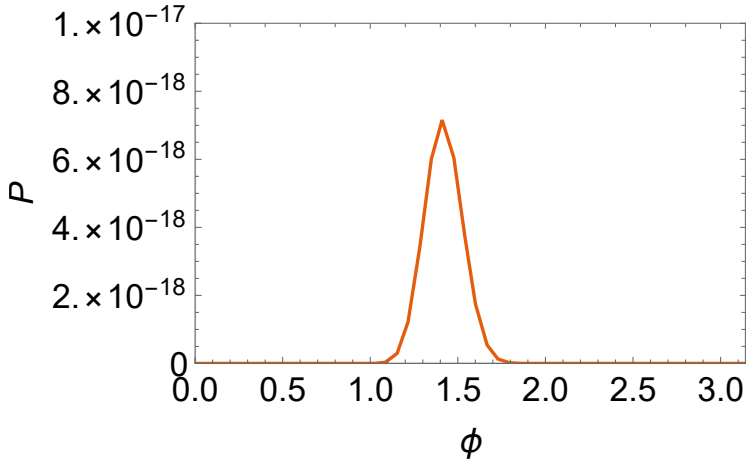

Figure 3.4: The approximate unnormalised probability density given by Eq. (3.37) with the parameters $\tau = 1$, $\omega = 2\pi$. We note that out of all the possible trajectories that are stationary in the rotating coordinates we may identify one which occurs with a maximum likelihood.

This exponent is equivalent to the stochastic Lagrangian Eq. (3.27) in rotating coordinates. This equivalence is most clearly shown by evaluating Eq. (3.27) on a trajectory characterised by $\dot{\tilde{\phi}} = 0$. For $T = 1$ and $\tilde{\phi}_{st} = \tilde{\phi}(t)$ this expression is given by

$$P[\phi_{st}] \propto \exp\left[-\frac{1}{2}\int_0^1 \left(\tau\omega^2 \csc^2(\tilde{\phi_{st}}) - 2\omega\cot(\tilde{\phi_{st}}) + \frac{1}{\tau}\right) dt\right] \tag{3.37}$$

$$\propto \exp\left[-\frac{1}{2}\left(\tau\omega^2 \csc^2(\tilde{\phi_{st}}) - 2\omega\cot(\tilde{\phi_{st}}) + \frac{1}{\tau}\right)\right]. \tag{3.38}$$

This is equivalent to Eq. (3.27) evaluated with $\dot{\theta} = \omega$. We display the probability density Eq. (3.37) for trajectories that perfectly synchronise with the motion of the measurement axis in Fig. 3.4. Note that $\tilde{\phi}_{st} = 0 \implies P(\tilde{\phi}_{st}) = 0$ for all τ (except $\tau \neq 0$). Across all ranges of measurement strengths, the probability density for a quantum trajectory that closes aligned precisely with the measurement axis is vanishingly small.

3.3 Topological Features of the Open Geometric Phase

The action (Eq. (3.16)) and its associated extremization in Eq. (3.17) allow us to determine the properties of the most likely geometric phases induced by Gaussian measurements for any given boundary conditions. However, before exploring new subsets of geometric phases, like optimal self-closing ones, we first determine the properties of the open geometric phases under Gaussian measurements, in particular, their topological features.

Gaussian measurements have been involved in researching this type of topological transition [34]. Dual readout Gaussian measurements on a qutrit were used to reproduce the effect of the null-type measurements on a two-level sub-system. Here we are concerned with Gaussian measurements in their own right, specifically in the protocol outlined in Section 3.1.1. In this case, a continuous mapping between the two spheres is no longer constrained to the null-type post-selection and more general post-selections can be imposed on the measurement readout. Quite generally, we expect that a rotating measurement protocol with $(\theta_i = \Theta, \phi_i = 0)$ features a topological transition for post-selected record function $r(t) > 0$, this condition ensures the system is driven towards the measurement axis at all times during the measurement induced dynamics. For the special case when $\Theta = \frac{\pi}{2}$, the Bloch sphere equator corresponds to an invariant subspace for every Kraus operator in the measurement sequence: states initialized on the equator remain therein. This feature of the system's accessible trajectories manifest in the available geometric phases $\{\frac{\pi}{2}n | n \in \mathbb{Z}\}$ on the equator; each is associated with a definite winding number characterizing the number of times a trajectory wraps around the Bloch sphere equator. This applies irrespective of the state preparation used.

As a first example, it is possible to ascertain the topological transition for the family of most likely trajectories spanned by initial states that coincide with the measurement axis. These most-probable post-selected optimal trajectories are

(a)

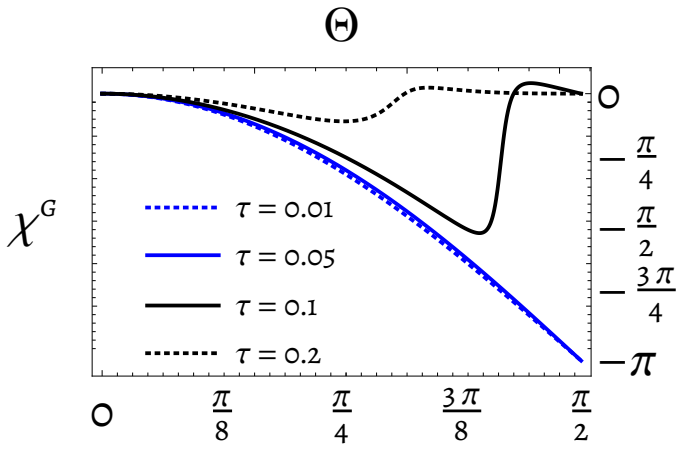

(b)

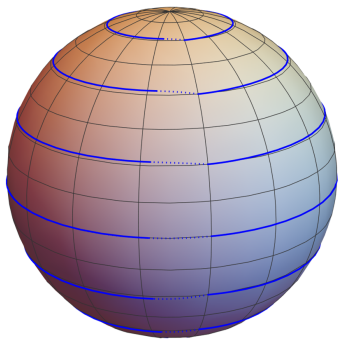

(c)

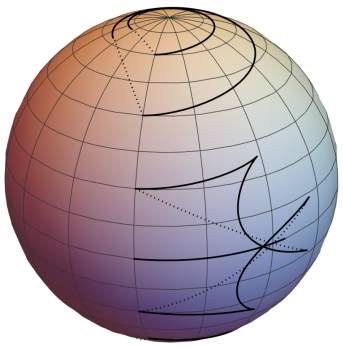

Figure 3.5: **Global Optimal quantum trajectories and their geometric phases**. (a) Geometric phase $\chi^g(\Theta)$ for a range of measurement strengths below (blue) and above (black) the inverse critical measurement strength $\tau_c/T \approx 0.1$. Quantum trajectories on the Bloch sphere with closing geodesics (dotted) for $\tau/T = 0.05$ (c) and $\tau/T = 0.2$ (b). The family of trajectories covers the Bloch sphere for measurements stronger than the critical value (b) and does not otherwise (c).

obtained from the observation that at each time-step, the most probable outcome is given by $\langle r \rangle = a(\Theta, t)$ (cf. Eq. (3.9)). Hence, substituting the time continuous version, $r(t) = a(t)$ from Eq. (3.10) into Eq. (3.12)- (3.14), with the initial conditions $\theta(0) = \Theta$ and $\phi(0) = \Phi(0)$, produces the required optimum quantum trajectory. A topological transition is observed in this case, as illustrated in Fig. 3.5, where the family of quantum trajectories — including the closing geodesic— for strong measurements (small τ/T) wrap the Bloch sphere (Fig. 3.7b), while for weak measurements (large τ/T) they do not (Fig. 3.7c). The transition measurement strength is determined numerically from the dependence $\chi^g(\Theta)$, which is reported in Fig 3.5a. For $\tau < \tau_c$ the geometric phase evolve continuously from 0 to $-\pi$, while for $\tau > \tau_c$, $\chi(\pi/2) = \chi(0)$. We estimate that the transition occurs for $\tau_c/T \approx 0.1$, The transition is further confirmed by a direct numerical evaluation of the Chern number using Eq. (2.49).

A second kind of variation of the protocol concerns the state preparation. So far we have only considered state initializations with the form $\theta(0) = \Theta$ and $\phi(0) = \Phi(0)$, however, it is possible to relax this assumption. From numerical simulation of a range of cases, it appears that the initialization of the system does not affect the topological nature of the transition and the associated phenomenology of the geometric phase provided the state initialization $\theta_i(\Theta(0))$ spans the entire range of the polar angle, is monotonic, and satisfies $\theta_i(0) = 0$, $\theta_i(\frac{\pi}{2}) = \frac{\pi}{2}$, and $\theta(\pi) = \pi$ with $\lim_{\tau \to 0} \phi_i = \Phi(0)$. Note we are explicitly allowing for the possibility of a measurement strength-dependent state preparation so $\theta(0) = \theta_i(\tau)$ and $\phi(0) = \phi_i(\tau)$. We are particularly interested in using this freedom to choose a new state preparation that, similar to the choice $\theta_i = \Theta$ $\phi_i = \Phi(0)$, will also continuously recover the projective measurement limit - where states are initialized along the measurement axis and meticulously follow the axis for their entire evolution. This then requires a state initialization that gives $\theta_i \to \Theta(0)$ and $\phi_i \to \Phi(0)$ in the strong measurement limit.

A natural case, which will be relevant later on for closed geometric phases, has

(a)

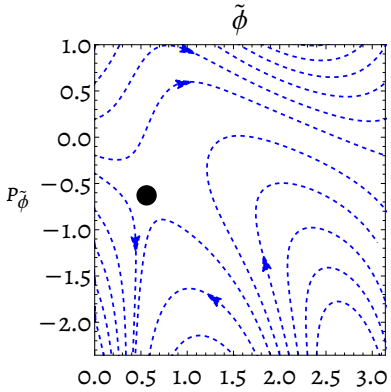

(b)

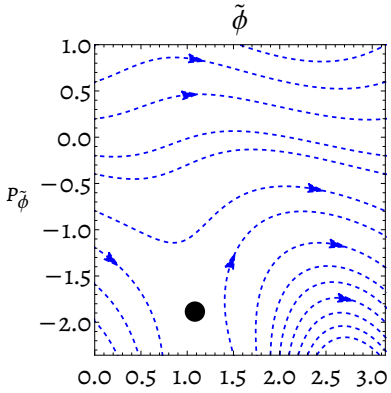

(c)

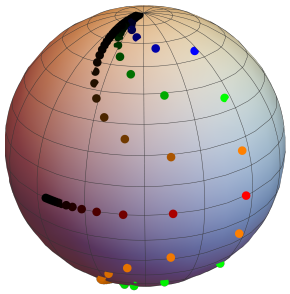

Figure 3.6: **Equilibrium state**. Flow of Hamilton's equations in the CDJ Phase Space at $\theta = \pi/2$ (Eq. (3.17)) in the co-rotating coordinate system for $\tau = 0.1$, $\Theta = \frac{\pi}{2}$ (panel a) and $\tau = 0.3$, $\Theta = \frac{\pi}{2}$ (panel b). The black dot indicates the equilibrium point. Panel c): Dependence of the equilibrium points (θ_e, ϕ_e) on Θ and τ. For each value of Θ ($\frac{\pi}{6}$ (blue), $\frac{2\pi}{7}$ (green), $\frac{2\pi}{5}$ (orange), $\frac{\pi}{2}$(red), $\frac{3\pi}{5}$(orange), $\frac{5\pi}{7}$ (green)) darker shades corresponding to weaker measurements from $\tau/T = 0.1$ to $\tau/T = 10$.

the initial state chosen to coincide with a fixed point (so $\theta_i = \theta_e$ and $\phi_i = \phi_e$) of the optimal trajectory dynamics in the co-rotating coordinate frame. This equilibrium point in the co-rotating dynamics (θ_e, ϕ_e) is defined by $\dot{\tilde{\phi}} = 0$, $\dot{\tilde{\theta}} = 0$, $\dot{\tilde{p}}_\phi = 0$, $\dot{\tilde{p}}_\theta = 0$. Hamilton's equations for the action (Eq. (3.25)) can be solved to determine a closed-form expression,

$$\theta_e = \arctan\left(\frac{\tan(\Theta)}{\sqrt{4\pi^2\tau^2 + 1}}\right), \tag{3.39}$$

$$\phi_e = -\arctan(2\pi\tau). \tag{3.40}$$

Fig. 3.6 reports the phase space flow diagram from Hamilton's equations for the action in Eq. (3.25) for different values of the measurement strength [panels (a) and (b)] at $\theta = \Theta_0 = \pi/2$. For increasingly strong measurements, ϕ_e tends toward the measurement axis. The position of equilibrium points for generic latitudes on the Bloch sphere is reported in Fig. 3.6c, showing that this same limiting behaviour continues across the entire Bloch sphere. The quantum trajectories for this modified protocol (with a generic choice of post-selection $r(t) = 1$) are reported in Fig.(3.7[b-c]), where small τ/T (panel b) leads to trajectories wrapping the Bloch sphere and large τ/T (panel c) does not. Similarly to the case reported in Fig. 3.5, we can identify a topological transition from the behaviour of χ as a function of Θ [cf. Fig. 3.7a], which gives a critical measurement strength $\tau_c/T \approx 0.22$. From these examples, it emerges that, despite variations in the exact value of τ_c, the fundamental characteristics of the transition are unchanged for a wide range of state preparation protocols.

3.4 Topological Transition in the Optimal Closed Geometric Phase

We now use the developed action formalism to investigate the topological features of the closed geometric phase. This involves considering the set of self-closing trajectories generated solely by continuous monitoring, without a projective

(a)

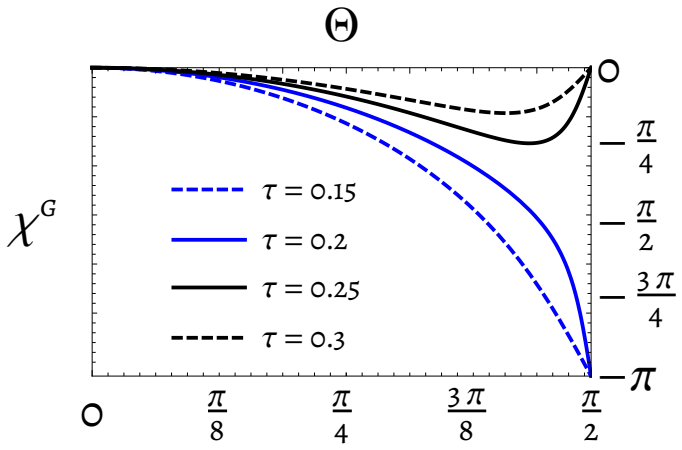

(b)

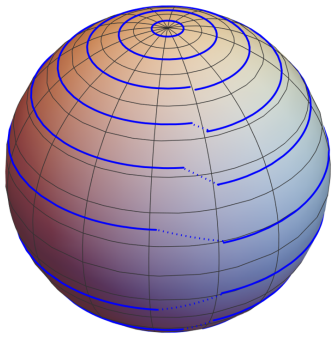

(c)

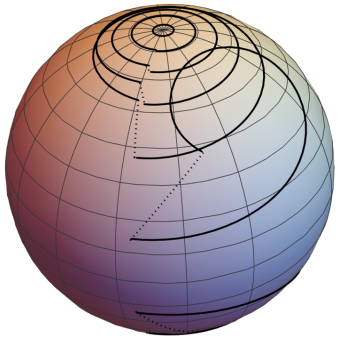

Figure 3.7: **Quantum trajectories and geometric phases with equilibrium state initialization**. Panel a) Geometric phase $\chi(\Theta)$ for a range of measurement strengths below (blue) and above (black) the inverse critical measurement strength $\tau_c \approx 0.22$. Quantum trajectories on the Bloch sphere with closing geodesics (dotted) for $\tau = 0.15$ (b) $\tau = 0.3$ (c). The family of trajectories covers the Bloch sphere for measurements stronger than the critical value (b) and does not otherwise (c).

measurement step. Since self-closing trajectories are not generally achievable by conditioning on any single measurement record function, we post-selected the most likely self-closing trajectory, corresponding to the most probable closed geometric phase attained during measurement. We denote the optimum phase as χ^{opt}. On the Bloch sphere equator, where quantum trajectories are restricted to S^1, the behaviour of χ^{opt} is fundamentally tied to the topology of S^1. Attaining only two possible values corresponding to the winding number of the associated equitorial quantum trajectory, either $-\pi$ or 0.

Care must be taken to find a state preparation that will produce χ^{opt} that recovers the projective measurement limit,

$$\lim_{\tau\to 0}\chi^{\text{opt}} \approx -2\pi\sin^2\left(\frac{1}{2}\Theta\right), \lim_{\tau\to\infty}\chi^{\text{opt}} \approx 0. \tag{3.41}$$

The state preparation $\theta(0) = \Theta$ and $\phi(0) = \Phi$, applied to Eq. (3.17), with self-closing boundary conditions produce a variety of candidate optimal geometric phases that satisfy Eq. (3.41). In the regime of strong measurements, one might anticipate an increased likelihood of candidate solutions with $\lim_{\tau\to 0}\chi^{\text{opt}} \approx -2\pi\sin^2\left(\frac{1}{2}\Theta\right)$. However, numerical assessment of the stochastic action reveals that these solutions remain vanishing improbable even in the strong measurement limit. This is demonstrated in Fig. 3.8 where the stationary phase approximation for Eq. (2.79) is used to produce an estimate

$$P(\tilde{\phi}_f|\tilde{\phi}_i) \approx P(\tilde{\phi}_{\text{op}}) \approx \exp(S[\phi, p_\phi, r]), \tag{3.42}$$

based on the probability density of the optimum trajectories. Numerical solutions for $\phi_{\text{op}}(t)$ are used to examine a series of probability density functions each with a different measurement strength. It is evident from every plot in Fig. 3.8 that winding self-closing ($\tilde{\theta}_f = 0$) trajectories occur with an vanishing probability. This phenomenon can be understood upon examining the characteristics of these candidate optima: spending the majority of their lifetime (approximately T) following the equilibrium trajectory (Eq. (3.39)), punctuated with rapid transitions to and from the measurement axis at the beginning and end of the protocol. It

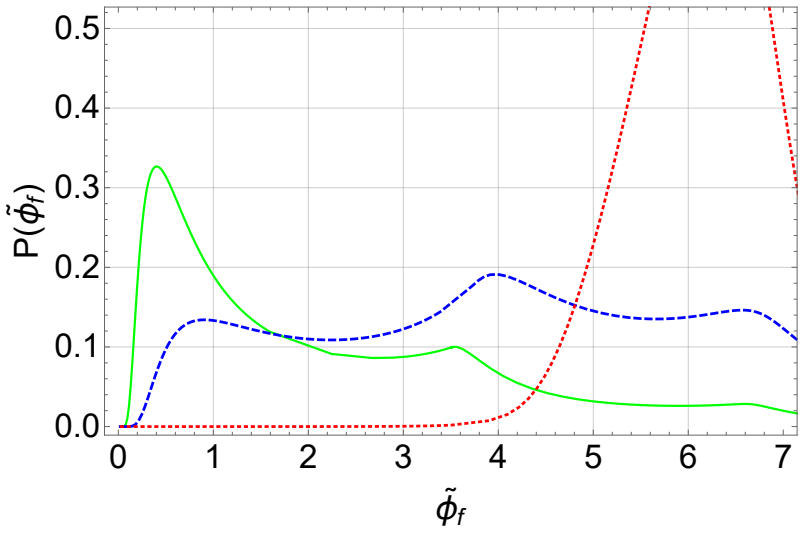

Figure 3.8: Given an initial state aligned with the measurement axis we plot the probability density as a function of the final state after the measurement axis has completed one full loop around the Bloch sphere. Red: $\frac{1}{\tau} = 1$. Blue: $\frac{1}{\tau} = 8$. Green: $\frac{1}{\tau} = 16$

is these rapid transitions that suppress the likelihood of the winding solution. Consequently, the solutions associated with a vanishing winding number dominate. This scenario leads to a χ^{opt} that does not satisfy Eq. (3.41). Instead, a suitable state preparation is provided by the equilibrium point introduced in Eq. (3.39). The equilibrium points span the entire range of latitudes, with $\theta \in [0, \pi]$. As we shall later demonstrate, with this particular initialization, the value of χ^{opt} adheres to the required limits given in Eq. (3.41). This establishes the mapping between measurement parameters (Θ, τ) and the optimal self-closing quantum trajectory and its associated closed geometric phase χ^{opt} that we use to establish a new topological transition.

3.4.1 Topological Transition

As discussed for the case of the open geometric phase, the topological properties of the mapping $\boldsymbol{n}(t) \to q(t)$ are dictated by the fixed points at $\Theta = 0$ and $\Theta =$

π. When $\Theta = \frac{\pi}{2}$, the simplest topological features can be investigated since here the accessible trajectories are each associated with a definite winding number n indexing the available closed geometric phases $\{\frac{\pi}{2}n \mid n \in \mathbb{Z}\}$. Hamilton's equations for the stochastic action, Eq. (3.17), restricted to the Bloch sphere equator, have multiple solutions after imposing boundary conditions $\phi(0) = \phi_e$ and $\phi(T) = \phi_e + 2\pi n$, generating a set of candidate most-likely self-closing quantum trajectories and phases. A single candidate solution is generated for each value of n corresponding to a local minimum of the action (or equivalently a local maximum of the probability density $\mathfrak{p}$ over the set of quantum trajectories).

To determine which candidate solution occurs with a higher probability, we evaluate and compare their actions. The solution corresponding to $n = 1$, equivalent to the equilibrium quantum trajectory in co-rotating coordinates, is $\phi(t)^{n=1}_{\Theta=\frac{\pi}{2}} = 2\pi t - \arctan 2\pi\tau$. By substituting this solution into Eq. (3.16), we find the associated probability density is given by $\mathfrak{p}^{n=1}_{\Theta=\frac{\pi}{2}} = e^{-2\pi^2\tau}$. For $n = 0$, a numerical solution to Eq. (3.17) is used to find $\phi(t)^{n=0}_{\Theta=\frac{\pi}{2}}$, which is then substituted directly into the stochastic action to evaluate $\mathfrak{p}^{n=0}_{\Theta=\frac{\pi}{2}}$. Both of these probability densities are plotted in Fig. 3.9a. Solutions for other values of n are found to have strictly lower probabilities. We, therefore, focus our analysis on the competition between the candidate optimum trajectories indexed by $n = 0$ and $n = 1$. The value of χ^{opt} is determined by the competition between the two most prominent candidate optimums. As evidenced by Fig. 3.9a, there is a measurement strength, $\tau_c/T \approx 0.11$, at which the optimum geometric phase jumps discontinuously from 0 to $-\pi$.

We now investigate if a transition of topological number in the optimal geometric phase occurs across the whole Bloch sphere. To address this question, we study the subset of solutions for Eq. (3.17) that generate optimal self-closing quantum trajectories (with $\theta(0) = \theta_e$, $\phi(0) = \phi_e$ and $\chi(0) = 0$) for all measurement latitudes. We identify one family of solutions (ϕ_{eq}) smoothly connected to $\phi(t)^{n=1}_{\Theta=\frac{\pi}{2}}$, specified by $\phi_{eq} = \phi_e + 2\pi t$ and $\theta(t) = \theta_e$. This closed-form solution may be substituted back

(a)

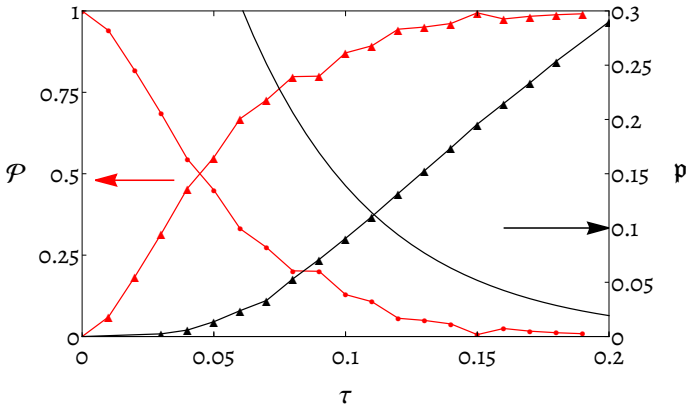

(b)

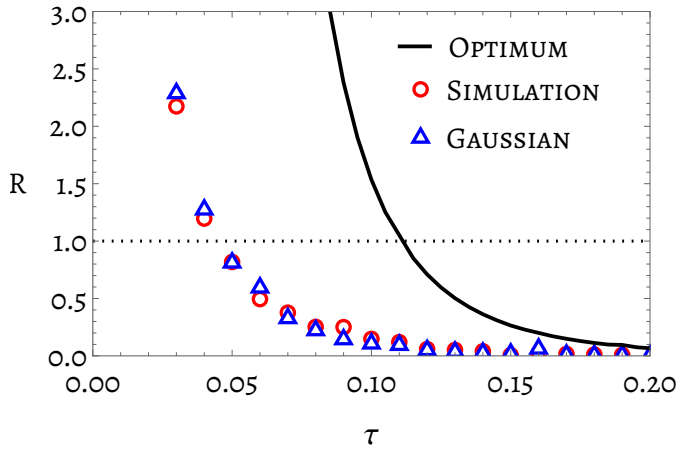

Figure 3.9: **Stochastic properties of winding and non-winding quantum trajectories on the Bloch sphere equator.** Panel a) Probability measure's $\mathfrak{p}^{n=1}$(solid black) and $\mathfrak{p}^{n=0}$ (black triangles) as functions of τ. Normalised self-closing conditional probability $\mathcal{P}$ (state initialization $(\theta_i = \theta_e, \phi_i = \phi_e)$) for non-winding trajectories (red triangles) and winding trajectories (red). $\mathcal{P}$ is obtained from numerical simulation of Eq. (3.2) and (3.3) with 100 time-steps and 500 quantum trajectories with bin size $\Delta\phi = 0.1$. Panel b) The τ dependence of the ratios $\mathfrak{R}$ and R (c.f. Section 3.5) calculated using numerical data in panel a and the results of Gaussian corrections of Section 3.5.

into Eq. (3.17) to find the corresponding geometric phase

$$\chi^{n=1} = -2\pi \sin^2\left(\frac{1}{2}\tan^{-1}\left(\frac{\tan(\Theta)}{\sqrt{4\pi^2\tau^2+1}}\right)\right), \tag{3.43}$$

which is proportional to the solid angle of the spherical cap defined at the latitude θ_e. We note that $\lim_{\tau\to 0}\chi^{n=1} = -2\pi\sin^2\left(\frac{1}{2}\Theta\right)$, and that $\chi^{n=1}$ decreases monotonically from 0 to $-\pi$ with increasing Θ. Similarly, we evaluate $S[\theta,\phi,p_\theta,p_\phi]$ on this $n=1$ family of solutions, finding the probability density of each single trajectory is given by

$$\mathfrak{p}^{n=1} = \exp\left(-\frac{2\pi^2\tau\sin^2(\Theta)}{2\pi^2\tau^2\cos(2\Theta)+2\pi^2\tau^2+1}\right). \tag{3.44}$$

Note that $\mathfrak{p}^{n=1}\to 1$ for $\tau\to 0$. These sets of solutions for different Θ form a submanifold of the Bloch sphere with $C=1$, independent of the measurement strength (see Fig. 3.10a). We may identify a second family of quantum trajectories: the most likely solutions excluding ϕ_{eq} [5] (see Fig. 3.10b). This set of solutions, $\phi(t)^{n=0}$, is determined by numerically computing the stochastic action in Eq. (3.16) and has no closed-form expression for either the accrued geometric phase or the associated probability density. The mapping between $(\Theta(t),\Phi(t))$ and $(\theta(t),\phi(t))$ in this case is always characterized by $C=0$. The optimal (most likely) value of the geometric phase, χ^{opt}, is then determined by the competition between these two families of solutions.

For strong measurements ($\tau \ll T$), solutions $\phi(t)^{n=0}$ are less probable than ϕ_{eq}, so the optimal geometric phase is given by Eq. (3.44). In the weak measurement regime ($\tau \gg T$), we have the converse, solutions $\phi(t)^{n=0}$ are more likely. We label Θ_{jump} the value of Θ, which for a given measurement strength, will delineate a discontinuity in χ^{opt}. Θ_{jump} has a τ dependence and separates two distinct types of behaviour of $\chi^{\text{opt}}(\Theta)$ as it approaches the strong measurement limit. At $\Theta_{\text{jump}}(\tau)$, χ^{opt} jumps discontinuously to the value determined by ϕ_{eq}, with τ_c marking the smallest value of τ for which this discontinuous jump occurs. This jump in the

[5] As for the solutions at the equator, multiple solutions of the Euler-Lagrange equations exist for given boundary conditions, corresponding to local minima of the actions

(a)

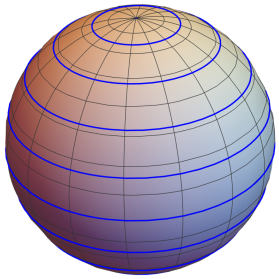

(b)

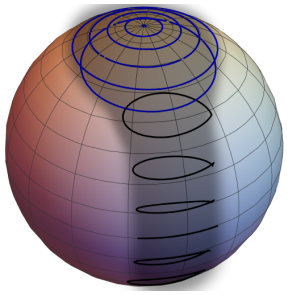

(c)

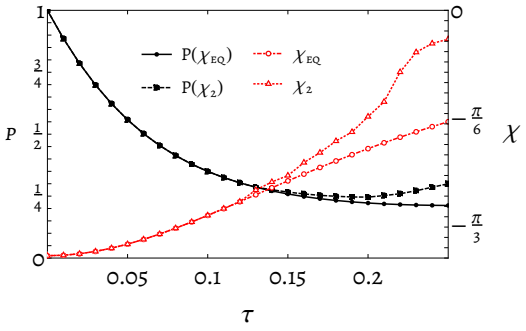

Figure 3.10: **Optimal self-closing quantum trajectories.** Equilibrium quantum trajectories ϕ_{eq} [panel (a)] and $\phi(t)^{n=0}$ [panel (b)]for various choices of Θ, with $\tau/T = 0.2$. The shaded region in panel (b) is a guide to the eyes highlighting the $C = 0$ submanifold on the Bloch sphere. The trajectories with $C = 1$ cover the whole sphere as shown in panel (a). Panel c) Candidate optimum geometric phases, χ_{eq} and χ_2 and corresponding probabilities, $P(\chi_{eq})$ and the competing optimum $P(\chi_2)$, at $\Theta = 0.9 < \Theta_c$ as a function of τ. The two candidate solutions merge into a single q-trajectory before the value of τ_c.

geometric phase is shown in Fig. 3.11. We name the largest value of Θ_{jump}, Θ_C, and it is determined to be $\Theta_C \approx 0.95$.

Below Θ_C, χ^{opt} tends smoothly towards the geometric phase associated with ϕ_{eq}. Numerical evidence suggests that the family of quantum trajectories $\phi(t)^{n=0}$ merge smoothly with the associated trajectory ϕ_{eq}. This behaviour is illustrated in Fig. 3.10b, where the blue-coloured quantum trajectories denote the region in which the family of trajectories $\phi(t)^{n=0}$ merges into ϕ_{eq}. This behaviour is quantified in Fig. 3.10c, which shows how, at $\Theta < \Theta_C$, the geometric phase from the $\phi(t)^{n=0}$ family of trajectories coincides with that from ϕ_{eq} at $\tau < \tau_c$. Crucially, this merger occurs above the critical measurement strength τ_c, suggesting that the value of τ_c as determined on the Bloch sphere equator does correspond to a topological transition across the entire Bloch sphere. This transition is manifest in the behaviour of χ^{opt} as a function of Θ (see Fig. 3.11), where τ_c separates phases that are continuous and monotonically decreasing (from 0 to π) and those which are non-monotonic (0 to 0). The transition in the topological number for optimal self-closing trajectories and the corresponding discontinuity in the geometric phase are distinct from the open geometric phase transition. While the latter is associated with a vanishing post-selection probability at the critical point [54], for self-closing trajectories, two trajectories from distinct families become equally likely at the transition point.

This topological transition is well defined in terms of the most likely trajectories belonging to either of the two families identified above. However, any experiment would not be able to access the most likely trajectories directly. This is due to the improbability of attaining exactly the required measurement record $r(t)$. This may be addressed by comparing the likelihood of trajectories which are approximately equivalent to the required paths. The sets of trajectories to be compared must necessarily include an ensemble of trajectories that are equivalent up to the precision of the experiment. The averaged geometric phase is expected to display a crossover as opposed to a sharp transition at τ_c. In a scenario with finite experimental precision, the value of τ_c will therefore be smeared out. However, a transition can

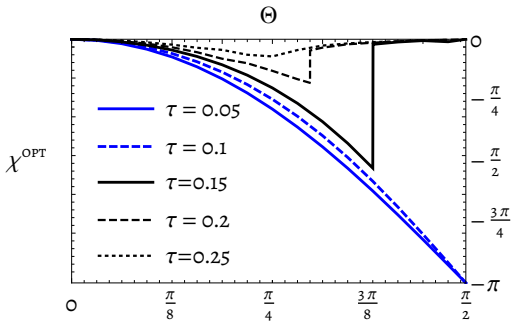

Figure 3.11: **Optimal geometric phases, $\chi^{\mathbf{opt}}$, as a function of Θ for a range of measurement strengths.** The critical measurement strength τ_c distinguishes the behaviour $\chi^{\text{opt}}(\Theta = \pi/2) = 0$ and $\chi^{\text{opt}}(\Theta = \pi/2) = -\pi$. The location of discontinuities specify Θ_{jump} we see for $\Theta > \Theta_C \approx 0.95$, the geometric phase can exhibit such a jump.

still be identified in terms of which of the ensembles (each associated with a distinct optimal geometric phase) is most probable. We calculate the effect this has on the value of τ_c in the next section.

3.4.2 Comparing Critical Measurement Strengths

We make a comparison between the critical measurement strength we have calculated for Gaussian measurements and the critical measurement strength described in Section 2.2.4. In order to make a meaningful comparison between the two distinct measurement strengths characterised by η and τ, we calculate the decoherence rate associated with both types of measurements to establish a map between the two measurement strength parameters η and τ.

Whenever our system, in a generic state Eq. (3.45), is measured by the null-weak measurement operators Eq. (2.45) its average post-measurement state will be given by Eq. (3.46),

$$\rho(t) = \begin{pmatrix} \rho_{11} & \rho_{12} \\ \rho_{21} & \rho_{22} \end{pmatrix}, \tag{3.45}$$

$$\begin{aligned}\langle\rho(t+\Delta t)\rangle &= \sum_r P(r)\frac{M_r\rho(t)M_r^\dagger}{P(r)} \\ &= \begin{pmatrix} \rho_{11} & \sqrt{1-\eta}\rho_{12} \\ \sqrt{1-\eta}\rho_{21} & \rho_{22}(|1-\eta|+|\eta|) \end{pmatrix}.\end{aligned} \tag{3.46}$$

During the quasi-continuous null type weak measurement protocol the measurement strength η depends on the total number of measurements during a cycle N (where we later have $N \to \infty$ or equivalently $\eta \to 0$) as $\eta = \frac{4c}{N}$. We may now say the total time, T, for a cycle is given by $T = N\Delta t$. Hence the change in the coherence of the average state after a single measurement, $\sqrt{1-\eta}$, has a dependence on Δt,

$$\sqrt{1-\eta} \to \sqrt{1-\frac{4c}{N}} \to \sqrt{1-\frac{4c\Delta t}{T}}. \tag{3.47}$$

From this, we see that the first-order change in the coherence as a function of Δt is given by

$$1 - \frac{2c\Delta \mathrm{t}}{T} + O\left(\Delta \mathrm{t}^2\right), \tag{3.48}$$

which uncovers the decoherence rate

$$\Gamma_{\text{Null}} = -\frac{2c}{T}. \tag{3.49}$$

Similarly, a qubit state (Eq. (3.45)) measured by a Gaussian measurement with the family of Kraus operators Eq. (3.4) will have an average post-measurement state given by

$$\begin{aligned}\langle\rho(t+\delta t)\rangle &= \int P(r)\frac{M_{\delta t}\rho(t)M_{\delta t}^\dagger}{P(r)}dr \\ &= \int M_{\delta t}\rho(t)M_{\delta t}^\dagger dr \\ &= \begin{pmatrix} \rho_{11} & \rho_{12}e^{-\frac{\delta \mathrm{t}}{2\tau}} \\ \rho_{21}e^{-\frac{\delta \mathrm{t}}{2\tau}} & \rho_{22} \end{pmatrix}.\end{aligned} \tag{3.50}$$

During the interval δt the coherence of the average post-measurement state reduces by a factor $\exp(-\frac{\delta t}{2\tau})$. Consequently, the first-order change in the state coherence as

a function of δt is

$$1 - \frac{\delta \mathrm{t}}{2\tau} + O\left(\delta \mathrm{t}^2\right). \tag{3.51}$$

This reveals a decoherence rate associated with Gaussian measurements

$$\Gamma = -\frac{1}{2\tau}. \tag{3.52}$$

For each measurement protocol ΓT is a meaningful dimensionless parameter and can be used to convert directly between the measurement parameters η and τ,

$$\Gamma_{\mathrm{Gauss}} T = \Gamma_{\mathrm{Null}} T. \tag{3.53}$$

From Eq. (3.49) we have $\Gamma_{\mathrm{Gauss}} T = 2c$. The critical measurement strength identified for a quasi-continuous loop of measurements is $c \approx 2.15$ [54], corresponding to $\Gamma_{\mathrm{Null}} T \approx 4.30$. For the Gaussian Measurement protocol $\Gamma_{\mathrm{Gauss}} T = \frac{T}{2\tau}$. In Section 3.4.1 we found that the dimensionless critical measurement strength $\tilde{\tau}_{\mathrm{crit}} \approx 0.11$ (when $\tau = T\tilde{\tau}$). Hence for $T = 1$, $\Gamma_{\mathrm{critical}} T \approx \frac{1}{2(0.11)} = 4.54$. As expected, the Gaussian critical measurement strength is similar, though not coincidental, to the binary critical measurement strength.

3.5 Gaussian Corrections

To incorporate multiple trajectories in the picture we include Gaussian corrections in the analyses of optimal self-closing trajectories. This method allows us to account for the effect of solutions that deviate slightly from the optimal solutions while still satisfying the required boundary conditions (and hence can be associated with distinct geometric phases). Operationally, the identification of τ_c when including extra trajectories is achieved by replacing a direct comparison of the measure of two individual quantum trajectories, with a comparison of the state transition probabilities,

$$\mathfrak{R} = \frac{\mathfrak{p}(\phi^{n=1}_{\Theta=\frac{\pi}{2}})}{\mathfrak{p}(\phi^{n=0}_{\Theta=\frac{\pi}{2}})} \to R = \frac{\mathcal{P}^{\mathrm{eq}}(2\pi + \phi_e|\phi_e)}{\mathcal{P}^{n=0}(\phi_e|\phi_e)}, \tag{3.54}$$

so that $\mathcal{P}^{eq}(2\pi + \phi_e|\phi_e)$ is the self-closing transition probability evaluated for trajectories close to ϕ_{eq} with geometric phases $-\pi$. $\mathcal{P}^{n=0}(\phi_e|\phi_e)$ is the self-closing transition probability evaluated for trajectories close to $\phi^{n=0}$ which are associated with a vanishing geometric phase. Here, we limit our analysis of Gaussian corrections to states initialized with $\Theta = \pi/2$ since the transition and its critical value are determined by the equatorial dynamics. The dynamics are then fully constrained to one dimension, parametrized by ϕ.

3.5.1 Phase Space Gaussian Fluctuations

$\mathcal{P}^{\text{eq}}$ and $\mathcal{P}^{n=0}$ can be evaluated using a saddle point approximation around their associated candidate optimum quantum trajectory. Computing saddle point approximations is a standard procedure explicated in Ref. [147]. The conventional algorithm consists of expanding the action around a chosen extremal trajectory by rewriting $\mathbf{q} = \mathbf{q}^* + \delta\mathbf{q}$ and $\mathbf{p} = \mathbf{p}^* + \delta\mathbf{p}$, where $\delta\mathbf{q}$ and $\delta\mathbf{p}$ are small deviations from the optimal values $\mathbf{q}^*$ and $\mathbf{p}^*$. The Gaussian terms in the path integral may then be evaluated, neglecting higher-order corrections. The result is an approximated probability,

$$\mathcal{P} = \mathcal{N} \int \mathcal{D}\mathbf{q}\mathcal{D}\mathbf{p}\ e^{S[\mathbf{q},\mathbf{p}]} \approx \mathcal{N} \sqrt{\frac{(2\pi)^n}{\det(\mathbf{A}|_{\mathbf{q}^*,\mathbf{p}^*})}} e^{S[\mathbf{q}^*,\mathbf{p}^*]}, \tag{3.55}$$

where $\mathbf{A}|_{\mathbf{q}^*,\mathbf{p}^*}$ is the functional hessian of the CDJ action evaluated on the optimum path with zero Dirichlet boundary conditions and $\mathcal{N}$ is an overall normalisation factor.

The challenging step to implementing Eq. (3.55) is the calculation of the functional determinant of the $\mathbf{A}|_{\mathbf{q}^*,\mathbf{p}^*}$. For the key case of interest on the Bloch sphere equator, we have the action-functional

$$S[\phi, p_\phi, r] = \int_0^T \left(-p_\phi \dot{\phi} + p_\phi \left(\dot{\Phi} - \frac{r}{\tau} \sin(\phi) \right) - \frac{r^2 - 2r\cos(\phi) + 1}{2\tau} \right) dt. \tag{3.56}$$

Since the stochastic action is in the form of an integral $\int F(\phi(t), p_\phi(t), r(t))dt$, an application of the Euler-Lagrange equations straightforwardly obtains the first

functional derivatives as follows:

$$\begin{aligned}
\frac{\delta S}{\delta \phi} &= \dot{p}_\phi - \frac{r p_\phi \cos(\phi) + r \sin(\phi)}{\tau}, \\
\frac{\delta S}{\delta p_\phi} &= \dot{\Phi} - \frac{r \sin(\phi)}{\tau} - \dot{\phi}, \\
\frac{\delta S}{\delta r} &= \frac{\cos(\phi) - p_\phi \sin(\phi) - r}{\tau}.
\end{aligned} \tag{3.57}$$

In preparation for applying another functional derivative Eq. (3.57) may be cast in the form of functionals with the dummy time variable s,

$$\begin{aligned}
\frac{\delta S}{\delta \phi(t_1)} &= \int_{-\infty}^{\infty} \frac{\tau p_\phi(s)\dot{\delta}(t_1 - s) - p_\phi(s) r(s) \delta(t_1 - s)\cos(\phi(s))}{\tau} ds, \\
\frac{\delta S}{\delta p_\phi(t_1)} &= \int_{-\infty}^{\infty} \frac{-r(s)\delta(t_1 - s)\sin(\phi(s)) + \dot{\Phi}\tau\delta(t_1 - s) - \tau\delta(t_1 - s)\dot{\phi}(s)}{\tau} ds, \\
\frac{\delta S}{\delta r(t_1)} &= \int_{-\infty}^{\infty} \frac{-2p_\theta(s)\delta(t_1 - s)\sin(\phi(s)) - 2r(s)\delta(t_1 - s) + 2\delta(t_1 - s)\cos(\phi(s))}{2\tau} ds.
\end{aligned} \tag{3.58}$$

Recall the definition of the functional derivative

$$\frac{\delta S}{\delta x_i(t_2)} = \lim_{\epsilon_1 \to 0} \frac{1}{\epsilon_1}(S[x_i + \epsilon_1 \delta] - S[x_i]). \tag{3.59}$$

Applying Eq. (3.59) to Eqs. (3.58) and naming $\Delta t = t_2 - t_1$ we obtain the following equations

$$\begin{aligned}
\frac{\delta}{\delta \phi(t_2)}\left(\frac{\delta S}{\delta \phi(t_1)}\right) &= \lim_{\epsilon_1 \to 0} \frac{1}{\epsilon}\Big[\Big(\frac{d}{dt_1} p_\phi(t_1) - \frac{r(t_1)\cos(\phi(t_1) + \epsilon\delta(\Delta t))p_\phi(t_1)}{\tau}\Big) \\
&\qquad - \Big(\frac{dp_\phi(t_1)}{dt_1} - \frac{p_\phi(t_1) r(t_1)\cos(\phi(t_1))}{\tau}\Big)\Big] \\
&= \frac{1}{\tau} p_\phi(t_1) r(t_1)\sin(\phi(t_1))\delta(\Delta t)
\end{aligned} \tag{3.60}$$

$$\begin{aligned}
\frac{\delta}{\delta p_\phi(t_2)}\left(\frac{\delta S}{\delta \phi(t_1)}\right) &= \lim_{\epsilon_1 \to 0} \frac{1}{\epsilon}\Big[\Big(\frac{d}{dt_1}(p_\phi(t_1) + \epsilon\delta(\Delta t)) - \frac{r(t_1)\cos(\phi(t_1))(p_\phi(t_1) + \epsilon\delta(\Delta t))}{\tau}\Big) \\
&\qquad - \Big(\frac{dp_\phi(t_1)}{dt_1} - \frac{p_\phi(t_1) r(t_1)\cos(\phi(t_1))}{\tau}\Big)\Big] \\
&= -\frac{d}{dt_1}\delta(\Delta t) - \frac{1}{\tau} r(t_1)\delta(\Delta t)\cos(\phi(t_1))
\end{aligned} \tag{3.61}$$

$$\frac{\delta}{\delta r(t_2)}\Big(\frac{\delta S}{\delta \phi(t_1)}\Big) = \lim_{\epsilon_1 \to 0} \frac{1}{\epsilon}\Big[\Big(\frac{d}{dt_1}p_\phi(t_1) - \frac{(r(t_1)+\epsilon\delta(\Delta t))\cos(\phi(t_1))p_\phi(t_1)}{\tau}\Big) - \Big(\frac{dp_\phi(t_1)}{dt_1} - \frac{p_\phi(t_1)r(t_1)\cos(\phi(t_1))}{\tau}\Big)\Big] = \frac{p_\phi(t_1)\delta(\Delta t)(-\cos(\phi(t_1))) - \delta(\Delta t)\sin(\phi(t_1))}{\tau} \tag{3.62}$$

$$\frac{\delta}{\delta \phi(t_2)}\Big(\frac{\delta S}{\delta p_\phi(t_1)}\Big) = \lim_{\epsilon_1 \to 0} \frac{1}{\epsilon}\Big[\Big(\dot{\Phi} - \frac{r(t_1)\sin(\phi(t_1)+\epsilon\delta(\Delta t))}{\tau} - \frac{d(\phi(t_1)+\epsilon\delta(\Delta t))}{dt_1}\Big) - \Big(\dot{\Phi} - \frac{r(t_1)\sin(\phi(t_1))}{\tau} - \frac{d}{dt_1}\phi(t_1)\Big)\Big] = \frac{d}{dt_1}\delta(\Delta t) - \frac{1}{\tau}r(t_1)\delta(\Delta t)\cos(\phi(t_1)) \tag{3.63}$$

$$\frac{\delta}{\delta p_\phi(t_2)}\Big(\frac{\delta S}{\delta p_\phi(t_1)}\Big) = \lim_{\epsilon_1 \to 0} \frac{1}{\epsilon}\Big[\Big(\dot{\Phi} - \frac{r(t_1)\sin(\phi(t_1))}{\tau} - \frac{d(\phi(t_1))}{dt_1}\Big) - \Big(\dot{\Phi} - \frac{r(t_1)\sin(\phi(t_1))}{\tau} - \frac{d}{dt_1}\phi(t_1)\Big)\Big] = 0 \tag{3.64}$$

$$\frac{\delta}{\delta r(t_2)}\Big(\frac{\delta S}{\delta p_\phi(t_1)}\Big) = \lim_{\epsilon_1 \to 0} \frac{1}{\epsilon}\Big[\Big(\dot{\Phi} - \frac{(r(t_1)+\epsilon\delta(\Delta t))\sin(\phi(t_1))}{\tau} - \frac{d(\phi(t_1))}{dt_1}\Big) - \Big(\dot{\Phi} - \frac{r(t_1)\sin(\phi(t_1))}{\tau} - \frac{d}{dt_1}\phi(t_1)\Big)\Big] = -\frac{\delta(\Delta t)\sin(\phi(t_1))}{\tau}$$

$$\frac{\delta}{\delta \phi(t_2)}\Big(\frac{\delta S}{\delta \phi(t_1)}\Big) = \lim_{\epsilon_1 \to 0} \frac{1}{\epsilon}\Big[\Big(\frac{-p_\phi(t_1)\sin(\phi(t_1)+\epsilon\delta(\Delta t)) - r(t_1) + \cos(\phi(t_1)+\epsilon\delta(\Delta t))}{\tau}\Big)\Big) - \Big(\frac{-p_\phi(t_1)\sin(\phi(t_1)) - r(t_1) + \cos(\phi(t_1))}{\tau}\Big)\Big] = \frac{p_\phi(t_1)\delta(\Delta t)(-\cos(\phi(t_1))) - \delta(\Delta t)\sin(\phi(t_1))}{\tau} \tag{3.65}$$

$$\frac{\delta}{\delta p_\phi(t_2)}\Big(\frac{\delta S}{\delta\phi(t_1)}\Big) = \lim_{\epsilon_1\to 0}\frac{1}{\epsilon}\Big[\Big(\frac{-(p_\phi(t_1)+\epsilon\delta(\Delta t))\sin(\phi(t_1)) - r(t_1)+\cos(\phi(t_1))}{\tau}\Big)\Big) - \Big(\frac{-p_\phi(t_1)\sin(\phi(t_1)) - r(t_1)+\cos(\phi(t_1))}{\tau}\Big)\Big] = -\frac{\delta(\Delta t)\sin(\phi(t_1))}{\tau} \tag{3.66}$$

$$\frac{\delta}{\delta r(t_2)}\Big(\frac{\delta S}{\delta\phi(t_1)}\Big) = \lim_{\epsilon_1\to 0}\frac{1}{\epsilon}\Big[\Big(\frac{-p_\phi(t_1)\sin(\phi(t_1)) - (r(t_1)+\epsilon\delta(\Delta t))+\cos(\phi(t_1))}{\tau}\Big)\Big) - \Big(\frac{-p_\phi(t_1)\sin(\phi(t_1)) - r(t_1)+\cos(\phi(t_1))}{\tau}\Big)\Big] = -\frac{\delta(\Delta t)}{\tau}. \tag{3.67}$$

These Eqs. (3.60)- (3.67) are organised into the matrix of operators

$$A(t_2,t_1) = \begin{pmatrix} \frac{\delta S}{\delta\phi(t_2)\delta\phi(t_1)} & \frac{\delta S}{\delta p(t_2)\delta\phi(t_1)} & \frac{\delta S}{\delta r(t_2)\delta\phi(t_1)} \\ \frac{\delta S}{\delta\phi(t_2)\delta p(t_1)} & \frac{\delta S}{\delta p(t_2)\delta p(t_1)} & \frac{\delta S}{\delta r(t_2)\delta p(t_1)} \\ \frac{\delta S}{\delta\phi(t_2)\delta r(t_1)} & \frac{\delta S}{\delta p(t_2)\delta r(t_1)} & \frac{\delta S}{\delta r(t_2)\delta r(t_1)} \end{pmatrix}. \tag{3.68}$$

When Eq. (3.68) is evaluated at the equilibrium quantum trajectory, it simplifies to:

$$A(t_2,t_1)|_{\phi_{\rm eq}} = \begin{pmatrix} -\frac{\sqrt{1-\dot\Phi^4\tau^4}}{\tau} & -\frac{d}{dt_1} - \frac{\sqrt{1-\dot\Phi^2\tau^2}}{\tau\sqrt{\dot\Phi^2\tau^2+1}} & 0 \\ \frac{d}{dt_1} - \frac{\sqrt{1-\dot\Phi^2\tau^2}}{\tau\sqrt{\dot\Phi^2\tau^2+1}} & 0 & -\frac{\dot\Phi}{\sqrt{\dot\Phi^2\tau^2+1}} \\ 0 & -\frac{\dot\Phi}{\sqrt{\dot\Phi^2\tau^2+1}} & -\frac{1}{\tau} \end{pmatrix}\delta(\Delta t). \tag{3.69}$$

Equipped with vanishing boundary conditions Eq. (3.69) has an empty spectrum. This presents an obstacle to evaluating $\mathrm{Det}[A(t_2,t_1)|_{\phi_{\rm eq}}]$, since $\mathrm{Det}[A(t_2,t_1)|_{\phi_{\rm eq}}]$ is defined to be the product of the operator eigenvalues. To make further progress, we integrate the measurement record function out. The functional determinant in Eq. (3.55) may be expressed as a path integral,

$$\int DxDyDz\exp\Big(\int\int dt_1dt_2\ \mathbf{x}^T A(t_2,t_1)|_{\mathbf{q}=\mathbf{q}_{\rm cl}}\mathbf{x}\Big) \tag{3.70}$$

Where $\mathbf{x}$ is the deviation from the classical trajectory

$$\mathbf{x} = \begin{pmatrix} x \\ y \\ z \end{pmatrix} = \begin{pmatrix} \delta\phi - \phi_{cl} \\ \delta p - p_{cl} \\ \delta r - r_{cl} \end{pmatrix}.$$

We may then perform the Gaussian integral over z using the general result

$$\begin{aligned} Dv(x) \exp\left(-\frac{1}{2}\int\int dx\, dx'\, v(x)A(x,x')v(x') + \int dx\, j(x)v(x)\right) \\ \propto (\det A)^{-\frac{1}{2}} \exp\left(\frac{1}{2}\int\int dx\, dx'\, j(x)A^{-1}(x,x')j(x')\right), \end{aligned} \tag{3.71}$$

where we have also used the definition of a Green's function

$$\int dx' A(x,x')A^{-1}(x',x'') = \delta(x - x''). \tag{3.72}$$

Naming the vector $\mathbf{y} = \begin{pmatrix} x \\ y \end{pmatrix}$ we obtain[6]

$$\int DxDyDz \exp\left(\int\int dt_1 dt_2\ \mathbf{x}^T A(t_2,t_1)|_{\phi_{eq}}\mathbf{x}\right) = \tag{3.73}$$

$$\int \mathcal{D}x\mathcal{D}y\mathcal{D}z \exp\left(\int\int dt_t dt_2 \mathbf{y}^T B(t_2,t_1)|_{\phi_{\rm eq}}\mathbf{y} - \frac{z(t_1)\delta(\Delta t)z(t_2)}{\tau}\right. \tag{3.74}$$

$$\left. - \int dt_2 \frac{2y(t_2)(\Theta(t_2) - \Theta(t_2 - T))z(t_2)}{\sqrt{1 + \dot{\Phi}^2\tau^2}}\right). \tag{3.75}$$

where we have isolated the simpler operator

$$B(t_2,t_1)|_{\phi_{\rm eq}} = \begin{pmatrix} -\frac{\sqrt{1-\dot{\Phi}^4\tau^4}}{\tau}\delta(\Delta t) & -\frac{d}{dt_1}\delta(\Delta t) - \frac{\sqrt{1-\dot{\Phi}^2\tau^2}}{\tau\sqrt{\dot{\Phi}^2\tau^2+1}}\delta(\Delta t) \\ \frac{d}{dt_1}\delta(\Delta t) - \frac{\sqrt{1-\dot{\Phi}^2\tau^2}}{\tau\sqrt{\dot{\Phi}^2\tau^2+1}}\delta(\Delta t) & 0 \end{pmatrix}. \tag{3.76}$$

Solving the z component by applying Eq. (3.71) to Eq. (3.70) we find the divergent pre-factor $\mathrm{Det}\left[-\frac{\delta(\Delta t)}{\tau}\right]^{-\frac{1}{2}}$, and the Green's function associated with $-\frac{\delta(\Delta t)}{\tau}$ is given by $-\tau\delta(\Delta t)$. By comparison with Eq. (3.71) we identify, $j(t_2) = -\frac{2\dot{\Phi}y(t_2)}{\sqrt{\dot{\Phi}^2\tau^2+1}}$. The

[6]Here we have repurposed the notion Θ to indicate the Heaviside function.

Gaussian corrections with the record function integrated out then become equivalent to the new path integral

$$\int DxDy \exp\left(\int dt_1 dt_2 - \frac{2\dot{\Phi}^2\tau y(t_1)\delta(\Delta t)y(t_2)}{\dot{\Phi}^2\tau^2+1}\right)\exp\left(\int\int dt_t dt_2 \mathbf{y}^T B(t_2,t_1)\mathbf{y}\right). \tag{3.77}$$

This path integral has the concomitant functional Hessian

$$C(t_2,t_1)|_{\phi_{\rm eq}} = \begin{pmatrix} -\frac{\sqrt{1-\dot{\Phi}^4\tau^4}}{\tau}\delta(\Delta t) & -\frac{d}{dt_1}\delta(\Delta t) - \frac{\sqrt{1-\dot{\Phi}^2\tau^2}}{\tau\sqrt{\dot{\Phi}^2\tau^2+1}}\delta(\Delta t) \\ \frac{d}{dt_1}\delta(\Delta t) - \frac{\sqrt{1-\dot{\Phi}^2\tau^2}}{\tau\sqrt{\dot{\Phi}^2\tau^2+1}}\delta(\Delta t) & -\frac{2\dot{\Phi}^2\tau\delta(\Delta t)}{\dot{\Phi}^2\tau^2+1} \end{pmatrix}. \tag{3.78}$$

In order to find the spectrum associated with this operator we set up the eigenvalue equation

$$\begin{pmatrix} -\frac{\sqrt{1-\dot{\Phi}^4\tau^4}}{\tau} & \frac{d}{dt_2} - \frac{\sqrt{1-\dot{\Phi}^2\tau^2}}{\tau\sqrt{\dot{\Phi}^2\tau^2+1}} \\ -\frac{d}{dt_2} - \frac{\sqrt{1-\dot{\Phi}^2\tau^2}}{\tau\sqrt{\dot{\Phi}^2\tau^2+1}} & -\frac{2\dot{\Phi}^2\tau}{\dot{\Phi}^2\tau^2+1} \end{pmatrix}\begin{pmatrix} x \\ y \end{pmatrix} = \eta\begin{pmatrix} x \\ y \end{pmatrix}. \tag{3.79}$$

However, once again we find that, subject to the boundary conditions that $x(0) = x(T) = 0$ and $y(0) = y(T) = 0$, there will be no corresponding solutions.

3.5.2 State Space Gaussian Fluctuations

Since we encounter these difficulties in the phase space formulation of the SPI we move on to expressing the stochastic path integral in the Lagrangian formulation Eq. (4.27). Despite the presence of the state-dependent functional measure in Eq. (3.28), we find that this form is more tractable. Simplifying Eq. (4.27), (3.28) and (3.27) with $\theta(t) = \frac{\pi}{2}$ and $\Theta = \frac{\pi}{2}$, and recalling the value of θ_e, the path integral we required for $\mathcal{P}^{\rm eq}(2\pi+\phi_e|\phi_e)$ is,

$$\mathcal{P}(2\pi+\phi_e|\phi_e) \propto \tag{3.80}$$

$$\int \mathcal{D}\phi \sqrt{\frac{\tau}{2\pi\sin^2(2\pi t-\phi)}} e^{\int\left(-\frac{1}{2}\tau\dot{\phi}^2\csc^2(2\pi t-\phi)+\dot{\phi}\cot(2\pi t-\phi)\right)dt} \tag{3.81}$$

$$\approx e^{S[\phi_{eq}]}\int \mathcal{D}\delta\phi\sqrt{\frac{\tau}{2\pi\sin^2(2\pi t-\phi_{eq})}} e^{\int \delta\phi\mathbf{A}|_{\phi_{eq}}\delta\phi dt}.$$

Following the method described in [158], we apply a time reparameterization around the equilibrium trajectory, so the new time variable u is determined by $u(t) = \frac{1}{\tau}\int_0^t \sin(2\pi t' - \phi_{eq}(t'))dt'$ with $u(0) = 0$. This acts as a local-scale transformation that eliminates the state-dependent functional measure, simplifying the path integral to

$$\mathcal{P}(2\pi + \phi_e|\phi_e) \approx \mathcal{N} e^{S[\phi_{eq}]} \int \mathcal{D}\delta\phi e^{\int \delta\phi \mathbf{\Sigma}|_{\phi_{eq}} \delta\phi du}. \tag{3.82}$$

This may then be evaluated using

$$\begin{aligned} e^{S[\phi_{eq}]} \int \mathcal{D}\delta\phi e^{\int \delta\phi \mathbf{\Sigma}|_{\phi_{eq}} \delta\phi du} &= e^{S[\phi_{eq}]} \Big(\det \mathbf{\Sigma}|_{\phi_{eq}} \Big)^{-\frac{1}{2}} \\ &= e^{S[\phi_{eq}]} \Big(\frac{\det\left[\Sigma|_{\phi_{eq}}\right]}{\det\left[\frac{d^2}{du^2}\right]} \Big)^{-\frac{1}{2}} \Big(\det_{\zeta}\left[\frac{d^2}{du^2}\right] \Big)^{-\frac{1}{2}}, \end{aligned} \tag{3.83}$$

where the final functional determinant is Riemann-Zeta regularized [147]. This regularized determinant would normally be absorbed in the functional measure, however, given the time parametrization we employed depends on the value of the state parameter we must include the state-dependent part of the Riemann Zeta regularised contribution of this term, which can be expressed as [158]

$$\det_{\zeta} \frac{d^2}{du^2} = \prod \pi^2 n^2 \prod \frac{1}{u(T)^2} = |u(T)| = \frac{4\pi^2\tau}{4\pi^2\tau^2 + 1}. \tag{3.84}$$

The ratio of functional determinants may be calculated by the Gelfand-Yaglom method [159] giving,

$$\frac{\det\left[\Sigma|_{\phi_{eq}}\right]}{\det\left[\frac{d^2}{du^2}\right]} = \frac{f(u|t=1)}{f^0(u|t=1)} = \frac{\tau \sinh\left(\frac{\sqrt{4\pi^2\tau^2+1}}{\tau}\right)}{\sqrt{4\pi^2\tau^2+1}}, \tag{3.85}$$

where $\Sigma|_{\phi_{eq}} f(u) = \lambda f(u)$ and $\frac{d^2}{du^2} f^0(u) = \lambda_i^0 f^0(u)$ with initial conditions $f^{(0)}(0) = 0$ and $\dot{f^{(0)}}(0) = 1$. For the winding trajectory, $\phi_{eq} = 2\pi t - \arctan(2\pi\tau)$, we find a closed-form expression for the probability density,

$$P(2\pi + \phi_e|\phi_e) \propto e^{-2\pi^2\tau} \left(\frac{4\pi^2\tau^2 \sinh\left(\frac{\sqrt{4\pi^2\tau^2+1}}{\tau}\right)}{(4\pi^2\tau^2+1)^{\frac{3}{2}}} \right)^{-\frac{1}{2}}. \tag{3.86}$$

For $\mathcal{P}^{n=0}(\phi_e|\phi_e)$, we employ the same method, however, there is no closed-form solution for the saddle point, we resort to a numerical approximation of each of the three contributing factors (equivalent to Eq. (3.83) evaluated around $\phi^{n=0}$) directly evaluating $e^{S[\phi^{n=0}]}$ and $|u(T)|$ numerically while approximating the ratio of the two functional determinants using the smallest N eigenvalues,

$$\frac{\det\left[\Sigma|_{\phi^{n=0}}\right]}{\det\left[\frac{d^2}{du^2}\right]} \approx \frac{\prod_i^N \lambda_i}{\prod_i^N \lambda_i^0}. \tag{3.87}$$

Using these results, the ratio R is plotted in Fig. (3.9b), where R is compared to $\mathfrak{R}$ and to the value of R computed using numerical simulations. We find that the effective value of $\tau_c^{\text{eff}} \approx 0.045$ is in excellent agreement with the results from trajectory simulations, substantiating the validity of the Gaussian approximation. This shows that the Gaussian action is a valid approximation to capture the whole statistics of quantum self-closing trajectories, and this might be valuable in any realization in which identifying the most probable trajectories might not be feasible.

3.6 Disscussion

In this chapter, we have added to the growing body of research into measurement-induced topological transitions, discovering a range of extensions to the post-selected geometric phase transition including post-selecting for the most probable readouts $r(t)$ and relaxing assumptions regarding the systems state preparation. We also uncover a qualitatively new type of transition which manifests for closed geometric phases and is only accessible through the study of self-closing quantum trajectories. Looking ahead, there may be analogous closed geometric phase transitions present in higher dimensional systems. The Gaussian fluctuation technique we demonstrate for our single qubit system may prove advantageous in the study of related phenomena present at the single qubit level, such as geometric dephasing, or may be applied to the dynamics of higher dimensional systems whenever the influence of multiple trajectories must be accounted for.

Chapter 4

Dual Qubit Entanglement Dynamics Under Measurement and Noise

In this chapter we study the effect of local unitary noise on the entanglement evolution of a two-qubit system subject to local monitoring and inter-qubit coupling. Recent studies have investigated the entanglement properties of monitored dual qubits systems [30, 160, 161]. We construct a CDJ path integral, as described in Section 2.3.2.2, for our system, and we extend the approach to account for the additional effect of unitary noise. Nascent features of the many-body competition between unitary evolution and monitoring in the entanglement dynamics can be identified even in two-qubit systems [162, 163, 164, 165, 166, 167] and the presence of a stochastic unitary component can have non-trivial effects in many-body MIPTs [168, 169, 170].

We use the stochastic action to identify the most probable quantum trajectories and their associated entanglement dynamics. We then use diagrammatic methods to obtain a closed-form approximation of the average entanglement dynamics, which exhibits an analytical dependence on the noise and measurement intensity. We find that both the optimal trajectory and diagrammatic expansion capture the

oscillations of entanglement at short times. A numerical investigation is required to probe the long-time steady-state entanglement, which reveals a non-monotonic relationship between concurrence and noise strength.

4.1 The Model: Two-Qubit Noisy Monitored Dynamics

Consider a two-qubit system, represented schematically in Fig. 4.1, subject to unitary noisy dynamics and continuous quantum monitoring. The unitary dynamics in the system are generated by the Hamiltonian H specified as

$$H = H_0 + H_n, \tag{4.1}$$

$$H_0 = i\hbar J(\sigma_{1,+}\sigma_{2,-} - \sigma_{1,-}\sigma_{2,+}), \tag{4.2}$$

$$H_n = 2\epsilon(t)\sigma_{1,y} + 2\lambda(t)\sigma_{2,y}, \tag{4.3}$$

where $\sigma_{i,j}$ is the j-th Pauli matrix acting on the i-th qubit, $\sigma_{i,\pm} = \sigma_{i,x} \pm i\sigma_{i,y}$. Fixing $\hbar = 1$, and $J = 1$ as an overall energy scale, ϵ and λ become randomly fluctuating dimensionless Gaussian noises, defined by $\langle\epsilon(t)\epsilon(t')\rangle = \langle\lambda(t)\lambda(t')\rangle = \Gamma\delta(t-t')$. The parameter Γ determines the noise strength, which we assume to be equal for both qubits.

The system is further subject to continuous Gaussian monitoring on each qubit [16, 17], which is described by the state update over an infinitesimal time δt as

$$|\psi_{t+\delta t}\rangle = \mathcal{N}^{-1} M_{1,r} \otimes M_{2,w} |\psi_t\rangle, \tag{4.4}$$

with the two Gaussian measurement operators (see Eq. (2.4)) acting on the first and second qubits, respectively, given by

$$M_r = \sqrt[4]{\frac{\delta t}{2\pi\tau}} \exp\left(-\frac{\delta t}{4\tau}(r - \sigma_{1,z})^2\right), \tag{4.5}$$

$$M_w = \sqrt[4]{\frac{\delta t}{2\pi\tau}} \exp\left(-\frac{\delta t}{4\tau}(w - \sigma_{2,z})^2\right), \tag{4.6}$$

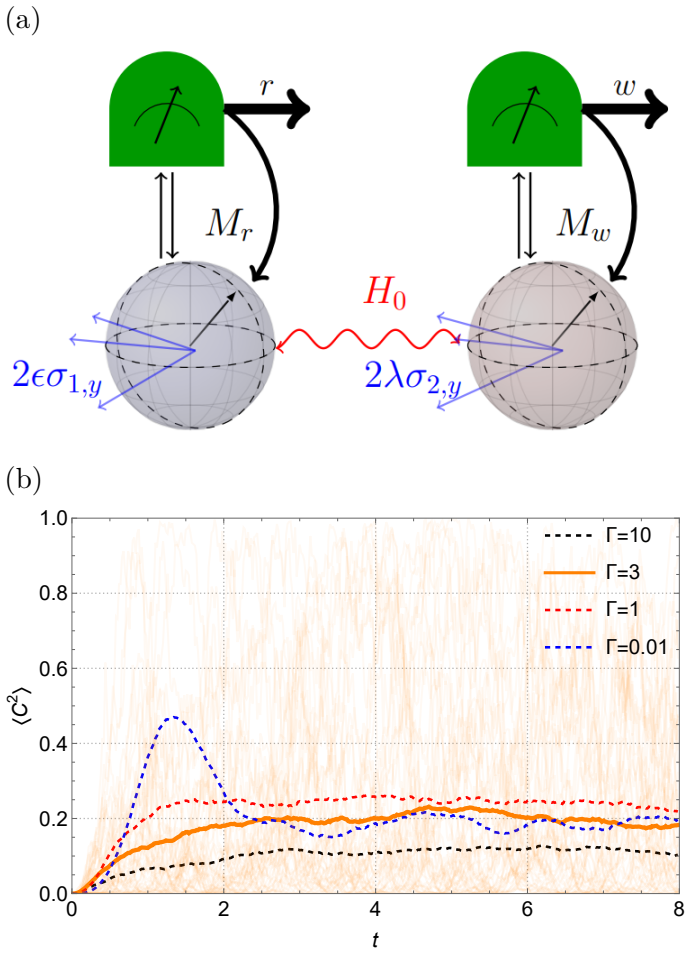

Figure 4.1: (a) Sketch of the two-qubit system we study. Two qubits (represented by single-qubit bock spheres) are coupled to quantum detectors (green) with output r, w and Kraus operator backaction M_r, M_w. The qubit unitary dynamics is generated by an inter-qubit interaction term (red wavy line) and local noisy Hamiltonian terms (blue arrows). (b) Stochastic trajectories of squared concurrence $\mathcal{C}^2$ (faded orange background) from numerical simulations with fixed measurement strength ($\tau = 0.2$) and noise strength ($\Gamma = 3$) and corresponding average (orange full line). The average $\mathcal{C}^2$ vs time is plotted for a range of noise strengths at fixed measurement strength ($\tau = 0.2$).

and the normalization $\mathcal{N}^{-1}$ set by $\langle\psi_{t+\delta t}|\psi_{t+\delta t}\rangle = 1$. Here, the measurement readouts r_k and w_k are drawn from the probability distributions

$$P(r_k) = \langle\psi_t|M_{r_k}^\dagger M_{r_k}|\psi_t\rangle, \tag{4.7}$$

$$P(w_k) = \langle\psi_t|M_{w_k}^\dagger M_{w_k}|\psi_t\rangle. \tag{4.8}$$

The measurement strength, τ, is the time required to separate the readout distributions for $|0\rangle$ and $|1\rangle$ by two standard deviations as explained in Section 2.1.2, where $|0\rangle$ and $|1\rangle$ correspond to a single qubit eigenstate of σ_z. In the limit $\delta t \to 0$, this formulation is equivalent to the stochastic Schrodinger equation (SSE) [16]

$$\begin{aligned} d|\psi\rangle = \Bigg[&- \frac{1}{\tau}(\sigma_{1,z}\sigma_{2,z} - \langle\sigma_{1,z}\sigma_{2,z}\rangle)^2 dt \\ &+ \sqrt{\frac{2}{\tau}}(\sigma_{1,z} - \langle\sigma_{1,z}\rangle)dW_1 + \sqrt{\frac{2}{\tau}}(\sigma_{1,z} - \langle\sigma_{1,z}\rangle)dW_2\Bigg]|\psi\rangle, \end{aligned} \tag{4.9}$$

with Gaussian noise increments dW_1 and dW_2 so that $\langle dW_1\rangle = \langle dW_2\rangle = 0$ and variance $dW_1^2 = dW_2^2 = dt$.

The evolution of the monitored system over a finite time t is obtained as a succession of N of these Kraus operators applied to the system so that $t = k\delta t$ with $\{k \in \mathbb{N} | k \leq N\}$. The limiting procedure, defined by $N \to \infty, \delta t \to 0$ while keeping $\delta t\ N = t$, defines a continuous monitoring process as per the stochastic evolution of the SSE in Eq. (4.9). A continuous stream of measurement readouts is obtained: so $\{r_k\} \to r$ and $\{w_k\} \to w$, become continuous random variables. We can conveniently group all the stochastic variables of the model in the vector $\mathbf{s} = (r, w, \epsilon, \lambda) \in \mathbb{R}^4$. We parameterised our system with the state parameter $\mathbf{q}_k = (a_k, c_k, \alpha_k, \gamma_k) \in \mathbb{R}^4$ so that,

$$|\psi_k\rangle = a_k|00\rangle + c_k|01\rangle + \alpha_k|10\rangle + \gamma_k|11\rangle. \tag{4.10}$$

After taking the continuous limit, these state parameters $\{\mathbf{q}_k\}$ also become continuous functions of time $\mathbf{q}(t)$.

We can formulate the time evolution from the combined quantum monitored and stochastic unitary evolution in a time-discretised formulation that is convenient for

both the action formulation and the numerical implementation. In the discrete limit, the Born rule gives the conditional probability of a pair of measurement readouts,

$$P(r_k, w_k|\psi_k, \lambda_k, \epsilon_k) = \langle\psi_k|E(r_k, w_k)^\dagger E(r_k, w_k)|\psi\rangle,$$
$$E(r_k, w_k) = e^{-iH\delta t}(M_{r_k} \otimes M_{w_k}). \tag{4.11}$$

Here the unitary transformation $e^{-iH\delta t}$ is considered to act across the interval $[t, t+\delta t]$ with noise variables drawn from the independent Gaussian distributions

$$P(\epsilon_k) = \sqrt{\frac{\delta t}{2\pi\Gamma}} e^{-\frac{\delta t}{2\Gamma}\epsilon_k^2}, \tag{4.12}$$

$$P(\lambda_k) = \sqrt{\frac{\delta t}{2\pi\Gamma}} e^{-\frac{\delta t}{2\Gamma}\lambda_k^2}, \tag{4.13}$$

across each time interval. The effect of the Hamiltonian Eq. (4.1) and continuous monitoring is combined in the state update given by,

$$|\psi_{k+1}\rangle = E(r_k)|\psi_k\rangle / \sqrt{P(r_k, w_k)}. \tag{4.14}$$

Taking this process back into the continuum limit produces dynamics that combine the effect of both the noisy Hamiltonian and the measurement (see Eq. (4.18)-(4.25))).

In the rest of the chapter, we will study the stochastic dynamics of the qubit entanglement within this model. The time evolution is such that if the state preparation satisfies, $\mathbf{q}(0) \in \mathbb{R}$, then $\mathbf{q}(t) \in \mathbb{R}$ at all subsequent times. For the sake of simplicity, we study qubit dynamics with the initially unentangled preparation $|\psi(0)\rangle = (\frac{1}{2}, \frac{1}{2}, \frac{1}{2}, \frac{1}{2})$. We do not expect the qualitative features of our analysis to be affected by this choice.

4.2 Optimal entanglement

We employ the concurrence, $\mathcal{C}$, as an entanglement monotone to quantify the entanglement in the system. For the 2-qubit state parameterised in Eq. (4.10), the concurrence is given by,

$$\mathcal{C} = 2|a\gamma - \alpha c|. \tag{4.15}$$

The deterministic component of the Hamiltonian, H_0, can generate entanglement between the two qubits. If the system is initialised in a separable state, H_0 drives oscillations of entanglement with a period of $t = \pi$. The local random Hamiltonians generically scramble these oscillations, leading to a stochastic evolution with a well-defined steady-state distribution of states and, hence, entanglement. The local monitoring, a stochastic process, also drives the system towards a well-defined steady-state entanglement distribution. However, the entanglement dynamics are controlled by the competition between the measurements, which reduce the entanglement, and the unitary dynamics, which typically establish it.

The stochastic entanglement evolution is reported in Fig. 4.1, showing the average squared concurrence as a function of time for a range of different noise strengths. Unless otherwise stated, results obtained from numerical simulations use the parameter $\delta t = 0.02$ and are based on a sample of size 400 trajectories for any given value of the protocol parameters. The average entanglement generically displays oscillations at short times before reaching a stated state value, which depends on the noise and measurement strength.

4.2.1 Chantasri-Dressel-Jordan Path Integral with unitary noise

We construct a path integral formulation of the probability distribution over quantum trajectories up to time T, $\mathcal{P}(\mathbf{q}(T))$ via the CDJ path integral (Section 2.3.2.2) to identify the optimal entanglement dynamics. The CDJ path integral is again constructed by noting that the full probability distribution for the measurement process can be expressed as a product of sequential conditional probabilities (cf. (2.74)) so

$$\mathcal{P}(\mathbf{q}(T), \mathbf{s}(T)|\mathbf{q}_i) = \mathcal{F}(t_0, t_N)\times \lim_{\delta t\to 0, N\to\infty} \prod_{k=0}^{N-1} P(\mathbf{q}_{k+1}|\mathbf{q}_k, \mathbf{s}_k) P(\mathbf{s}_k|\mathbf{q}_k), \tag{4.16}$$

where $\mathcal{F}(t_0, t_N) = \delta^3(\mathbf{q}(N) - \mathbf{q}_f)\delta^3(\mathbf{q}(0) - \mathbf{q}_i)$ sets the initial and final states to be $\mathbf{q}_i$ and $\mathbf{q}_f$.

The path integral (4.16) therefore requires two critical pieces of information: the infinitesimal state update $P(\mathbf{q}_{k+1}|\mathbf{q}_k, \mathbf{s}_k)$ and the conditional measurement readout probability distribution $P(\mathbf{s}_k|\mathbf{q}_k)$. The state updating term in Eq. (4.16) is deterministic, so it can be expressed as a delta function,

$$\begin{aligned} P(\mathbf{q}_{k+1}|\mathbf{q}_k, \mathbf{s}_k) &= \delta^d(\mathbf{q}_{k+1}|\mathbf{q}_k, \mathbf{s}(t)) \\ &= \left(\frac{1}{2\pi i}\right)^d \int_{-i\infty}^{i\infty} d^d\mathbf{p} e^{-\mathbf{p}_p\cdot(\mathbf{q}_k)}. \end{aligned} \tag{4.17}$$

This step introduces conjugate momenta [1] $\mathbf{p}_k = (p_a, p_c, p_\alpha, p_\gamma)$. Expanding both sides of Eq. (4.14) up to the first order in δt, we obtain, in the continuum limit, the stochastic differential equations for the evolution of the state parameters,

$$\dot{a} = A - c\lambda - \alpha\epsilon, \tag{4.18}$$

$$\dot{c} = C + \alpha + a\lambda - \gamma\epsilon, \tag{4.19}$$

$$\dot{\alpha} = D - c + a\epsilon - \gamma\lambda, \tag{4.20}$$

$$\dot{\gamma} = Y + c\epsilon + \alpha\lambda, \tag{4.21}$$

where

$$A = \frac{aw}{\tau}(c^2 + \gamma^2) + \frac{ar}{\tau}(\alpha^2 + \gamma^2), \tag{4.22}$$

$$C = \frac{cw}{\tau}(c^2 + \gamma^2 - 1) + \frac{cr}{\tau}(\alpha^2 + \gamma^2), \tag{4.23}$$

$$D = \frac{\alpha w}{\tau}(c^2 + \gamma^2) + \frac{r\alpha}{\tau}(\alpha^2 + \gamma^2 - 1), \tag{4.24}$$

$$Y = \frac{\gamma w}{\tau}(c^2 + \gamma^2 - 1) + \frac{r\gamma}{\tau}(\alpha^2 + \gamma^2 - 1). \tag{4.25}$$

Eq. (4.22-4.25) contain the effect of the measurement on the state dynamics. In the absence of these terms, Eq. (4.18-4.21), describe the effect of any unitary noise

[1] Similar to the discussion of the CDJ action in chapter 3.2.1, the integrals in Eq. (4.17) are taken over the imaginary axis but the conjugate momentum variables are treated as real since this reproduces the Lagrange multiplier optimization of $\lim \delta to \to 0 \prod_{k=0}^{N-1} P(\mathbf{s}_k|\mathbf{q}_k)$.

$\lambda(t), \epsilon(t)$ on the system dynamics. We observe the noise free ($\lambda = 0, \epsilon = 0$) and measurement-free oscillations[2] ($r = 0, w = 0$) given by $\dot{c} = \alpha$, $\dot{\alpha} = -c$, are contained within Eq. (4.18-4.21) as expected.

The probability $P(\mathbf{s}_k|\mathbf{q}_k)$ may be expressed as the product $P(\epsilon_k)P(\lambda_k)P(r_k, w_k|\mathbf{q}_k)$ and the factor $P(\epsilon_k)P(\lambda_k)$ is defined in Eq. (4.12). Expanding Eq. (4.11) to leading (first) order in time, we find that the state-dependent conditional probability density is,

$$P(r_k, w_k|\mathbf{q}_k) = \frac{\delta t}{2\pi\tau} e^{-\frac{\delta t}{2\tau}(r_k^2 + w_k^2 - 2w_k\bar{w}_k - 2r_k\bar{r}_k + 2)}, \tag{4.26}$$

where the mean readouts of the detectors are $\bar{w}_k = (2c_k^2 + 2\gamma_k^2 - 1)$, $\bar{r}_k = (2\alpha_k^2 + 2\gamma_k^2 - 1)$. Following the usual procedure for constructing path integrals set out in Section 2.3.2.2, extraneous factors of δt are absorbed into the functional measure, we express $\mathcal{P}$ in terms of an action $\mathcal{S}[\mathbf{q}, \mathbf{p}, \mathbf{s}]$,

$$\mathcal{P}(\mathbf{q}(T), \mathbf{s}(T)|\mathbf{q}_i) \propto \int D\mathbf{q} D\mathbf{p} D\mathbf{s} e^{-S[\mathbf{q},\mathbf{p},\mathbf{s}]}. \tag{4.27}$$

The functional S, acting on the whole set of quantum trajectories is given by

$$S[\mathbf{q}, \mathbf{p}, \mathbf{s}] = \int_0^T \Big(- \mathbf{p} \cdot \dot{\mathbf{q}} + \mathcal{H} \Big) dt. \tag{4.28}$$

Here $\mathcal{H}$ is expressed as

$$\begin{aligned} \mathcal{H} &= p_a A + p_c C + p_\alpha D + p_\gamma Y - \frac{\lambda^2 + \epsilon^2}{2\Gamma} \\ &+ \frac{1}{2\tau}\left(r^2 + w^2 - 2r\bar{r} - 2w\bar{w} + 2 \right), \end{aligned} \tag{4.29}$$

and is referred to as stochastic Hamiltonian [28, 29, 30, 31], in analogy with the Hamiltonian formulation of a classic system. From this formulation, we see that the conjugate momenta act as Legendre multipliers, enforcing constraints on the rate of change of the state parameters. We will utilise this action formulation to investigate the optimal entanglement growth in the system.

[2]Demanding r and w identically vanish forces the measurement operators to become identically unity - hence they induce no backaction on the state.

4.2.2 Optimal Squared Concurrence

Extremising the CDJ stochastic action (Eq. (4.28)) via Hamilton's equation's $-\partial_{\mathbf{q}}\mathcal{H} = \dot{\mathbf{p}}, \partial_{\mathbf{p}}\mathcal{H} = \dot{\mathbf{q}}, \partial_{\mathbf{r}}\mathcal{H} = 0$ leads to equations of motion that specify quantum trajectories that are extremal points of the action. Solutions of Eq. (4.18) combined with Eq. (4.30 - 4.37) therefore constitute either most probable, least probable or saddle point trajectories for any given boundary conditions. The nature of any given solution is most easily determined by evaluating the action and comparing the solution with a nearby quantum trajectory. So for any accessible initial and final boundary conditions, we can use these equations (Eqs. 4.28, 4.18 and 4.30-4.37) to determine the most likely quantum trajectory.

The extremization of Eq. (4.28) is carried out explicitly, resulting in

$$\lambda = -\Gamma(-ap_c + cp_a + p_\alpha\gamma - p_\gamma\alpha) \tag{4.30}$$

$$\epsilon = \Gamma(ap_\alpha + cp_\gamma - p_a\alpha - p_c\gamma) \tag{4.31}$$

$$\begin{aligned} r = {} & ap_a\alpha^2 + ap_a\gamma^2 + cp_c\alpha^2 + cp_c\gamma^2 + p_\alpha\alpha\gamma^2 + p_\alpha\alpha^3 \\ & - p_\alpha\alpha + p_\gamma\alpha^2\gamma + p_\gamma\gamma^3 - p_\gamma\gamma - 2\alpha^2 - 2\gamma^2 + 1, \end{aligned} \tag{4.32}$$

$$\begin{aligned} w = {} & ac^2p_a + ap_a\gamma^2 + c^2p_\alpha\alpha + c^2p_\gamma\gamma + cp_c\gamma^2 + c^3p_c \\ & - cp_c - 2c^2 + p_\alpha\alpha\gamma^2 + p_\gamma\gamma^3 - p_\gamma\gamma - 2\gamma^2 + 1. \end{aligned} \tag{4.33}$$

Eqs. (4.30-4.33) express each stochastic variable in terms of the state parameters and conjugate momentum. These, in turn, are determined by the evolution of the system state parameters obtained earlier (Eq. (4.18)), along with four further expressions

for the evolution of the conjugate momentum variables, given by

$$\dot{p_a} = -\frac{1}{\tau}\Big(c^2 p_a w + p_a r\alpha^2 + p_a r\gamma^2 + p_a \gamma^2 w + \tau p_\alpha \epsilon + \tau p_c \lambda\Big) \tag{4.34}$$

$$\dot{p_c} = \frac{1}{\tau}\Bigg(- 2acp_a w - 2cp_\alpha \alpha w - 2cp_\gamma \gamma w - 3c^2 p_c w + 4cw + \tau p_\alpha + \tau p_a \lambda$$
$$- p_c r\alpha^2 - p_c r\gamma^2 - p_c \gamma^2 w + p_c w - \tau p_\gamma \epsilon\Bigg) \tag{4.35}$$

$$\dot{p_\alpha} = \frac{1}{\tau}\Bigg(- 2ap_a r\alpha + c^2(-p_\alpha)w - 2cp_c r\alpha - \tau p_c - 3p_\alpha r\alpha^2 - p_\alpha r\gamma^2 + p_\alpha r$$
$$- p_\alpha \gamma^2 w + \tau p_a \epsilon - 2p_\gamma r\alpha\gamma - \tau p_\gamma \lambda + 4r\alpha\Bigg) \tag{4.36}$$

$$\dot{p_\gamma} = \frac{1}{\tau}\Bigg(- 2ap_a r\gamma - 2ap_a \gamma w - 2cp_c r\gamma - 2cp_c \gamma w + c^2(-p_\gamma)w - 2p_\alpha r\alpha\gamma + \tau p_\alpha \lambda$$
$$- 2p_\alpha \alpha\gamma w - p_\gamma r\alpha^2 - 3p_\gamma r\gamma^2 + p_\gamma r - 3p_\gamma \gamma^2 w + p_\gamma w + \tau p_c \epsilon + 4r\gamma + 4\gamma w\Bigg). \tag{4.37}$$

Eqs. (4.30-4.33) can be substituted into the remaining equations of motion, resulting in an 8-dimensional system of ODEs in phase space. The state initialisation $a(0) = c(0) = \alpha(0) = \gamma(0) = \frac{1}{2}$, may then be combined with a final time boundary condition (or equivalently, with a choice of initial momentum) to generate extremal quantum trajectories. While the exact solutions obtained from Eq. (4.30-4.37) depends on the initial state, we expect that the ensuing set of optimal trajectories will exhibit qualitatively and quantitatively similar behaviour in terms of their dynamic entanglement properties for generic non-entangled initial states.

To determine the most likely quantum trajectory for a given initial and final concurrence, we evaluate the probability of each candidate's optimal quantum trajectory over the equivalence class of final state conditions with equal entanglement monotone value (see Eq. (4.15)). In other words, we find candidate optimal trajectories that share an equal final concurrence, then search this set for the most probable overall trajectory. Examples of these optimal entanglement dynamics are provided in Fig. 4.2, where they are compared to the associated post-selected

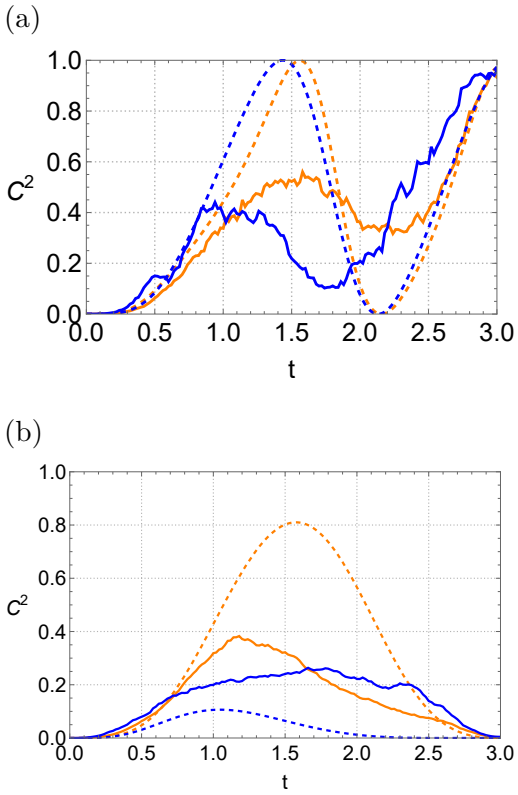

Figure 4.2: Squared concurrence vs time for post-selected trajectories to maximum entanglement [panel (a)] and minimum entanglement [panel (b)] at $t = 3$. Solid lines are for the average squared concurrence, and dashed lines are for the most probable trajectory with the specified boundary conditions for different noise strengths of $\Gamma = 0.01$ (Orange) and $\Gamma = 0.5$ (Blue). In all cases, $\tau = 0.2$. Across a range of noise strengths, an optimal concurrence track with a maximum concurrence at $t = \pi$ approximately reproduces the system's deterministic oscillations. The optimal path with a final minimum entanglement is sensitive to changes in Γ.

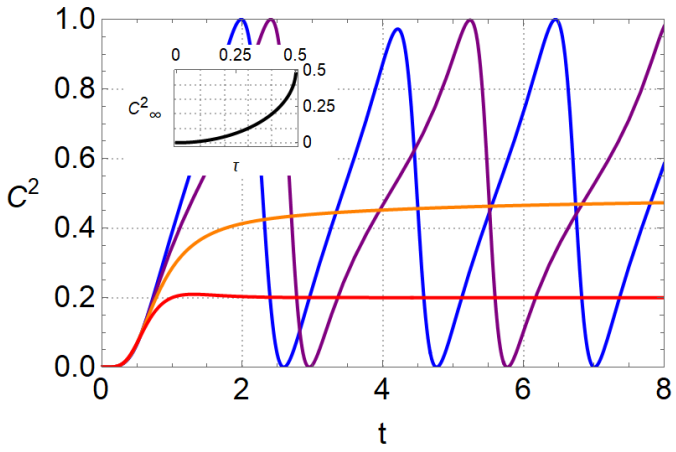

Figure 4.3: Global optimum squared concurrence vs time for $\tau = 0.6$ (Purple), $\tau = 0.7$ (Blue), $\tau = 0.4$ (Orange) and $\tau = 0.3$ (Red). For $\tau > 0.5$, $\mathcal{C}^2$ along the global optimal trajectory oscillates, while for $\tau < 0.5$, it saturates to fixed values after a few units of time. Inset: Plot of the steady-state global optimum concurrence against measurement strength for $\tau < 0.5$.

average concurrence. We observe that the optimal entanglement captures some general features of the post-selected averages, particularly the number of inflexion points reproduced. However, these optimal curves are poor estimates of the average entanglement growth and attenuation.

In addition to the most probable trajectories for given initial and final conditions, we may also identify the most probable concurrence globally (without any final boundary conditions). This is achieved by substituting in the values $\bar{w} = 1 - 2c^2 - 2\gamma^2, \bar{r} = 1 - 2\alpha^2 - 2\gamma^2, \lambda = 0, \epsilon = 0$ (the mean values of these stochastic variables at each time step, as can be identified from Eq. (4.26) into Eqs. (4.18)-(4.21). The result is a set of ODEs that generated the global optimum trajectory. We see that the resulting equations of motion are then independent of Γ, hence the global optimum concurrence is independent of the noise strength. This is expected given that the unitary noise is independent of the system's state; hence, the noise fluctuations play no role.

As shown in Fig. 4.3 the qualitative behaviour of the globally most probable

entanglement undergoes a transition at $\tau \approx 0.5$. Above $\tau \approx 0.5$, the globally optimum concurrence oscillates continuously as a function of time - dominated by the influence of the driving Hamiltonian. The concurrence saturates to a fixed value below $\tau \approx 0.5$. This phenomenology is illustrated in Fig. 4.3. It is a monotonically decreasing function of the measurement strength, as might be expected in the strong measurement regime since measurement attenuates the entanglement. We note that the average concurrence also achieves a steady state - however, this occurs across all ranges of τ and generally saturates at a value distinct from the corresponding optimum concurrence.

4.3 diagrammatic Approximation for the Average Squared Concurrence

Besides the optimal behaviour, further analytical insight into the stochastic entanglement dynamics can be obtained for weak coupling/short-time dynamics, for which diagrammatic methods can be applied considering a suitable reformulation of the stochastic action [29]. We follow the procedure described in [29, 10] to construct a second stochastic action, again using Eq. (4.16) as the starting point, which models the systems dynamics while enabling diagrammatic methods. We will use a diagrammatic weak coupling expansion to find a closed-form expression for the average squared concurrence as a function of time that shows excellent agreement with the results of simulations in combined weak measurement weak noise regimes.

4.3.1 Ito's Rule Formulation of the Stochastic Dynamics

As a first step, we transform the state update equations Eq. (4.18) into stochastic differential equations using Ito's rules, i.e. $\delta t^2 r^2 \rightarrow \delta t\tau, \delta t^2 w^2 \rightarrow \delta t\tau, \delta t^2 \epsilon^2 \rightarrow \Gamma\delta t, \delta t^2\lambda^2 \rightarrow \Gamma\delta t$. We apply these rules to the second-order expansion of the state update equation Eq. (4.14) to properly account for the noise fluctuations. The

measurement record functions are then approximated as their mean values plus some Gaussian noise, $r \to -\bar{r} + \sqrt{\tau}\theta, w \to -\bar{w} + \sqrt{\tau}\phi$. Here, θ and ϕ are new Gaussian noise variables with mean 0 and variance δt^{-1}. Additionally, we re-scale the earlier Gaussian noise variables with the transformation $\lambda \to \sqrt{\Gamma}\lambda, \epsilon \to \sqrt{\Gamma}\epsilon$ λ ϵ so they also have a variance of δt^{-1}. From this, we find the following SDEs governing the system state parameters

$$\dot{a} = -dt\left(\frac{a}{\tau}\tilde{A} + a\Gamma\right) + \frac{a\lambda}{\sqrt{\tau}}\left(\alpha^2+\gamma^2\right) + \frac{a\lambda}{\sqrt{\tau}}(c^2+\gamma^2) - \sqrt{\Gamma}c\theta - \sqrt{\Gamma}\alpha\phi, \tag{4.38}$$

$$\dot{c} = dt\left(\alpha - \Gamma c + \frac{c}{\tau}\tilde{C}\right) + \frac{c\lambda}{\sqrt{\tau}}(\gamma^2+c^2-1) + \frac{c\epsilon}{\sqrt{\tau}}(\alpha^2+\gamma^2) - \sqrt{\Gamma}\gamma\phi + \sqrt{\Gamma}a\theta, \tag{4.39}$$

$$\dot{\alpha} = dt\left(\frac{\alpha}{\tau}\tilde{D} - c - \Gamma\alpha\right) + \frac{\alpha\lambda}{\sqrt{\tau}}(\gamma^2+c^2) + \frac{\alpha\epsilon}{\sqrt{\tau}}(\gamma^2+\alpha^2-1) + \sqrt{\Gamma}a\phi - \sqrt{\Gamma}\gamma\theta, \tag{4.40}$$

$$\dot{\gamma} = dt\left(\frac{\gamma}{\tau}\tilde{Y} - \Gamma\gamma\right) + \frac{\lambda}{\sqrt{\tau}}(c^2\gamma+\gamma^3-\gamma) + \frac{\epsilon}{\sqrt{\tau}}(\alpha^2\gamma+\gamma^3-\gamma) + \sqrt{\Gamma}c\phi + \sqrt{\Gamma}\alpha\theta, \tag{4.41}$$

where

$$\begin{aligned}
\tilde{A} &= \left(c^2\gamma^2 + \frac{c^4}{2} + \alpha^2\gamma^2 + \frac{\alpha^4}{2} + \gamma^4\right), \\
\tilde{C} &= (-\alpha^2\gamma^2 - \frac{\alpha^4}{2} - c^2\gamma^2 + \gamma^2 - \gamma^4 - \frac{c^4}{2} + c^2 - \frac{1}{2}), \\
\tilde{D} &= (-c^2\gamma^2 - \frac{c^4}{2} - \alpha^2\gamma^2 + \gamma^2 - \gamma^4 - \frac{\alpha^4}{2} + \alpha^2 - \frac{1}{2}), \\
\tilde{Y} &= (-c^2\gamma^2 + c^2 - \frac{c^4}{2} - \alpha^2\gamma^2 + \alpha^2 - \frac{\alpha^4}{2} + \gamma^4 + 2\gamma^2 - 1).
\end{aligned}$$

We observe that in the limit where Γ approaches zero, Eqs. (4.38)-(4.41) recover the stochastic Schrödinger equation (Eq. (4.9)). These SDEs are utilized in the creation of a new path integral in the same manner as Eqs. (4.18)- (4.21); each state parameter acquires a corresponding conjugate momentum through the Fourier representation of a Dirac delta function (Eq. (4.17)) in Eq. (4.16). We reuse the notation $\mathbf{p} = (p_a, p_c, p_\alpha, p_\gamma)$ to index these new conjugate momenta.

Each new Gaussian random variable, in discrete time, has an accompanying state-independent probability distribution, $P(\theta) = \sqrt{\frac{\delta t}{2\pi}} e^{-\frac{\delta t}{2}\theta^2}$ and $P(\phi) = \sqrt{\frac{\delta t}{2\pi}} e^{-\frac{\delta t}{2}\phi^2}$. Along with the transformed distributions from Eq. (4.12), we multiply together these independent distributions to form the following probability density,

$$P(\theta, \phi, \lambda, \epsilon) = \frac{\delta t^2}{4\pi^2} e^{-\frac{\delta t}{2}(\theta^2+\phi^2+\epsilon^2+\lambda^2)} d\theta d\phi d\lambda d\epsilon. \tag{4.42}$$

This stochastic action component is considerably simplified compared to its equivalent in Eq. (4.26).

A second stochastic path integral may be constructed from this new model of the system [10, 29] substituting in time discretised versions of the Fourier-transformed Dirac delta distributions associated with Eq. (4.38) and the distribution of Eq. (4.42) into Eq. (4.16). Taking this into the continuum limit and then integrating out all four Gaussian noises from the resulting path integral produces a phase space path integral

$$\mathcal{P} \propto \int \mathcal{D}\mathbf{q}\mathcal{D}\mathbf{p} e^{\tilde{S}}. \tag{4.43}$$

The stochastic action $\tilde{S}$ is composed of three parts

$$\tilde{S} = \tilde{S}_f + \tilde{S}_i + \tilde{S}_b. \tag{4.44}$$

The free action, $\tilde{S}_f$, contains all bilinear terms of the action

$$\begin{aligned} \tilde{S}_f = \int & p_a \dot{a} + \Gamma a p_a + p_c \dot{c} + c p_\alpha + \Gamma c p_c + \frac{c p_c}{2\tau} - p_c \alpha \\ & + p_\alpha \dot{\alpha} + \Gamma p_\alpha \alpha + \frac{p_\alpha \alpha}{2\tau} + p_\gamma \dot{\gamma} + \Gamma p_\gamma \gamma + \frac{p_\gamma \gamma}{\tau} dt. \end{aligned} \tag{4.45}$$

The interaction action, $\tilde{S}_i$, contains all remaining terms

$$\tilde{S}_i = \sum_\rho \mathcal{F}_\rho a^{n_a} c^{n_c} \alpha^{n_\alpha} \gamma^{n_\gamma} p_a^{m_a} p_c^{m_c} p_\alpha^{m_\alpha} p_\gamma^{m_\gamma}, \tag{4.46}$$

where the sum is over all the strings $\rho = \{n_a, n_c, n_\alpha, n_\gamma, m_a, m_c, m_\alpha, m_\gamma\}$ such that $\sum_j n_j \leq 6$ and the coefficients of each terms are explicitly given in Section 4.3.1.1 in Eq. (4.48). The final term in the action expresses the boundary conditions

$$\tilde{S}_b = \frac{1}{2}\delta(t) p_a + \frac{1}{2}\delta(t) p_c + \frac{1}{2}\delta(t) p_\alpha + \frac{1}{2}\delta(t) p_\gamma. \tag{4.47}$$

We used the state normalization condition, $a^2 + c^2 + \alpha^2 + \gamma^2 = 1$, to simplify the result. One advantage of having the action in this form is that the free part of the action in Eq. (4.45) is exactly solvable, and it becomes possible to apply various diagrammatic methods. In the following section, we use this path integral to find a closed-form approximation for concurrence as a function of time.

4.3.1.1 Interaction Action

We report the full expression for the interaction action $\tilde{S}_i$ in Eq. (4.44) used in the diagrammatic approximation of $\langle \mathcal{C}^2 \rangle$. The expression consists of 127 distinct terms, each associated with an interaction vertex.

$$\tilde{S}_i = \frac{1}{\tau}\int dt \Bigg[\frac{p_c^2c^6}{2} + ap_ap_cc^5 + \frac{p_cc^5}{2} + p_cp_\alpha\alpha c^5 + p_cp_\gamma\gamma c^5 + \frac{a^2p_a^2c^4}{2} + \frac{p_\alpha^2\alpha^2c^4}{2} \tag{4.48}$$

$$+ p_c^2\gamma^2c^4 + \frac{p_\gamma^2\gamma^2c^4}{2} + \frac{ap_ac^4}{2} + ap_ap_\alpha\alpha c^4 + \frac{p_\alpha\alpha c^4}{2} + ap_ap_\gamma\gamma c^4 + \frac{p_\gamma\gamma c^4}{2} + p_\alpha p_\gamma\alpha\gamma c^4$$

$$- p_c^2c^4 + 2p_cp_\gamma\gamma^3c^3 + 2ap_ap_c\gamma^2c^3 + p_c\gamma^2c^3 + 2p_cp_\alpha\alpha\gamma^2c^3 - ap_ap_cc^3 - p_cc^3$$

$$- p_cp_\alpha\alpha c^3 - 2p_cp_\gamma\gamma c^3 + \frac{p_c^2\alpha^4c^2}{2} + p_c^2\gamma^4c^2 + p_\gamma^2\gamma^4c^2 + 2ap_ap_\gamma\gamma^3c^2 + p_\gamma\gamma^3c^2 + 2p_\alpha p_\gamma\alpha\gamma^3c^2$$

$$+ \frac{1}{2}\Gamma p_a^2c^2 + \frac{p_c^2c^2}{2} + \frac{1}{2}\Gamma p_\gamma^2c^2 + a^2p_a^2\gamma^2c^2 + p_c^2\alpha^2\gamma^2c^2 + p_\alpha^2\alpha^2\gamma^2c^2 + ap_a\gamma^2c^2 + 2ap_ap_\alpha\alpha\gamma^2c^2$$

$$+ p_\alpha\alpha\gamma^2c^2 - p_c^2\gamma^2c^2 - p_\gamma^2\gamma^2c^2 - ap_ap_\gamma\gamma c^2 - p_\gamma\gamma c^2 - p_\alpha p_\gamma\alpha\gamma c^2 + p_cp_\alpha\alpha^5c$$

$$+ 2p_cp_\gamma\gamma^5c + ap_ap_c\alpha^4c + \frac{p_c\alpha^4c}{2} + 2ap_ap_c\gamma^4c + p_c\gamma^4c + 2p_cp_\alpha\alpha\gamma^4c + 2p_cp_\gamma\alpha^2\gamma^3c$$

$$+ 2p_cp_\alpha\alpha^3\gamma^2c + 2ap_ap_c\alpha^2\gamma^2c + p_c\alpha^2\gamma^2c - \Gamma ap_ap_cc + \Gamma ap_\alpha p_\gamma c - 2\Gamma p_ap_\gamma\alpha c + p_cp_\gamma\alpha^4\gamma c$$

$$+ \Gamma p_ap_\alpha\gamma c - \Gamma p_cp_\gamma\gamma c + p_cp_\gamma\gamma c - p_cp_\alpha\alpha^3c - 3p_cp_\gamma\gamma^3c - ap_ap_c\gamma^2c - p_c\gamma^2c$$

$$- 2p_cp_\alpha\alpha\gamma^2c - p_cp_\gamma\alpha^2\gamma c + \frac{p_\alpha^2\alpha^6}{2} + p_\gamma^2\gamma^6 + ap_ap_\alpha\alpha^5 + \frac{p_\alpha\alpha^5}{2} + 2ap_ap_\gamma\gamma^5 + p_\gamma\gamma^5$$

$$+ 2p_\alpha p_\gamma\alpha\gamma^5 + \frac{a^2p_a^2\alpha^4}{2} + \frac{ap_a\alpha^4}{2} + a^2p_a^2\gamma^4 + p_\alpha^2\alpha^2\gamma^4 + p_\gamma^2\alpha^2\gamma^4 + ap_a\gamma^4 + 2ap_ap_\alpha\alpha\gamma^4$$

$$+ p_\alpha\alpha\gamma^4 + 2p_\alpha p_\gamma\alpha^3\gamma^3 + 2ap_ap_\gamma\alpha^2\gamma^3 + p_\gamma\alpha^2\gamma^3 + \frac{1}{2}\Gamma a^2p_c^2 + \frac{1}{2}\Gamma a^2p_\alpha^2 + \frac{1}{2}\Gamma p_a^2\alpha^2 + \frac{p_\alpha^2\alpha^2}{2}$$

$$+ \frac{1}{2}\Gamma p_\gamma^2\alpha^2 + p_\alpha^2\alpha^4\gamma^2 + \frac{p_\gamma^2\alpha^4\gamma^2}{2} + 2ap_ap_\alpha\alpha^3\gamma^2 + p_\alpha\alpha^3\gamma^2 + \frac{1}{2}\Gamma p_c^2\gamma^2 + \frac{1}{2}\Gamma p_\alpha^2\gamma^2 + p_\gamma^2\gamma^2$$

$$+ a^2p_a^2\alpha^2\gamma^2 + ap_a\alpha^2\gamma^2 - \Gamma ap_ap_\alpha\alpha + \Gamma ap_cp_\gamma\alpha + p_\alpha p_\gamma\alpha^5\gamma + ap_ap_\gamma\alpha^4\gamma + \frac{p_\gamma\alpha^4\gamma}{2} - 2\Gamma ap_cp_\alpha\gamma$$

$$+ \Gamma p_ap_c\alpha\gamma - \Gamma p_\alpha p_\gamma\alpha\gamma + p_\alpha p_\gamma\alpha\gamma - p_\alpha^2\alpha^4 - 2p_\gamma^2\gamma^4 - ap_ap_\alpha\alpha^3 - p_\alpha\alpha^3 - 2ap_ap_\gamma\gamma^3 - 2p_\gamma\gamma^3$$

$$- 3p_\alpha p_\gamma\alpha\gamma^3 - p_\alpha^2\alpha^2\gamma^2 - p_\gamma^2\alpha^2\gamma^2 - ap_ap_\alpha\alpha\gamma^2 - p_\alpha\alpha\gamma^2 - 2p_\alpha p_\gamma\alpha^3\gamma - ap_ap_\gamma\alpha^2\gamma - p_\gamma\alpha^2\gamma \Bigg] \tag{4.49}$$

4.3.2 Diagrammatic Approximation for the Squared Concurrence

We aim to compute the moments of the squared concurrence $\langle \mathcal{C}^2 \rangle = 4(\langle a^2\gamma^2 \rangle - 2\langle ac\alpha\gamma \rangle + \langle \alpha^2c^2 \rangle)$. To this end, various approximation techniques [10, 9] may be

applied to Eq. (4.43). We are interested specifically in a diagrammatic method for a weak coupling approximation [10] that gives a closed-form expression for the squared concurrence. A weak coupling approximation involves expanding around the free action $\tilde{S}_f$, for which we have a closed-form expression for the Green's function G associated with the free propagator,

$$G(t,t') = \Theta(\Delta t) e^{\frac{-(2\Gamma\tau+1)\Delta t}{2\tau}} P, \tag{4.50}$$

where $\Theta(t)$ is the Heaviside function (with $\Theta(0) = 0$ due to Ito's condition and $\lim_{\Delta t\to 0^+} \Theta(\Delta t) = 1$) and P is a matrix of differential operators which act on a vector of four-dimensional real-valued functions $\boldsymbol{q}(t) = (q_1, q_2, q_3, q_4) = (a, c, \alpha, \gamma)$,

$$P = \begin{pmatrix} e^{-\Delta t(2\Gamma+\frac{1}{2\tau})} & 0 & 0 & 0 \\ 0 & \cos(\Delta t) & \sin(\Delta t) & 0 \\ 0 & -\sin(\Delta t) & \cos(\Delta t) & 0 \\ 0 & 0 & 0 & e^{-\Delta t(2\Gamma+\frac{3}{2\tau})} \end{pmatrix}, \tag{4.51}$$

with $\Delta t = t - t'$. We may consider the (i,l)-th component of the matrix corresponding to pre-multiplication by the p_l component ($\boldsymbol{p}(t) = (p_1, p_2, p_3, p_4) = (p_a, p_c, p_\alpha, p_\gamma)$), of momenta and post multiplication with the q_j state parameter. This free propagator will be the basis to evaluate Feynman diagrams for averages of state-dependent quantities and expansion of the interaction action $\tilde{S}_i$.

We associate a Feynmann diagram with the average of a monomial in the state and momentum variables. Averages are performed over the free action and are computed via the Green's function in Eq. (4.50). Following the general construction in [10], each term in $\tilde{S}_i$ is associated with a single vertex in a Feynman diagram characterised by the edges it connects with. Different edges, labelled by different lines (full/dashed/dotted/wiggly), correspond to different state parameters as per the correspondence in Table 4.1. To fully specify the diagram, we further associate ingoing arrows with state parameters and outgoing arrows with conjugate momenta.

State Variable	Momentum	Edge
a	p_a	
c	p_c	
α	p_α	
γ	p_γ	

Table 4.1: Association between edge type and state variable type for the construction of Feynmann diagrams.

For example, the vertex associated with $\alpha\gamma p_a p_c$, which corresponds to the factor $\Gamma \int_0^T p_a p_c \alpha\gamma dt$ in Eq. (4.48), is given by the diagram in Fig. 4.5(a). Similarly, the vertex associated with $p_c c\gamma^2$ ($\int_0^T p_c c\gamma^2 dt$ in Eq. (4.48)) is shown in Fig. 4.5(b). The vertex in Fig. 4.5(a) consists of two state parameters and two conjugate momenta and the corresponding diagram features two ongoing and two outgoing edges; the vertex in Fig. 4.5(b) instead includes three state parameters but only one momentum and its diagram accordingly requires three ingoing and one outgoing edge. For vertices that include no state parameters, such as p_a, which corresponds to the term $\frac{1}{2}\int_0^T p_a \delta(t) dt$ in $\tilde{S}_b$, the diagrams are simple, consisting of a single outgoing edge. As an example, the diagram for $\frac{1}{2}\int_0^T p_a \delta(t) dt$ is given in Fig. 4.5(c).

When computing averages of state-dependent quantities perturbatively, the monomials to average will be included as edges of the Feynman diagrams. Specifically, the squared concurrence of interest here, $\langle \mathcal{C}^2 \rangle = 4(\langle a^2\gamma^2 \rangle - 2\langle ac\alpha\gamma \rangle + \langle \alpha^2 c^2 \rangle)$, consists of three terms, each with four state parameters. Each of the three terms may be approximated separately. For example, for the term $\langle ac\alpha\gamma \rangle$, one of Feynman's diagrams contributing to the average to order five interaction vertices (IV) is presented in Fig. 4.5(d). The state parameters are associated with vertices (grey-coloured vertices in Fig. 4.4), placed at the final time position in our Feynman diagrams. The remaining vertices (black) are from the expansion of the interaction action.

Time-directed (right to left) Feynman diagrams may now be constructed by

selecting all combinations of interaction vertices that can be connected to the appropriate final time vertices. All diagrams contributing non-vanishingly to this approximation must connect with final vertices determined by the state parameters we are averaging, with no unconnected edges left over (see Fig. 4.4). Note that since the quadratic action mixes terms with different state parameters and conjugates momenta, the propagators can connect different types of edges.

We sum up all such Feynman diagrams and then convert them into equations according to the following rules [10]

1a. For every interaction vertex in the diagram, a prefactor of $-\frac{1}{n!}$ is added where n is the count of conjugate momenta in that vertex.

1b. If the same vertex occurs k times in a diagram, then there is an additional factor of $\frac{1}{k!}$.

1c. If there are m distinct ways of connecting edges to vertices that yield the same diagram there is a final prefactor factor of m. This is the combinatorial factor determined by the number of unique Wick contractions leading to the same diagram.

2. Each edge between time t_j and t_k is replaced with the q_i-th p_l-th component of the free propagator $G_{p_l,q_i}(t_j, t_k)$.

3. Integrate from 0 to ∞ over the time index associated with each interaction vertex.

We organise our approximation by the number of interaction vertices used. We include terms up to five IVs to obtain a closed form expression for $\langle \mathcal{C}^2 \rangle$ in Eq. (4.52). Note that three or fewer IV diagrams leave unconnected edges, and using only four IVs is equivalent to only solving the linear component of Eq. (4.38). This linear approximation is given by the first term in Eq. (4.52), which corresponds to diagrams with four vertices, while subsequent terms are built from five IV.

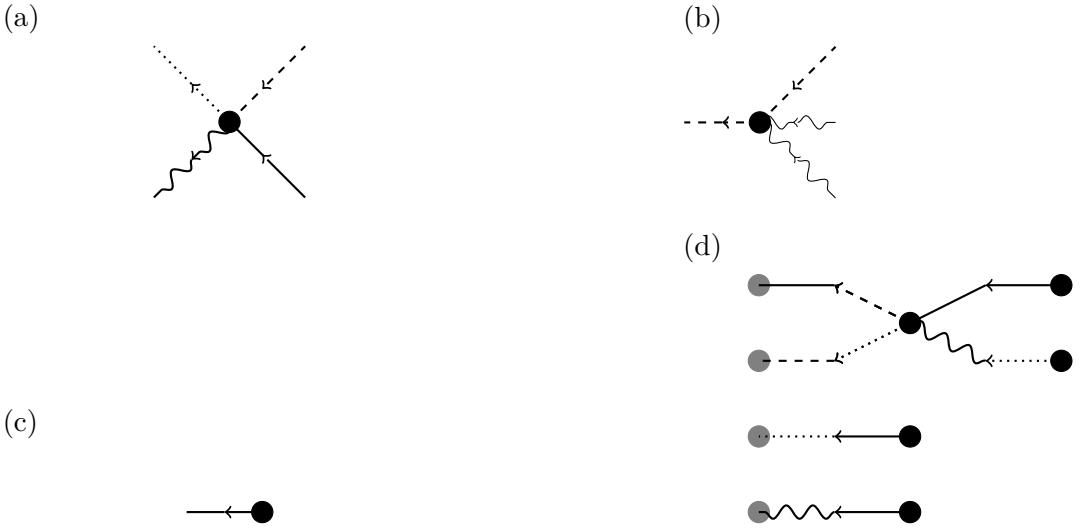

Figure 4.4: (a)-(c) Examples of interaction vertices associated with terms in Eq. (4.48). (d) An example of a Feynman diagram which contributes to the calculation of $\langle ac\alpha\gamma\rangle$.

$$\langle C^2\rangle \approx \sin^4(t)e^{-2t(2\Gamma+\frac{1}{\tau})} + \frac{1}{8\tau}e^{-2t\left(2\Gamma+\frac{1}{\tau}\right)}\left(\frac{64\Gamma\tau^4\sinh\left(\frac{t}{\tau}\right)}{4\tau^2+1} - \frac{32\Gamma\tau^3\sin(2t)}{4\tau^2+1}\right.$$
$$\left. - 4\Gamma\tau\sin(4t) + 2t(8\Gamma\tau-5)\cos(2t) + 9t + \sin(2t) - \sin(4t) + 3t\cos(4t)\right) \quad (4.52)$$

We plot Eq. (4.52) for a selection of measurement and noise strength choices in Fig. 4.5. The diagrammatic approximation is valid for a combination of weak noise and measurement strength. Eq. (4.52) outperforms the linear approximation, which consists of only the first term in Eq. (4.52), (also plotted in Fig. 4.5): the latter captures the oscillations with the correct frequency at short times, but misses the correct values of amplitudes. Notably, it is evident from Fig. 4.5 that, after a period of oscillating behaviour, the system's average entanglement will eventually enter a steady state (cf. Fig. 4.7). We note that our weak coupling approximation at five IVs fails to capture this regime across all values of the measurement and noise strength; in fact, the long time limit of Eq. (4.52) corresponds to a vanishing entanglement.

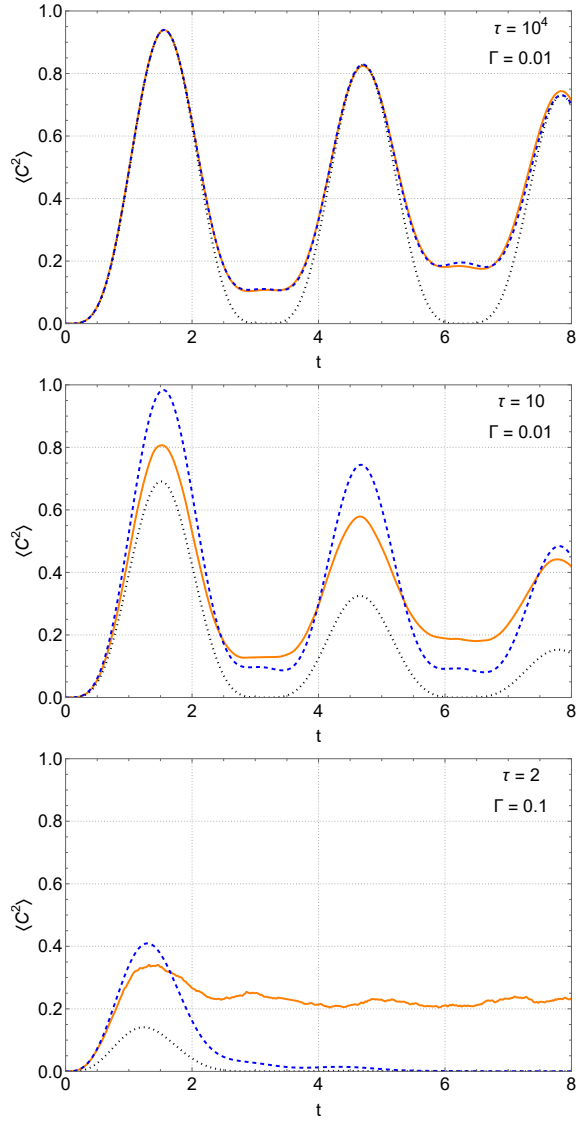

Figure 4.5: Average squared concurrence against time. Numerical simulations (solid orange lines) are compared with the linear approximation (dotted black) and the weak coupling approximation —Eq. (4.52)— (dashed blue) for different measurement and noise strengths. The weak coupling approximation outperforms the linear approximation and shows excellent agreement with numerical simulations in the weak measurement regime

4.4 Steady-State Entanglement

While the diagrammatic approximation developed above can only capture the entanglement dynamics at short times and predicts vanishing steady-state concurrence, the system is generically expected to reach an average steady-state entanglement from the competition of the unitary entangling terms and measurement disentangling effects. This competition is the source of measurement-induced entanglement transitions in many-body systems, and a steady-state interplay is already present at the level of 2 qubits.

4.4.1 A Simplified SDE Model for Steady-State Concurrence

Having obtained a system of SDEs governing the system's dynamics with Eq. (4.38), we seek simplifications that may be made to the model to obtain an expression for the entanglement. In particular, we seek an expression that saturates at some non-vanishing steady state. One method to achieve this is to combine the SDEs of Eq. (4.38) such that the only independent state parameter is an entanglement monotone. So here we attempt to extract an ODE in terms of $\mathcal{C}$ from our system of SDEs.

We first observe that the evolution of the concurrence is subject to the identity,

$$2\mathcal{C}\dot{\mathcal{C}} = 8(a\gamma - c\alpha)[a\dot{\gamma} + \dot{a}\gamma - c\dot{\alpha} - \dot{c}\alpha]. \tag{4.53}$$

We further note that, $\frac{a\gamma - c\alpha}{|a\gamma - c\alpha|} = \frac{1}{\mathrm{sgn}(a\gamma - c\alpha)}$, converting the identity Eq. (4.53) into

$$\dot{\mathcal{C}} = \frac{2}{\mathrm{sgn}(a\gamma - c\alpha)}[a\dot{\gamma} + \dot{a}\gamma - c\dot{\alpha} - \dot{c}\alpha]. \tag{4.54}$$

We may then substitute the set of SDEs (Eq. (4.38)) into Eq. (4.54), discarding terms that have more than four state parameters multiplied together. This step is motivated by the observation that the normalisation of real numbers will cause the numerical value of these terms to be, on average, lower than the others. We

additionally apply the equation $\frac{a\gamma - c\alpha}{\text{sgn}(a\gamma - c\alpha)} = \frac{C}{2}$ to Eq. (4.54), resulting in,

$$\dot{\mathcal{C}} \approx -(2\Gamma + \frac{1}{\tau})\mathcal{C} + 2\left(\frac{c^2 - \alpha^2}{\text{sgn}(a\gamma - c\alpha)}\right) + \frac{c\alpha\lambda}{\sqrt{\tau}} - \frac{a\gamma\epsilon}{\sqrt{\tau}}. \tag{4.55}$$

We have not yet successfully excised the state variables from Eq. (4.55). Although we acknowledge the stochastic nature of the state parameters, and the interdependence between $\mathcal{C}$ and the system's state, we proceed by treating the expressions that depend on state parameters as some arbitrary unknown functions of time. The resulting SDE in the variable $\mathcal{C}$ has an exact closed-form solution contingent on the unknown functions is provided by the ODE,

$$\langle\dot{\mathcal{C}}\rangle \approx -(2\Gamma + \frac{1}{\tau})\langle\mathcal{C}\rangle + 2\langle\frac{c^2 - \alpha^2}{\text{sgn}(a\gamma - c\alpha)}\rangle. \tag{4.56}$$

Naming the expression $K(t) = \langle\frac{c^2-\alpha^2}{\text{sgn}(a\gamma - c\alpha)}\rangle$. Eq. (4.56) has a closed-form solution for the average concurrence,

$$\langle\mathcal{C}(t)\rangle \approx e^{\frac{t}{\tau}+2\Gamma t}\int dt' 2e^{\frac{t'}{\tau}+2\Gamma t'}K(t). \tag{4.57}$$

The function $K(t)$ may be computed directly from numerical simulation. The results of using a numerically calculated $K(t)$ in Eq. (4.57) is plotted in Fig. 4.6 where we see good agreement with the results from simulations in the regime of weak noise. This experimental approximation tends to be steady, although it significantly underestimates $\langle\mathcal{C}^2\rangle_\infty$ in the strong measurement regime.

4.4.2 Numerical Simulation

Having made only limited progress in capturing the steady state analytically, we study the steady state of the system numerically. The results, which confirm the existence of the non-monotonic effect of noise on entanglement, are reported in Fig. 4.7 for both entanglement monotones of interest.

In the absence of measurements, the combination of unitary dynamics and Gaussian noise is expected to lead to a uniformly distributed 'ergodic' steady state, where every accessible final state is realised with equal probability. Using the

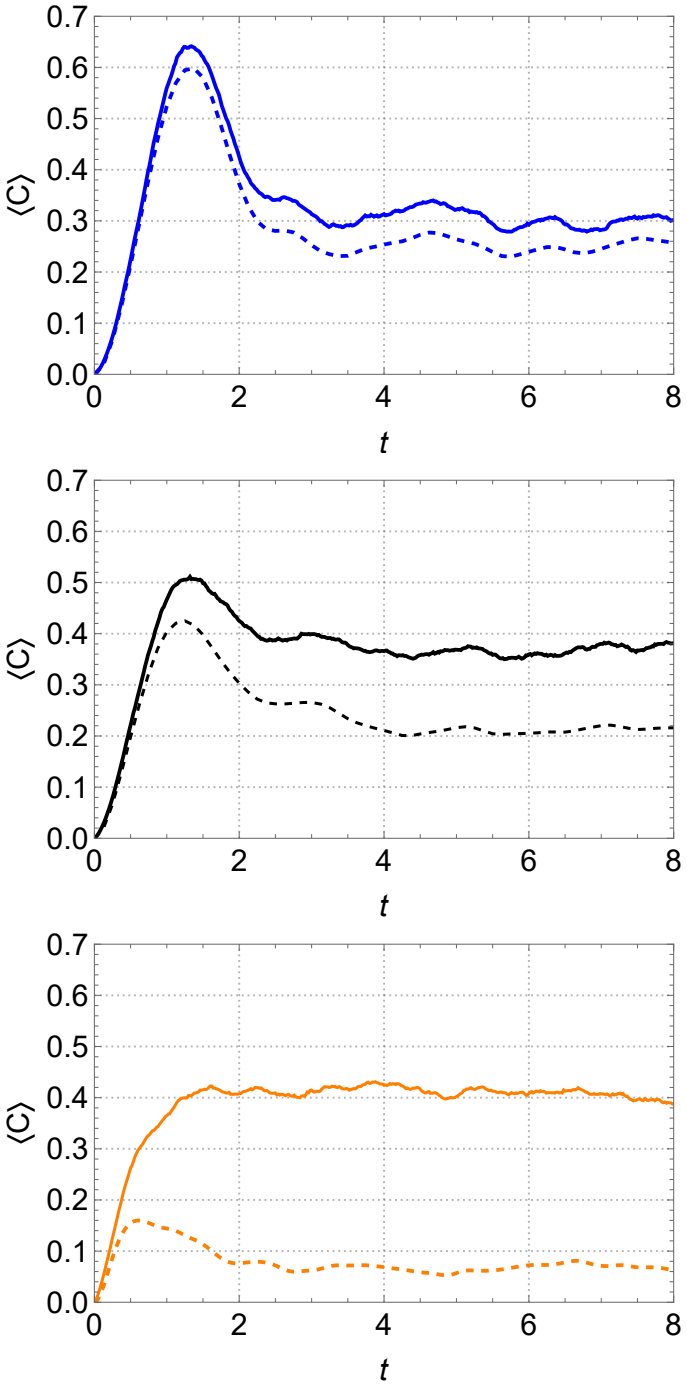

Figure 4.6: Comparisonn of the steady-state approximation — Eq. (4.56)— (dotted lines) and full numerical solutions (full lines) for the average concurrence as a function of time for $\tau = 0.2$ and a range of noise strengths $(0.05, 0.3, 1)$. The approximation underestimates the steady-state concurrence, with significant discrepancies at strong noise.

values of $\langle C^2 \rangle_\infty$ in the ergodic case is helpful as a reference point. Parametrizing a generic final state of the system as $|\psi\rangle$ with $a = \cos(\psi)$,$c = \sin(\psi)\cos(\theta)$, $\alpha = \sin(\psi)\sin(\theta)\cos(\phi)$ and $\gamma = \sin(\psi)\sin(\theta)\sin(\phi)$, the measure on the state parameters becomes $d\mu = \sin(\theta)\sin^2(\psi)d\theta d\phi d\psi$. In the ergodic regime, where all states are equally likely, the average squared concurrence is given by

$$\langle C^2 \rangle = \frac{1}{2\pi^2} \int\int\int 4\sin^2(\theta)\sin^2(\psi) Z(\theta,\psi,\phi)^2 d\mu = \frac{1}{3}, \tag{4.58}$$

where $Z(\theta,\psi,\phi) = \cos(\psi)\sin(\phi) - \cos(\theta)\sin(\psi)\cos(\phi)$, which agrees with the no-measurement limit in the numerical simulations. (c.f. Fig.(4.7)). Remarkably, increasing the noise strength under continuous monitoring has a non-monotonic effect on the concurrence. In particular, at any measurement strength, weak noise in the system increases the total steady-state entanglement, while larger noise strength induces a decrease in concurrence.

The effect can be understood by observing that, for low noise, increasing noise generically increases the probability of exploring larger parts of the Hilbert space (with higher entangled states). In contrast, larger local noise tends to induce large fluctuations of the local energy levels, which hinder the entangling effect of the two-qubit Hamiltonian. This effect becomes inappreciable for vanishing measurements when the steady-state distribution tends to Eq. (4.58), i.e. it is mainly independent of the noise strength. It also becomes gradually less pronounced for strong measurements where the disentangling effect of measurements dominates over the noise.

4.5 Discussion

We combined the effects of monitoring with independent external noise into an SPI formalism. This extension of the CDJ formalism can be the basis for the efficient study of noisy measurement-induced dynamics in more complex systems. We used the formalism to extract optimum entanglement dynamics; however, incorporating noise into the CDJ formalism enables predictions of optimal quantum trajectories for

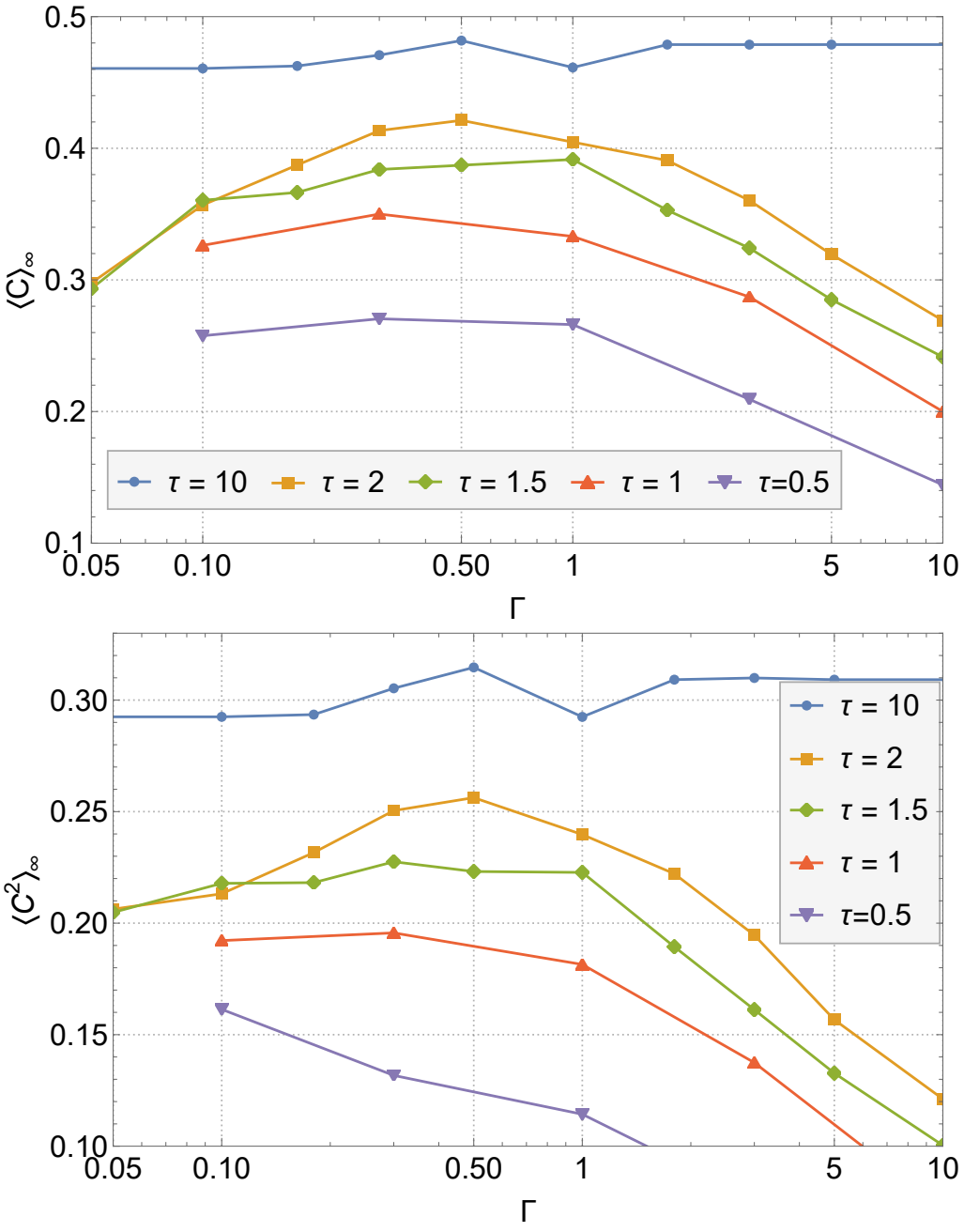

Figure 4.7: (a) Steady State concurrence vs noise intensity, Γ, for a range of measurement strengths. (b) Steady State squared concurrence vs noise intensity, Γ, for a range of measurement strengths. Entanglement exhibits a non-monotonic dependence on noise strength.

a variety of noisy systems. This is particularly relevant given experimental advances that allow for the tracking of individual quantum trajectories. We also apply path integral methods on stochastic quantum dynamics to find the average entanglement dynamics, finding good agreement between theory and simulations. The approach we have applied for the squared concurrence may be extended to any multinomial function of quantum state parameters, enabling the approximation of moments and response functions.

Chapter 5

Testing a Nonequilibrium Fluctuation Theorem for Qubit Dynamics

Our primary objective in this chapter is to design an experimental setup to validate Manzano's fluctuation theorem (MFT), described in Section 2.4.2, using the most straightforward quantum system - a single qubit. First, we need to identify some qubit dynamics that meet the fundamental criteria for applying MFT (Eq. (2.103)) while also being feasible for experimental implementation. To demonstrate the unique features of Eq. (2.103), we design a test that applies to qubit dynamics that earlier quantum fluctuation theorems [91, 92, 93, 94, 95]would not govern. We achieve this goal by utilising a generalised measurement approach. Furthermore, we elaborate on this generalised measurement procedure's basic operator algebra description by mathematically modelling the ancillary qubit system necessary for executing the generalised measurement. This comprehensive schematic description will offer experimentalists a ready-made two-qubit experimental design. Lastly, we broaden the applicability of our research beyond its initial scope, exploring extensions to the original fluctuation theorem that are of additional interest [102].

The reader will notice that we break with our usual procedure since our analysis

of MFT will not involve any path integral methods. We consider our qubit system driven by a CPTP map as described in Section 2.1.3. These dynamics are equivalent to an unselective measurement process, hence why they may be investigated using a generalised measurement process- however, unlike the processes we applied the CDJ method to, the induced quantum trajectories involve discontinuous dynamics in the qubit state space. While treating such a system with a stochastic path integral formulation is possible, we see no advantages to applying such a sophisticated approach. Instead, we opt to examine trajectories directly using measurement operators.

5.1 Finding Candidate Quantum Channels

5.1.1 Criterion for Testable Qubit Dynamics

We explore a range of possible Markovian open qubit dynamics to ascertain the simplest possible dynamics for which a meaningful test of the fluctuation theorem in Eq. (2.103) may be performed. As discussed in Section 2.4.2, the Kraus operator representation must admit a dual reverse dynamics Eq. (2.99) that satisfies a detailed balance relation Eq. (2.101) with its associated forward dynamics. For this to hold, we require that the Kraus operator decomposition satisfies the condition in Eq. (2.98). This equation places a restriction equivalent to requiring that each Kraus operator is a ladder operator inducing jumps between eigenstates of π with a fixed nonequilibrium potential $\Delta\Phi$

$$[M_k, \ln(\pi)] = \Delta\phi_\pi(k) M_k, \tag{5.1}$$

$$[M_k^\dagger, \ln(\pi)] = -\Delta\phi_\pi(k) M_k^\dagger. \tag{5.2}$$

whereas discussed in Section 2.4.2, $\Delta\phi(k)$ is a quantity (nonequilibrium potential) associated with each Kraus operator.

A set of Kraus operators $\{N_j\}$ provides a new Kraus representation of the quantum channel $\mathcal{E}$ if and only if it is related to the original Kraus representation

$\{M_i\}$ by some unitary matrix U as

$$N_j = \sum_i U_{ij} M_i. \tag{5.3}$$

If we suppose that the original set of Kraus operators obeys the detailed balance equation (Eq. (2.101)) with their dual counterparts

$$M_i = e^{\Delta\Phi_i}\tilde{M}_i = e^{\Delta\Phi_i}\mathcal{A}\pi^{\frac{1}{2}}M_i\pi^{-\frac{1}{2}}\mathcal{A}^\dagger, \tag{5.4}$$

$$\sum_j U_{ij}^\dagger N_j = e^{\Delta\Phi_i}\mathcal{A}\pi^{\frac{1}{2}}\Big(\sum_j U_{ij}^\dagger N_j\Big)\pi^{-\frac{1}{2}}\mathcal{A}^\dagger. \tag{5.5}$$

It is clear from Eq. (5.5) that this new set of equations cannot generally be brought into the form $N_i = e^{\Delta\Phi_i^N}\tilde{N}_i$, so the new Kraus representation does not satisfy a simple detailed balance relation with its dual Kraus operator, clarifying the importance of the particular unravelling chosen for the channel.

In addition to finding open dynamics with a particular Kraus representation satisfying detailed balance, we require two further requirements to be satisfied. First, the chosen dynamics must be readily experimentally implementable. Secondly, we demand the set $\Delta\phi_\pi(k)$ are not all zeros (i.e. the requirements for MFT are satisfied in a non-trivial way). A great variety of qubit quantum channels satisfy Eq. (2.98) but do so with vanishing nonequilibrium potentials ($\Delta\phi_\pi(k) = 0$). Vanishing potentials will be induced whenever the invariant state of the CPTP map under consideration is the maximally mixed state. Hence, the Kraus operators associated with the measurement outcomes should not, for example, all be Hermitian.

The FT may apply both to a single application of a CPTP map (see Section 2.1.3), multiple concatenations of these channels or even a concatenation of many infinitesimal CPTP maps (see Section 2.1.4) specified in the form of a lindblad equation. We first examine qubit dynamics in the Lindblad form.

5.1.2 Candidate Lindblad Dynamics

For a system evolving according to some Lindblad equation with Lindblad jump operators $\{L_k\}$,

$$\mathcal{L}(\rho) = -i[H, \rho] + \sum_k D[L_k]\rho. \tag{5.6}$$

Eq. (2.103) may be applied to this qubit system by considering the evolution in infinitesimal time steps, Eq. (2.18). In this case, the Kraus operators take the form.

$$M_0 = \mathbb{I} - \left(iH + \frac{1}{2}\sum_k L_k^\dagger L_k\right)\delta t \tag{5.7}$$

$$M_k = \sqrt{L_k}\delta t. \tag{5.8}$$

In particular, a concatenation of these Kraus operators defines a quantum trajectory, and the application of Eq. (2.99) defines the dual Kraus operators, where the invariant state π is defined by $\mathcal{L}(\pi) = 0$. The Kraus operators (Eq. (5.7)) must satisfy the same criterion as discussed above, with the additional observation that the invariant state must be diagonal in the energy eigenbasis.

Here, we give several Lindblad operators that satisfy non-trivially the fluctuation theorem. Consider a simple stochastic process $\mathcal{L}_1$ that induces jumps towards the poles of the Bloch sphere (in the σ_z basis) and with no driving Hamiltonian. A parameter ν controls the relative frequency of the two possible quantum jumps[1]

$$\mathcal{L}_1\rho = \nu\mathcal{D}[\sigma_-] + (1-\nu)\mathcal{D}[\sigma_+]. \tag{5.9}$$

The stationary state for this Lindblad, specified by $\mathcal{L}_1\pi_1 = 0$, and the corresponding three infinitesimal Kraus operators are specified in Eq. (5.11) are given by

$$\pi_1 = \begin{pmatrix} \nu & 0 \\ 0 & 1-\nu \end{pmatrix}, \tag{5.10}$$

$$M_{1,0} = \begin{pmatrix} 1-\frac{\delta t}{2} & 0 \\ 0 & 1-\frac{\delta t}{2} \end{pmatrix}, M_{1,1} = \sqrt{\delta t}\begin{pmatrix} 0 & 0 \\ 1 & 0 \end{pmatrix}, M_{1,2} = \sqrt{\delta t}\begin{pmatrix} 0 & 1 \\ 0 & 0 \end{pmatrix}. \tag{5.11}$$

[1]Here the dissipators $\mathcal{D}$ are defined in Sec. 2.1.4

$\mathcal{L}_1$ non trivially satisfies the requirements of MFT and may be a good basis for an experimental test. A driving Hamiltonian σ_z may introduce more complexity into these dynamics. Incorporating this unitary evolution into the stochastic dynamics, the Lindblad operator $\mathcal{L}_2$ comes with an unchanged invariant state $\pi_2 = \pi_1$, although the infinitesimal Kraus operators (5.13) has a modified drift term.

$$\mathcal{L}_2\rho = -i\frac{1}{2}[\sigma_z, \rho] + \nu\mathcal{D}[\sigma_-] + (1-\nu)\mathcal{D}[\sigma_+], \tag{5.12}$$

$$M_{2,0} = \begin{pmatrix} 1-(\frac{1}{2}+i)\delta t & 0 \\ 0 & 1-(\frac{1}{2}-i)\delta t, \end{pmatrix} M_{2,1} = \sqrt{\delta t}\begin{pmatrix} 0 & 0 \\ 1 & 0 \end{pmatrix}, M_{2,2} = \sqrt{\delta t}\begin{pmatrix} 0 & 1 \\ 0 & 0 \end{pmatrix}. \tag{5.13}$$

Note that by introducing a driving Hamiltonian in $\mathcal{L}_2$, we require that the invariant state of the quantum channel must be diagonal in the energy eigenbasis - which holds for π_2.

Considering the Lindblad $\mathcal{L}_3$, which is made even more general through the additional parameters γ and Ω, which control the ratio of unitary evolution to stochastic jumping we then substantively modify the dynamics by choosing a driving Hamiltonian that rotates the qubit state around the x-axis in the Bloch sphere

$$\mathcal{L}_3\rho = -i\frac{\Omega}{2}[\sigma_x, \rho] + \gamma\nu\mathcal{D}[\sigma_-] + \gamma(1-\nu)\mathcal{D}[\sigma_+]. \tag{5.14}$$

These dynamics have the invariant state

$$\pi_3 = \begin{pmatrix} \frac{\nu\gamma^2+\Omega^2}{\nu^2+2\Omega^2} & i(2\nu-1)\frac{\gamma\Omega}{\nu^2+2\Omega^2} \\ -i(2\nu-1)\frac{\gamma\Omega}{\nu^2+2\Omega^2} & \frac{\nu\gamma^2+\Omega^2}{\nu^2+2\Omega^2} \end{pmatrix}, \tag{5.15}$$

and infinitesimal Kraus operators given by

$$M_{3,0} = \begin{pmatrix} 1-\frac{dt}{2}dt & -idt \\ -idt & 1-\frac{dt}{2}dt \end{pmatrix}, M_{3,1} = \sqrt{dt}\begin{pmatrix} 0 & 0 \\ 1 & 0 \end{pmatrix}, M_{3,2} = \sqrt{dt}\begin{pmatrix} 0 & 1 \\ 0 & 0 \end{pmatrix}. \tag{5.16}$$

MFT cannot be applied to these system dynamics since π_3 fails to be diagonal in the σ_x basis. Despite this, we note that the fixed state tends to be the maximally

mixed state for $\Omega \gg \gamma$, the limit where only the unitary dynamics are relevant. In this case, $\mathcal{L}_3$ would trivially satisfy the MFT desideratum.

To provide an example of a Lindblad operator that satisfies Manzano's FT trivially, we look at $\mathcal{L}_4$, which has been experimentally realised for a driven transmon qubit circuit which is capacitively coupled to waveguide cavity [38]. A homodyne measurement along some quadrature of the electromagnetic field $ae^{-i\phi} + a^\dagger e^{i\phi}$, constitutes a weak measurement along the corresponding dipole of the transmon qubit, $\sigma^+ e^{-i\phi} + \sigma^- e^{i\phi}$. The time-dependent field H drives the qubit

$$H = \hbar\Omega \cos\Big(\omega t + \phi\Big)\sigma_y, \tag{5.17}$$

where ω is the resonance frequency of the qubit and Ω is the Rabi drive frequency. The homodyne readout dV_t obtained over the time interval $(t, t+\delta t)$ is given by $dV_t = \sqrt{\eta\gamma}\hbar\sigma_x\delta t + \sqrt{\gamma}dr$, where η is the quantum efficiency of the homodyne detection, γ is the radiative decay rate, and dr is a zero-mean Gaussian random variable with variance δt. $\mathcal{L}_4$ is then given by

$$\mathcal{L}_4\rho = -\frac{i}{\hbar}[H,\rho] + \gamma\mathcal{D}[\sigma_-]\rho + \sqrt{\eta\gamma}\mathcal{H}[\sigma_- r]\rho, \tag{5.18}$$

where the jump superoperator acts as $\mathcal{H}[O](\tilde{\rho}) = O\tilde{\rho} + \tilde{\rho}O^\dagger - \mathrm{tr}[(O+O^\dagger)\tilde{\rho}]\tilde{\rho}$. From the relation

$$M_r = \sqrt[4]{\frac{\eta}{2\pi\delta t}}\exp\Big(-\frac{\eta r^2}{4\delta t}\Big)\Big(1 - \frac{i}{\hbar}H dt - \frac{1}{2}\hat{c}^\dagger\hat{c}\delta t + \sqrt{\eta}\hat{c}r\Big) \tag{5.19}$$

the infinitesimal Kraus operators associated with the quantum channel are

$$M_r = \sqrt[4]{\frac{\eta}{2\pi\delta t}}\exp\Big(-\frac{\eta r^2}{4\delta t}\Big)\begin{pmatrix} 1-\frac{\gamma\delta t}{2} & -\delta t\Omega\hbar\cos(\phi - t\omega) \\ \delta t\Omega\hbar\cos(\phi - t\omega) + r\sqrt{\gamma\eta} & 1 \end{pmatrix}. \tag{5.20}$$

With stochastic dynamics obeying $\rho(t+dt) = \frac{M_r\rho M_r^\dagger}{\mathrm{Tr}[M_r\rho M_r^\dagger]}$, we average over the measurement readouts keeping only terms up to first order in time,

$$\rho(t+dt) = \int_{-\infty}^{\infty}\frac{M_r\rho M_r^\dagger}{\mathrm{Tr}[M_r\rho M_r^\dagger]}dr = \begin{pmatrix} \rho_{00} & \rho_{01} \\ \rho_{10} & \rho_{11} \end{pmatrix}$$
$$+ dt\begin{pmatrix} -\gamma\rho_{00} - \Omega(\rho_{01}+\rho_{10})\cos(\phi - t\omega) & \Omega(\rho_{00}-\rho_{11})\cos(\phi - t\omega) - \frac{1}{2}\gamma\rho_{01} \\ \Omega(\rho_{00}-\rho_{11})\cos(\phi - t\omega) - \frac{1}{2}\gamma\rho_{10} & \gamma\rho_{00} + \Omega(\rho_{01}+\rho_{10})\cos(\phi - t\omega) \end{pmatrix}.$$

From this, we see that the channel characterised by the Hamiltonian in Eq. (5.17) is equivalent to the Lindblad $\dot{\rho} = -\frac{i}{\hbar}[H, \rho] + \gamma\mathcal{D}[\sigma_y]\rho$. This channel is unital since

$$-\frac{i}{\hbar}[H, \mathbb{I}] + \sigma_y \mathbb{I} \sigma_y^\dagger - \frac{1}{2}\left(\sigma_y^\dagger \sigma_y \mathbb{I} + \mathbb{I}\sigma_y^\dagger \sigma_y\right) = 0. \tag{5.21}$$

Any unital quantum channel can never accumulate a nonvanishing nonequilibrium potential.

5.1.3 Discrete Qubit Measurements

5.1.3.1 Binary Qubit Measurements

We find that, for a qubit, quantum channels decomposed into only two Kraus operators will either fail to have defined dual dynamics or their possible dual trajectories always occur with equal probability to their forward trajectories. We demonstrate this by systematically examining all possible forms of dual Kraus operator representations. First, we assume that an invariant state of some qubit channel $\mathcal{E}$ exists; we then choose the diagonal basis of the invariant space to represent the Kraus operators. Eq. (2.98) severely constrains the form the measurement operators can take; all such Kraus operators may be specified using at most four arbitrary complex numbers $\alpha, \beta, \gamma, \delta$. We then test all possible combinations to the generic state $\rho = \begin{pmatrix} \rho_{00} & \rho_{01} \\ \rho_{10} & \rho_{11} \end{pmatrix}$, the resulting non-selective post-measurement state may then be analysed.

For the first set of channels, without loss of generality, we choose $M_1 = \begin{pmatrix} \alpha & 0 \\ 0 & 0 \end{pmatrix}$. For the first two cases, the channel is necessarily unital and, therefore, will be unsuitable for testing.

$$M_{a,2} = \begin{pmatrix} 0 & 0 \\ 0 & \beta \end{pmatrix}, \quad \mathcal{E}_a(\rho) = \begin{pmatrix} \rho_{00} & 0 \\ 0 & \rho_{11} \end{pmatrix}. \tag{5.22}$$

$$M_{b,2} = \begin{pmatrix} \beta & 0 \\ 0 & \gamma \end{pmatrix}, \qquad \mathcal{E}_b(\rho) = \begin{pmatrix} \rho_{00} & \beta\gamma^*\rho_{01} \\ \gamma\beta\rho_{10} & \rho_{11} \end{pmatrix}. \tag{5.23}$$

For this next type of map, the fixed state is pure, which is another disqualifying characteristic

$$M_{c,2} = \begin{pmatrix} 0 & \beta \\ 0 & 0 \end{pmatrix}, \qquad \mathcal{E}_c(\rho) = \begin{pmatrix} \rho_{00} + \rho_{11} & 0 \\ 0 & 0 \end{pmatrix}. \tag{5.24}$$

The last operator to check in conjunction with M_1, is $M_{d,2} = \begin{pmatrix} 0 & 0 \\ \beta & 0 \end{pmatrix}$, however, such a Kraus operator decomposition is impossible for any CPTP map, so this combination may be disqualified immediately.

The next three cases to check are associated with $M_1 = \begin{pmatrix} 0 & 0 \\ 0 & \alpha \end{pmatrix}$. We note that there is one fewer combination to check, as the operator ordering is irrelevant. We find that our first channel $\mathcal{E}_e$ is unital, and therefore trivial

$$M_{e,2} = \begin{pmatrix} \beta & 0 \\ 0 & \gamma \end{pmatrix} \quad \mathcal{E}_e(\rho) = \begin{pmatrix} \rho_{00} & \beta\gamma^*\rho_{01} \\ \gamma\beta^*\rho_{10} & \rho_{11} \end{pmatrix}. \tag{5.25}$$

The next channel $\mathcal{E}_f(\rho)$ projects the system's final state into a pure state, again disqualifying it from consideration

$$M_{f,2} = \begin{pmatrix} 0 & 0 \\ \beta & 0 \end{pmatrix} \quad \mathcal{E}_f(\rho) = \begin{pmatrix} 0 & 0 \\ 0 & 1 \end{pmatrix}. \tag{5.26}$$

Taking $M_{g,2} = \begin{pmatrix} 0 & \beta \\ 0 & 0 \end{pmatrix}$ will fail to produce a CPTP channel. For the next two cases we take $M_1 = \begin{pmatrix} \alpha & 0 \\ 0 & \beta \end{pmatrix}$. Examining the form of these channels reveals that the fluctuation theorem cannot apply to either channel since, in both cases, the fixed state is necessarily pure

$$M_{h,2} = \begin{pmatrix} 0 & \gamma \\ 0 & 0 \end{pmatrix} \quad \mathcal{E}_h(\rho) = \begin{pmatrix} \rho_{00} + |\gamma|^2\rho_{11} & \alpha\beta^*\rho_{01} \\ \beta\alpha^*\rho_{10} & (1 - |\gamma|^2)\rho_{11} \end{pmatrix} \tag{5.27}$$

$$M_{i,2} = \begin{pmatrix} 0 & 0 \\ \gamma & 0 \end{pmatrix} \quad \mathcal{E}_i(\rho) = \begin{pmatrix} (1 - |\gamma|^2)\rho_{00} & \alpha\beta^*\rho_{01} \\ \beta\alpha^*\rho_{10} & \rho_{11} + |\gamma|^2\rho_{00} \end{pmatrix} \tag{5.28}$$

In the final case, we take $M_1 = \begin{pmatrix} 0 & \alpha \\ 0 & 0 \end{pmatrix}$, the ensuing channel is unital and therefore trivial

$$M_{j,2} = \begin{pmatrix} 0 & 0 \\ \beta & 0 \end{pmatrix} \quad \mathcal{E}_j(\rho) = \begin{pmatrix} \rho_{11} & 0 \\ 0 & \rho_{00} \end{pmatrix}. \tag{5.29}$$

5.1.3.2 Triple Readout Protocol

Inspired by Eq. (5.13), we examine the non-infinitesimal version of these measurement operators that take the same form as those associated with $\mathcal{L}_1$ and $\mathcal{L}_2$. Again parameterising these operators using generic complex numbers $\alpha, \beta, \gamma, \delta$,

$$M_0 = \begin{pmatrix} \alpha & 0 \\ 0 & \beta \end{pmatrix}, M_1 = \begin{pmatrix} 0 & \gamma \\ 0 & 0 \end{pmatrix}, M_2 = \begin{pmatrix} 0 & 0 \\ \delta & 0 \end{pmatrix}, \tag{5.30}$$

subject to the conditions $|\alpha|^2 + |\delta|^2 = 1$ and $|\gamma|^2 + |\beta|^2 = 1$. Two key properties of the channel defined by the operators Eq. (5.30) are the unique invariant state π (Eq. 5.31) and the three possible changes in nonequilibrium potential specified in Eq. (5.32),

$$\pi = \begin{pmatrix} \frac{|\gamma|^2}{|\gamma|^2 - |\alpha|^2 + 1} & 0 \\ 0 & 1 - \frac{|\gamma|^2}{|\gamma|^2 - |\alpha|^2 + 1} \end{pmatrix} = \begin{pmatrix} \pi_{00} & 0 \\ 0 & 1 - \pi_{00} \end{pmatrix}, \tag{5.31}$$

$$\begin{aligned} \Delta\Phi_\pi(0) &= 0, \\ \Delta\Phi_\pi(1) &= 2\tanh^{-1}\left(\frac{2\left(|\alpha|^2 - 1\right)}{|\gamma|^2 - |\alpha|^2 + 1} + 1\right), \\ \Delta\Phi_\pi(2) &= -2\tanh^{-1}\left(\frac{2\left(|\alpha|^2 - 1\right)}{|\gamma|^2 - |\alpha|^2 + 1} + 1\right). \end{aligned} \tag{5.32}$$

This particular Kraus operator decomposition of $\mathcal{E}$ has, in combination with a freely chosen symmetry operator A, a dual map $\tilde{\mathcal{E}}$ with dual Kraus operators. Using Eq. (2.99) and choosing the trivial symmetry operator $A = \mathbb{I}$, we find the associated dual Kraus operators

$$\tilde{M}_0 = \begin{pmatrix} \alpha^* & 0 \\ 0 & \beta^* \end{pmatrix}, \tag{5.33}$$

$$\tilde{M}_1 = \begin{pmatrix} 0 & 0 \\ \sqrt{\frac{1-|\alpha|^2}{|\gamma|^2}}\gamma^* & 0 \end{pmatrix}, \quad \tilde{M}_2 = \begin{pmatrix} 0 & \sqrt{\frac{|\gamma|^2}{1-|\alpha|^2}}\delta^* \\ 0 & 0 \end{pmatrix}.$$

5.2 Developing and Refining a Measurement Protocol

We take the set of Kraus operators in Eq. (5.30) to be suitable to test; we take these instead of the infinitesimal time case since we can exert more direct control over the process and use the same experimental platform to drive the dual dynamics. To actively test Eq. (2.103), it is necessary to determine the accumulated nonequilibrium potential and the probability for all quantum trajectories generated during the dynamics. A straightforward experimental sketch is as follows:

1. Associate each measurement readout with a change in the nonequilibrium potential, and then implement the forward measurement process:
   (a) Prepare an initial mixed state
   (b) Perform an initial protective measurement of this state on some orthonormal basis
   (c) Implement the chosen series of generalised measurements
   (d) Take a final projective measurement onto another chosen orthonormal basis.
2. Repeat step one until the statistical properties of the generalised measurement readouts become clear. From this data calculate $P(\gamma)$ for every possible γ and associate an $\sum_{r=1}^{R} \Delta\Phi_{\pi(r)}(k_r)$ with each γ.
3. Implement the dual measurement process:
   (a) Prepare an initial mixed state
   (b) Project this state onto the orthonormal basis related by the chosen symmetry operator A to the basis used in step 3a.

(c) Implement the chosen series of dual generalised measurements

(d) Take a final projective measurement onto the orthonormal basis related by the chosen symmetry operator A to the basis used in step 3a.

4. Repeat step three until the statistical properties of the dual generalised measurement readouts become clear. Then, verify the relationship between the accumulated nonequilibrium potential along the trajectories and their statistical relationship with their associated dual trajectories.

This procedure is easier sketched than executed. As discussed in Section 2.1, to perform such a measurement, we need at least a three-level ancillary system to perform the generalised measurement. However, three-level systems (qutrits) are more challenging to fabricate than qubits primarily due to their higher dimensionality and heightened noise sensitivity, making it harder to maintain coherence and perform precise operations. Moreover, the lack of established platforms and control techniques for qutrits makes them an unattractive platform for implementing an FT test.

The forward generalised measurements process described in step two may be implemented using a single ancillary qubit if we allow each generalised measurement operator to be performed in two substeps. One possible experimental architecture for this design, discussed with K. Murch [171], is cross-shaped transmon qubits, a type of quantum bit that uses a superconducting circuit composed of a Josephson junction crossed by another junction to create a cross-shaped structure [172]. This type of qubit has a reduced sensitivity to charge noise compared to standard transmon qubits, and it may be readily coupled to other qubits and control mechanisms. The coupling between the system and ancillary qubit could be achieved by coupling via a third detuned qubit: this would be a qubit whose energy level is shifted away from resonance with control signals or neighbouring qubits. The system and ancillary

qubit would be governed by the Hamiltonian H_c with a coupling strength c

$$H_c = \begin{pmatrix} 0 & 0 & 0 & 0 \\ 0 & 0 & c & 0 \\ 0 & c & 0 & 0 \\ 0 & 0 & 0 & 0 \end{pmatrix}. \tag{5.34}$$

To perform a two substep measurement equivalent to Eq. (5.30), we first assume the system is in the separable state $|\psi_0\rangle = (a|0\rangle + b|1\rangle) \otimes |0\rangle$, where the second qubit is the ancillary system. In the first substep, we apply an iSWAP gate[2] to the system and then measure the ancillary qubit. Let H_c drive the system, then the interaction duration t controls the degree of rotation between $|01\rangle$ and $|10\rangle$ up to the desired rotation angle θ. At this stage, the system is in the state

$$|\psi_1\rangle = a|0\rangle \otimes |0\rangle - ib\sin(\theta/2)|0\rangle \otimes |1\rangle + b\cos(\theta/2)|1\rangle \otimes |0\rangle. \tag{5.35}$$

A projective measurement of the ancillary qubit in the σ_z basis produces back-action on the system state, which depends on the measurement readout; the system qubit updates to $a|0\rangle + b\cos(\theta/2)|1\rangle$ if the detector registers 0 and $-ib\sin(\theta/2)|0\rangle$ if the detector registers 1. We begin the second substep by flipping the ancillary qubit (corresponding to a π rotation on the Bloch sphere) irrespective of the first measurement readout. Then, another iSWAP gate may be applied in the manner as before with the rotation angle ϕ. The two conditional quantum states of the system are then $a\cos(\phi/2)|0\rangle \otimes |1\rangle - ia\sin(\phi/2)|1\rangle \otimes |0\rangle + b\cos(\theta/2)|1\rangle \otimes |1\rangle$ and $-ib\sin(\theta/2)|0\rangle \otimes |0\rangle$ for 1. We then complete the second substep by performing another Von-Neuman measurement on the ancillary qubits computational basis. This procedure effectively implements the measurements

$$M_0 = \begin{pmatrix} \cos(\frac{\phi}{2}) & 0 \\ 0 & \cos(\frac{\theta}{2}) \end{pmatrix}, M_1 = \begin{pmatrix} 0 & -i\sin(\frac{\theta}{2}) \\ 0 & 0 \end{pmatrix}, M_2 = \begin{pmatrix} 0 & 0 \\ -i\sin(\frac{\phi}{2}) & 0 \end{pmatrix}. \tag{5.36}$$

[2] $\text{iSWAP} = \begin{pmatrix} 1 & 0 & 0 & 0 \\ 0 & 0 & i & 0 \\ 0 & i & 0 & 0 \\ 0 & 0 & 0 & 1 \end{pmatrix}$

$$\Delta\Phi_0 = 0, \Delta\Phi_1 = \log\left(\frac{\cos(\phi)-1}{\cos(\theta)-1}\right), \Delta\Phi_2 = \log\left(\frac{\cos(\theta)-1}{\cos(\phi)-1}\right). \tag{5.37}$$

Where the readout $(0,0)$ is associated with M_2, $(0,1)$ with M_0 and $(1,0)$ is equivalent to M_1. We note that $(1,1)$ occurs with zero probability in our scheme.

A small modification of this procedure may be used to implement the dual process; we need to add a negative sign to the rotation angle of both iSWAP gates. The corresponding Kraus operators then are

$$\tilde{M}_0 = \begin{pmatrix} \cos(\phi/2) & 0 \\ 0 & \cos(\theta/2) \end{pmatrix}, \quad \tilde{M}_1 = \begin{pmatrix} 0 & 0 \\ i\sin(\phi) & 0 \end{pmatrix}, \quad \tilde{M}_2 = \begin{pmatrix} 0 & i\sin(\theta) \\ 0 & 0 \end{pmatrix}. \tag{5.38}$$

Any experiment will necessarily introduce sources of error; therefore, it is essential to be aware of what deviation from theory these imperfections are likely to introduce. Analytically calculating this behaviour is not advantageous since the deviation from the expected behaviour will depend on each particular trajectory chosen. Therefore, our experimental collaborators [171], using detailed knowledge of the decoherence and readout fidelity effects introduced by their experimental instruments, simulate the expected behaviour of a short implementation of our experimental design.

A readout fidelity f implies the measurement device registers the wrong reading $(1-f)$ fraction of readouts, so the probabilities for the readouts $(0,0)$, $(0,1)$, $(1,0)$, and $(1,1)$ to correspond to the purported post-measurement states are f^2, $f(1-f)$, $f(1-f)$, and $(1-f)^2$. To account for this source of error, the post-measurement state for the projective readout $(0,0)$ is taken to be a convex combination,

$$\rho = f^2\rho^{00} + f(1-f)\rho^{01} + f(1-f)\rho^{10} + (1-f)^2\rho^{11}. \tag{5.39}$$

where ρ^{ij} is the system state with $f = 1$ and readout (i,j). The post-measurement state for the other readouts is calculated similarly. The effect of decoherence is incorporated after each projective measurement by multiplying e^{-t/T_1} by ρ'_{11}, adding

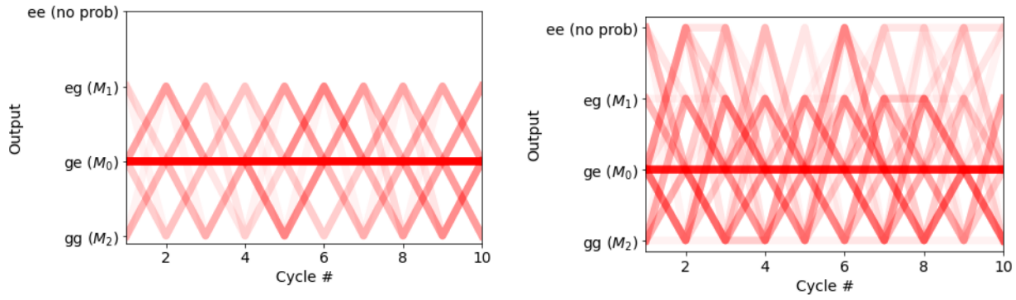

Figure 5.1: Reproduced with permission from K. Murch and X. Linpeng [171]. [Panel a] Readout trajectories of the forward dynamics in the ideal case. [Panel b] Readout trajectories in the case with readout fidelity $f = 0.9$, $T_1 = T_2 = 30$ µs, and readout time $t = 2$ µs. The target Kraus operator are arbitrarily chosen to be $\theta = \phi = \pi/4$. These simulations are performed for ten generalised measurements. The colour concentration corresponds to the probability of the readout.

$(1 - e^{-t/T_1})\rho'_{11}$ to ρ'_{00}, and multiplying $e^{-t/2T_1 - t/T_2}$ to ρ'_{01} and ρ'_{10}. Here, ρ' is the reduced density matrix for the system qubit, t is the time of one readout, and T_1, T_2 are the timescale over which the quantum coherence of the qubit's state is preserved. T_1 is the characteristic time for the qubit to relax to its ground state, and T_2 is the dephasing time, the timescale over which the phase coherence of the qubit's superposition states is lost.

Fig. 5.1 shows readout trajectories for the forward dynamics in the ideal case and the realistic case that includes readout fidelity and decoherence. In the latter case, obtaining the readouts $(1, 1)$ is possible. Fig. 5.2 shows the degree of agreement between the results of numerical simulations and the detailed balance relation Eq. (2.103) for a selection of readout fidelities decoherence times. Here, the forward trajectory $(M_2, M_1, M_2, M_1, M_2)$ and its dual reverse $(\tilde{M}_2, \tilde{M}_1, \tilde{M}_2, \tilde{M}_1, \tilde{M}_2)$ are used. Significant deviations are predicted when the measurement fidelity ≤ 0.9 and the coherence time is less than 10 µs.

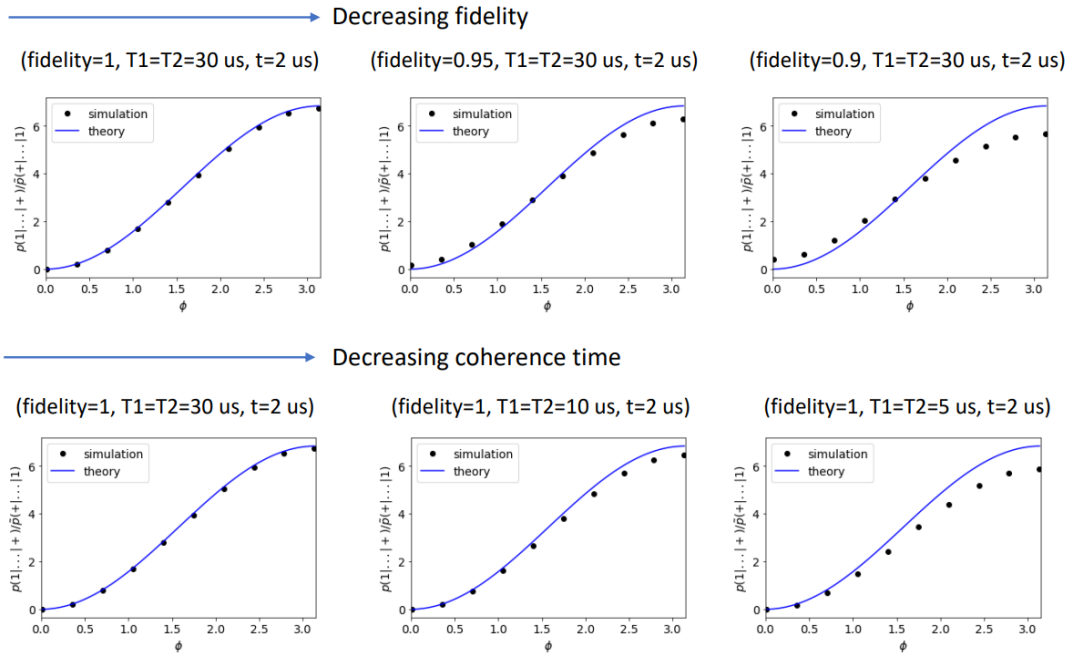

Figure 5.2: Ratio between the forward and reverse trajecories against ϕ. Reproduced with permission from K. Murch and X. Linpeng [171]. The theoretical detailed balance relation is compared to the results from numerical simulation for a range of readout fidelities and decoherence times. θ is set at $\pi/4$ and ϕ is varied from 0 to π.

5.3 Beyond a Theoretical Validation

In addition to merely testing a known theoretical result, we briefly explore ways our measurement scheme may be used to explore new theoretical questions. In particular, we look at a convex combination of CPTP maps constrained by Eq. (2.103), finding the new nonequilibrium potentials combine non-trivially. We additionally explore how well the nonequilibrium potentials constrain the statistics of open dynamics that are only approximately governed by Eq. (2.103).

5.3.1 Convex Combination of Nonequilibrium Potentials

Consider a convex combination of CPTP maps,

$$\mathcal{E} = p\mathcal{E}^a + (1-p)\mathcal{E}^b, \tag{5.40}$$

where we assume both subchannels are constrained by MFT. To apply Eq. (2.103) to $\mathcal{E}$, we require that this aggregate channel independently satisfies the MFT requirements. Once this is established it becomes logical to consider how the nonequilibrium potentials of $\mathcal{E}^a$ and $\mathcal{E}^b$ combine to produce new nonequilibrium potentials.

In general, the invariant states of two channels do not obey any simple combination algorithm under a convex combination of their channels. Eq. (5.41) demonstrates that a convex combination of invariant states fails to be invariant for a convex combination of channels

$$\begin{aligned}\mathcal{E}(q\pi^a + (1-q)\pi^b) &= p\mathcal{E}^a(q\pi^a + (1-q)\pi^b) + (1-p)\mathcal{E}^b(q\pi^a + (1-q)\pi^b) \\ &= pq\pi^a + (1-p)(1-q)\pi^b + p\mathcal{E}^a((1-q)\pi^b) + \mathcal{E}^b(q\pi^a).\end{aligned} \tag{5.41}$$

This suggests that the nonequilibrium potentials will also fail to satisfy any simple combination rule.

We illustrate this nontrivial behaviour by considering the simple case of two CPTP maps, $\mathcal{E}_a$ and $\mathcal{E}_b$, with simultaneously diagonalisable fixed points and Kraus representations of the same form. Imposing these two strict conditions, we see

immediately that the combined channel will also be constrained by Eq. (2.103); we label these two sets of Kraus operators

$$M_1^a = \begin{pmatrix} \alpha_a & 0 \\ 0 & \beta_a \end{pmatrix}, M_2^a = \begin{pmatrix} 0 & \gamma_a \\ 0 & 0 \end{pmatrix}, M_3^a = \begin{pmatrix} 0 & 0 \\ \delta_a & 0 \end{pmatrix}, \tag{5.42}$$

$$M_1^b = \begin{pmatrix} \alpha_2 & 0 \\ 0 & \beta_2 \end{pmatrix}, M_2^b = \begin{pmatrix} 0 & \gamma_2 \\ 0 & 0 \end{pmatrix}, M_3^b = \begin{pmatrix} 0 & 0 \\ \delta_2 & 0 \end{pmatrix}. \tag{5.43}$$

Separately, these two channels have fixed points π^a and π^b and the combined invariant state is given by π^{ab}

$$\pi^{a/b} = \begin{pmatrix} \frac{|\beta_{1/2}|^2-1}{|\beta_{1/2}|^2+|\delta_{1/2}|^2-2} & 0 \\ 0 & 1-\frac{|\beta_{1/2}|^2-1}{|\beta_{1/2}|^2+|\delta_{1/2}|^2-2} \end{pmatrix} \tag{5.44}$$

$$\pi^{ab} = \begin{pmatrix} \frac{(p-1)|\beta_2|^2-p|\beta_1|^2+1}{(p-1)(|\alpha_2|^2+|\beta_2|^2)-p(|\alpha_1|^2+|\beta_1|^2)+2} & 0 \\ 0 & \frac{(p-1)|\alpha_2|^2-p|\alpha_1|^2+1}{(p-1)(|\alpha_2|^2+|\beta_2|^2)-p(|\alpha_1|^2+|\beta_1|^2)+2} \end{pmatrix} \tag{5.45}$$

Correspondingly, each map individually has the changes in nonequilibrium potentials given by Eq. (5.46) and, in combination, is associated with the potentials in Eq. (5.47). Eq. (5.47) cannot be decomposed into terms that depend only on one subchannel.

$$\Delta\phi^{a/b} = 0, \Delta\phi^{a/b} = \pm 2\tanh^{-1}\left(\frac{|\delta_{1/2}|^2-|\beta_{1/2}|^2}{|\beta_{1/2}|^2+|\delta_{1/2}|^2-2}\right) \tag{5.46}$$

$$\Delta\phi = 0, \Delta\phi = \pm 2\tanh^{-1}\left(\frac{(p-1)|\alpha|^2-p(|\alpha_1|^2-|\beta_1|^2+|\beta_2|^2)+|\beta_2|^2}{(p-1)(|\alpha_2|^2+|\beta_2|^2)-p(|\alpha_1|^2+|\beta_1|^2)+2}\right) \tag{5.47}$$

An example of how the channel potentials combine is demonstrated in Fig. 5.3.

5.3.2 Deviations from the Detailed Balance Relation

In addition to the primary measurement protocol, we include the effect of an additional qubit rotation on the system. The aim is to stop MFT from applying to the system. Physically this involves allowing processes that affect a coherent evolution between states and which may not share a common nonequilibrium

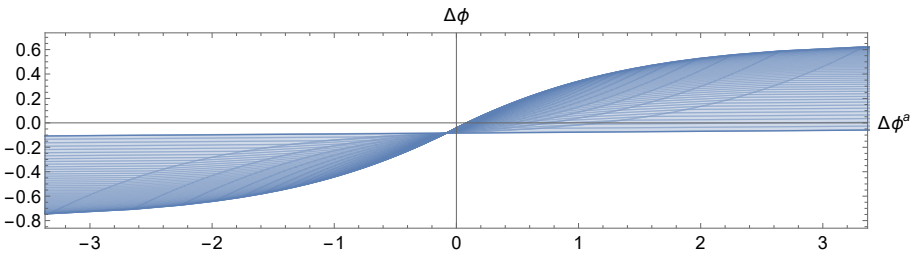

Figure 5.3: A parametric plot of the pair $(\Delta\phi^a(\alpha_1,\beta_1),\Delta\phi(\alpha_1,\beta_1))$ showing an example of how the nonequilibrium potentials for CPTP maps Eq. (5.42) and Eq. (5.43) may combine for $p=\frac{1}{2}$ and fixed $\Delta\phi^b=-\frac{1}{10}$. This illustrates how the non-equilibrium potentials of a sub-channel may constrain the non-equilibrium potential of the overall dynamics.

potential difference $\Delta\phi$. By including a tunable rotation deviations from the FT can be investigated in a controlled way. We consider the measurement of the form Eq. (5.30) implemented by the same two sub-step measurement protocol described in Section 5.2. However, we introduce an additional qubit rotation on the system before the final ancilla measurement. Suppose the final ancillary readout registers the zero state. In that case, we apply a rotation $\Gamma=R_x(\gamma)\otimes\mathbb{I}$ directly to the system degree of freedom with the new parameter γ,

$$\Gamma=\begin{pmatrix}\cos\left(\frac{\gamma}{2}\right) & -i\sin\left(\frac{\gamma}{2}\right)\\ -i\sin\left(\frac{\gamma}{2}\right) & \cos\left(\frac{\gamma}{2}\right)\end{pmatrix}\otimes\mathbb{I}. \tag{5.48}$$

If the final ancillary readout registers 1 no additional action is taken.

Applying the additional qubit rotation only to states that register a 0 readout in the first measurement step ensures that there will continue to be only three Kraus operators since the $(1,1)$ readout still occurs with vanishing probability. The

resulting Kraus operators

$$N_0 = \begin{pmatrix} \cos\gamma\cos\frac{\phi}{2} & -i\cos\frac{\theta}{2}\cos\frac{\phi}{2}\sin\gamma \\ -i\sin\gamma & \cos\gamma\cos\frac{\theta}{2} \end{pmatrix}, N_1 = \begin{pmatrix} 0 & 0 \\ -i\sin\frac{\phi}{2}\cos\gamma & -\cos\frac{\theta}{2}\sin\frac{\phi}{2}\sin\gamma \end{pmatrix},$$
$$N_2 = \begin{pmatrix} 0 & -i\sin\frac{\theta}{2} \\ 0 & 0 \end{pmatrix} \tag{5.49}$$

violate the MFT. Any set of Kraus operators of this form in the eigenbasis of their invariant state cannot satisfy the FT, as they are a linear combination of all jump operators. The size of the violation is controlled by the parameter γ.

Since the form of the Kraus operators is changed by the inclusion of γ, as noted above, a jump in the nonequilibrium potential cannot be directly associated with each Kraus operator. However, given that γ is small, a nonequilibrium potential jump may be associated with each operator unambiguously. These approximate nonequilibrium potentials come from the eigenvalues of the new invariant state. Recall that the critical feature of Manzano's FT is that, for some arbitrary states $|\psi\rangle$ and $|\phi\rangle$ (with the symmetry operator set to the identity)

$$\frac{p(\phi,k|\psi)}{p(\psi,k|\phi)} = \frac{|\langle\phi|M_k|\psi\rangle|^2}{|\langle\psi|\tilde{M}_k|\phi\rangle|^2} = e^{-\Delta\Phi_k}. \tag{5.50}$$

Note that this ratio is independent of ψ and ϕ. While Eq. (5.50) is typically extended to incorporate more Kraus operators, it is sufficient to consider the application of a single map.

To investigate how the extra small qubit rotation affects MFT, we calculate numerically the real ratio between the forward and dual processes

$$\frac{p(\phi,k|\psi)}{p(\psi,k|\phi)} = \frac{|\langle\phi|N_k|\psi\rangle|^2}{|\langle\psi|\tilde{N}_k|\phi\rangle|^2} \tag{5.51}$$

and compare this with the ratio we would expect had the MFT held

$$\frac{p(\phi,k|\psi)}{p(\psi,k|\phi)} \overset{?}{\approx} e^{-\Delta\Phi_k}. \tag{5.52}$$

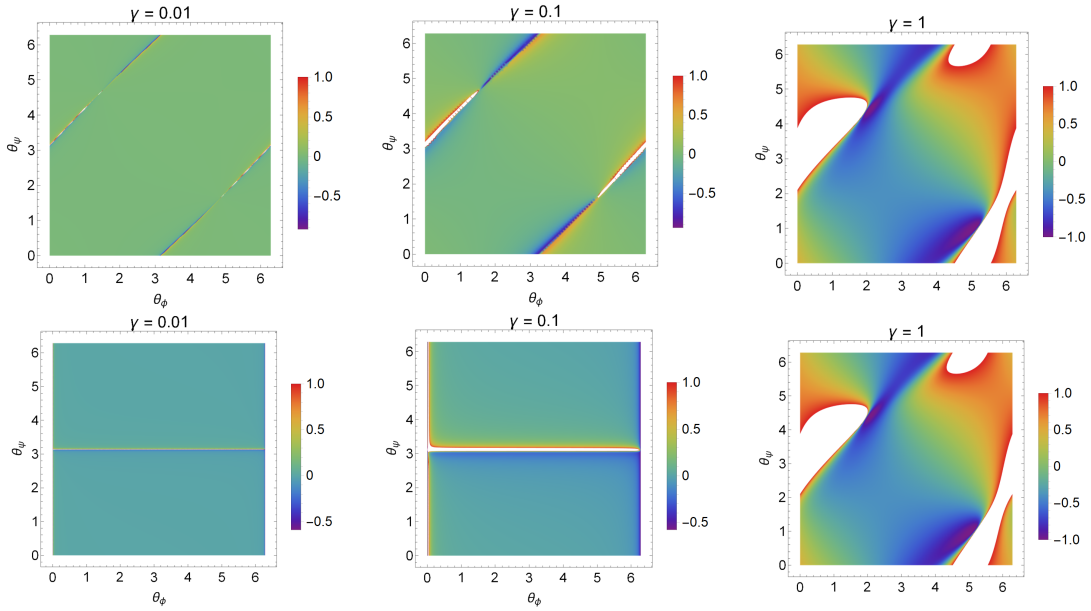

Figure 5.4: The numerical difference between the left-hand side and right-hand side of Eq. (5.52) as a function of θ_ψ and θ_ϕ. The two additional parameters ϕ_ψ and ϕ_ϕ are set equal to 1. This deviation is illustrated for a selection of rotation values $\gamma \in 0.01, 0.1, 1$. [Top Row]corresponds to the back-action N_0. [Bottom Row] corresponds to the back-action N_1. .

Let $|\psi\rangle$ and $|\phi\rangle$ be parameterised in standard Bloch sphere coordinates by (θ_ψ, ϕ_ψ) and (θ_ϕ, ϕ_ϕ) respectively. The results of this numerical calculation are shown in Fig. 5.4.

We observe several notable features; firstly, the independence of the ratio on the choice of ψ and ϕ no longer holds. Secondly, for a wide range of the parameter space $(\theta_\psi, \phi_\psi, \theta_\phi, \phi_\phi)$, the non-equilibrium potential provides a good approximation for constraining the trajectory statistics. Finally, deviations from the ratio predicted from the nonequilibrium potential are the most pronounced when: the final projective measurement is applied along a Bloch sphere angle $\Delta\theta = \pi$ relative to the forward process state initialisation (the N_0 case), and the forward process is initialised on the Bloch sphere equator (the N_1 case).

5.4 Discussion

We have identified an example of open qubit CPTP dynamics that is realizable by a generalized measurement scheme and would produce quantum trajectories that are governed by Manzano's fluctuation theorem. Our chosen measurement scheme is general enough to investigate the non-trivial implications of MFT. Working with experimentalists we ensured our proposed experiment would be realistically achievable using, as an example of an experimental protocol, Xmon qubits in a quantum circuit. Numerical simulations showed that even in the presence of some detector error and loss of coherence an experimental implementation should still attain good agreement with theory. We also demonstrated how our proposed experimental protocol could be readily modified to explore stochastic dynamics that extend beyond those covered by MFT.

Chapter 6

Conclusions

In this thesis, we have developed a comprehensive action formalism rooted in the Chantasri–Dressel–Jordan (CDJ) framework to describe various features of the dynamics of continuously monitored single-qubit and coupled two-qubit systems. We have also designed a measurement protocol to test an open single-qubit system's thermal and statistical properties. The entire work is underpinned by a unifying thread: the examination of the properties of individual measurement-induced quantum trajectories.

For the single-qubit case, we established a path integral formalism incorporating a global phase parameter, facilitating the determination of statistical properties of measurement-induced geometric phases. Performing the passage between the phase and state space forms of the path integral defined a Lagrangian density associated with nonholonomic constraints. Using this formulation, we analysed the topological properties of the open geometric phase for post-selected quantum trajectories with various initial conditions, revealing a general topological transition phenomenon.

More significantly, we explored geometric phases associated with self-closing trajectories, unveiling a measurement-induced topological transition that is present across the entire Bloch sphere, although the underlying mechanism differed from that of open-geometric phases. For the closed geometric phase, the transition is dictated by the competition of local most likely trajectories, whereas for open

geometric phases, the phase becomes unobservable (occurring with vanishing probabilities) at the transition point. Furthermore, we have shown that including the effects of trajectories around an optimal trajectory via Gaussian fluctuations is an excellent approximation of the entire distribution simulated numerically and leads to modifications of the transition critical point; this has practical implications on experimentally identifying the transition.

Extending the CDJ formalism to coupled two-qubit systems, we derived stochastic actions incorporating continuous monitoring and Gaussian noise fluctuations by combining the CDJ path integral with the standard SPI on Gaussian noise fluctuations. We identified optimal quantum trajectories and analysed their associated concurrence, capturing features of the general entanglement dynamics like their oscillations and non-monotonicity. However, while these paths offer some insights into the systems' overall qualitative behaviour, they fall short in quantitatively reproducing specifics, e.g., oscillation amplitudes and max/min values. For the global optimal trajectory, the associated most likely entanglement can also capture a transition from an oscillating behaviour at short times to an overdamped approach to a steady state as a function of the measurement strength. While such behaviour has a counterpart in the average dynamics, the optimal trajectory does not capture the correct steady-state dependence of the entanglement and misses the effect of the Gaussian noise.

To address these limitations we use a diagrammatic approach, which allows us to capture more features of the systems entanglement dynamics, especially for short-timescales and weak noise and measurement strengths. While the leading-order term in the diagrammatic expansion captures the entanglement oscillations at short times with the appropriate frequency, the next non-trivial term showed a much better agreement with the oscillations' amplitudes. Notably, finite order expansion of the perturbation will generically lead to a vanishing steady state concurrence, which does not agree with the numerical simulation. This hints at the need for some form of infinite resummation of the perturbation series to capture the long-

time steady-state behaviour.

Numerical simulations demonstrated non-monotonic relationships between the steady-state entanglement and noise strength. These effects can be uniquely attributed to the entanglement along quantum trajectories as determined by measurement- and Hamiltonian-induced fluctuations and can serve as a first test of the ability to track non-linear quantum resources, like entanglement, along quantum trajectories.

We concluded our investigation of qubit quantum trajectories by designing an experimental protocol to study quantum fluctuation theorems. In particular, our protocol demonstrates the significance of the nonequilibrium potential, a quantity introduced in Manzano's fluctuation theorem (MFT) as a precursor to entropy production and which serves to constrain trajectory statistics during open system dynamics. We collaborated closely with experimentalists to ensure the feasibility of our protocol. As part of the experimental design phase, we explored the thermal properties of an assortment of qubit CPTP maps. We demonstrated how our measurement protocol could probe the limits of MFT and considered the possible sub-structures that might be present in the thermodynamic properties of a convex combination of quantum channels.

The formalism developed here shows that an action formalism can capture geometric phases and entanglement dynamics and shed new light on these phenomena using path integral techniques, such as the least action principle, Gaussian fluctuations, and diagrammatics. While our work sets the basis for addressing these features in single and dual qubit systems, geometric phases and entanglement are critical concepts in many-body quantum dynamics. As such, our work sets the first steps to devise more methods and approximate treatments of many-body complex dynamics like topological order control and measurement-induced many-body phase transitions.

References

[1] **Dominic Shea** and Alessandro Romito. "Action formalism for geometric phases from self-closing quantum trajectories". In: *Journal of Physics A: Mathematical and Theoretical* 57.31 (July 2024), p. 315303. DOI: 10.1088/1751-8121/ad5e4b. URL: https://dx.doi.org/10.1088/1751-8121/ad5e4b.

[2] **Dominic Shea** and Alessandro Romito. *Stochastic action for the entanglement of a noisy monitored two-qubit system.* 2024. arXiv: 2403.08422 [quant-ph].

[3] R. P. Feynman. "Space-Time Approach to Non-Relativistic Quantum Mechanics". In: *Rev. Mod. Phys.* 20 (2 Apr. 1948), pp. 367–387. DOI: 10.1103/RevModPhys.20.367. URL: https://link.aps.org/doi/10.1103/RevModPhys.20.367.

[4] Werner Karl Heisenberg. "Über quantentheoretische Umdeutung kinematischer und mechanischer Beziehungen". In: *Z. Phys.* 33 (1925), pp. 879–893. URL: https://cds.cern.ch/record/439964.

[5] Paul Adrien Maurice Dirac and Ralph Howard Fowler. "On the theory of quantum mechanics". In: *Proceedings of the Royal Society of London. Series A, Containing Papers of a Mathematical and Physical Character* 112.762 (1926), pp. 661–677. DOI: 10.1098/rspa.1926.0133. eprint: https://royalsocietypublishing.org/doi/pdf/10.1098/rspa.1926.0133. URL:

https://royalsocietypublishing.org/doi/abs/10.1098/rspa.1926.0133.

[6] E. Schrödinger. "Quantisierung als Eigenwertproblem". In: *Annalen der Physik* 386.18 (1926), pp. 109–139. DOI: https://doi.org/10.1002/andp.19263861802. eprint: https://onlinelibrary.wiley.com/doi/pdf/10.1002/andp.19263861802. URL: https://onlinelibrary.wiley.com/doi/abs/10.1002/andp.19263861802.

[7] M.E. Peskin and D.V. Schroeder. *An Introduction To Quantum Field Theory*. Frontiers in Physics. Avalon Publishing, 1995. ISBN: 9780813345437. URL: https://books.google.co.uk/books?id=EVeNNcslvX0C.

[8] H. Kleinert. *Path Integrals In Quantum Mechanics, Statistics, Polymer Physics, And Financial Markets (5th Edition)*. World Scientific Publishing Company, 2009. ISBN: 9789814365260. URL: https://books.google.co.uk/books?id=dJ3FCgAAQBAJ.

[9] H.S. Wio. *Path Integrals for Stochastic Processes: An Introduction*. World Scientific, 2013. ISBN: 9789814449045. URL: https://books.google.co.uk/books?id=jpG6CgAAQBAJ.

[10] Carson C. Chow and Michael A. Buice. "Path Integral Methods for Stochastic Differential Equations". In: *The Journal of Mathematical Neuroscience (JMN)* 5 (1 2015), p. 8. DOI: https://doi.org/10.1186/s13408-015-0018-5.

[11] Norbert Wiener. "The Average of an Analytic Functional1". In: *Proceedings of the National Academy of Sciences* 7.9 (1921), pp. 253–260. DOI: 10.1073/pnas.7.9.253. eprint: https://www.pnas.org/doi/pdf/10.1073/pnas.7.9.253. URL: https://www.pnas.org/doi/abs/10.1073/pnas.7.9.253.

[12] Norbert Wiener. "The Average of an Analytic Functional and the Brownian Movement". In: *Proceedings of the National Academy of Sciences* 7.10 (1921), pp. 294–298. DOI: 10.1073/pnas.7.10.294. eprint: https://www.pnas.

org/doi/pdf/10.1073/pnas.7.10.294. URL: https://www.pnas.org/doi/abs/10.1073/pnas.7.10.294.

[13] Vadim Linetsky. "The Path Integral Approach to Financial Modeling and Options Pricing". English (US). In: *Computational Economics* 11.1-2 (1997), pp. 129–163. ISSN: 0927-7099. DOI: 10.1023/a:1008658226761.

[14] Michael A Buice, Jack D Cowan, and Carson C Chow. "Systematic fluctuation expansion for neural network activity equations". In: *Neural computation* 22.2 (2010), pp. 377–426.

[15] Paul Cecil Martin, ED Siggia, and HA Rose. "Statistical dynamics of classical systems". In: *Physical Review A* 8.1 (1973), p. 423.

[16] Kurt Jacobs. *Quantum Measurement Theory and its Applications*. Cambridge University Press, 2014. DOI: 10.1017/CBO9781139179027.

[17] Kurt Jacobs and Daniel A. Steck. "A straightforward introduction to continuous quantum measurement". In: *Contemporary Physics* 47.5 (Sept. 2006), pp. 279–303. DOI: 10.1080/00107510601101934. URL: https://doi.org/10.1080%2F00107510601101934.

[18] M.A. Nielsen and I.L. Chuang. *Quantum Computation and Quantum Information*. Cambridge Series on Information and the Natural Sciences. Cambridge University Press, 2000. ISBN: 9780521635035. URL: https://books.google.co.uk/books?id=aai-P4V9GJ8C.

[19] A.N. Jordan and I.A. Siddiqi. *Quantum Measurement: Theory and Practice*. Cambridge University Press, 2024. ISBN: 9781009100069. URL: https://books.google.co.uk/books?id=MRrxEAAAQBAJ.

[20] Christopher A. Fuchs. *QBism, the Perimeter of Quantum Bayesianism*. 2010. arXiv: 1003.5209 [quant-ph].

[21] P. Busch et al. *Quantum Measurement*. Theoretical and Mathematical Physics. Springer International Publishing, 2016. ISBN: 9783319433899. URL: https://books.google.co.uk/books?id=MZflDAAAQBAJ.

[22] D.Z. Albert. *Quantum Mechanics and Experience*. Emersion: Emergent Village Resources for Communities of Faith Series. Harvard University Press, 1994. ISBN: 9780674741133. URL: https://books.google.co.uk/books?id=HYEZD0Mh8JEC.

[23] Howard E. Brandt. "Positive operator valued measure in quantum information processing". In: *American Journal of Physics* 67.5 (May 1999), pp. 434–439. ISSN: 0002-9505. DOI: 10.1119/1.19280. eprint: https://pubs.aip.org/aapt/ajp/article-pdf/67/5/434/10115735/434_1_online.pdf. URL: https://doi.org/10.1119/1.19280.

[24] J. von Neumann. *Mathematical Foundations of Quantum Mechanics*. Goldstine Printed Materials. Princeton University Press, 1955. ISBN: 9780691028934. URL: https://books.google.co.uk/books?id=JLyCo3RO4qUC.

[25] M.B. Mensky. *Continuous Quantum Measurements and Path Integrals*. Taylor & Francis, 1993. ISBN: 9780750302289. URL: https://books.google.co.uk/books?id=PAwMXu7IbJcC.

[26] M. B. Mensky. "Quantum restrictions for continuous observation of an oscillator". In: *Phys. Rev. D* 20 (2 July 1979), pp. 384–387. DOI: 10.1103/PhysRevD.20.384. URL: https://link.aps.org/doi/10.1103/PhysRevD.20.384.

[27] Carlton M. Caves. "Quantum mechanics of measurements distributed in time: A Path integral formulation". In: *Phys. Rev. D* 33 (1986), pp. 1643–1665. DOI: 10.1103/PhysRevD.33.1643.

[28] A. Chantasri, J. Dressel, and A. N. Jordan. "Action principle for continuous quantum measurement". In: *Physical Review A* 88.4 (Oct. 2013). DOI: 10.1103/physreva.88.042110. URL: https://doi.org/10.1103%2Fphysreva.88.042110.

[29] Areeya Chantasri and Andrew N. Jordan. "Stochastic path-integral formalism for continuous quantum measurement". In: *Physical Review A* 92.3 (Sept. 2015). DOI: 10.1103/physreva.92.032125. URL: https://doi.org/10.1103%2Fphysreva.92.032125.

[30] Areeya Chantasri et al. "Quantum Trajectories and Their Statistics for Remotely Entangled Quantum Bits". In: *Physical Review X* 6.4 (Dec. 2016). DOI: 10.1103/physrevx.6.041052. URL: https://doi.org/10.1103%2Fphysrevx.6.041052.

[31] Areeya Chantasri et al. "Simultaneous continuous measurement of noncommuting observables: Quantum state correlations". In: *Physical Review A* 97.1 (Jan. 2018). DOI: 10.1103/physreva.97.012118. URL: https://doi.org/10.1103%2Fphysreva.97.012118.

[32] Philippe Lewalle, Areeya Chantasri, and Andrew N. Jordan. "Prediction and characterization of multiple extremal paths in continuously monitored qubits". In: *Physical Review A* 95.4 (Apr. 2017). DOI: 10.1103/physreva.95.042126. URL: https://doi.org/10.1103%2Fphysreva.95.042126.

[33] Philippe Lewalle, John Steinmetz, and Andrew N. Jordan. "Chaos in continuously monitored quantum systems: An optimal-path approach". In: *Physical Review A* 98.1 (July 2018). DOI: 10.1103/physreva.98.012141. URL: https://doi.org/10.1103%2Fphysreva.98.012141.

[34] K. W. Murch et al. "Observing single quantum trajectories of a superconducting quantum bit". In: *Nature* 502.7470 (Oct. 2013), pp. 211–214. DOI: 10.1038/nature12539. URL: https://doi.org/10.1038%2Fnature12539.

[35] S. J. Weber et al. "Mapping the optimal route between two quantum states". In: *Nature* 511.7511 (July 2014), pp. 570–573. ISSN: 1476-4687. DOI: 10.1038/nature13559. URL: http://dx.doi.org/10.1038/nature13559.

[36] D. Tan et al. "Prediction and Retrodiction for a Continuously Monitored Superconducting Qubit". In: *Phys. Rev. Lett.* 114 (9 Mar. 2015), p. 090403. DOI: 10.1103/PhysRevLett.114.090403. URL: https://link.aps.org/doi/10.1103/PhysRevLett.114.090403.

[37] R. Vijay et al. "Stabilizing Rabi oscillations in a superconducting qubit using quantum feedback". In: *Nature* 490.7418 (Oct. 2012), pp. 77–80. ISSN: 1476-4687. DOI: 10.1038/nature11505. URL: http://dx.doi.org/10.1038/nature11505.

[38] M. Naghiloo et al. "Heat and Work Along Individual Trajectories of a Quantum Bit". In: *Phys. Rev. Lett.* 124 (11 Mar. 2020), p. 110604. DOI: 10.1103/PhysRevLett.124.110604. URL: https://link.aps.org/doi/10.1103/PhysRevLett.124.110604.

[39] Joschka Roffe. "Quantum error correction: an introductory guide". In: *Contemporary Physics* 60.3 (July 2019), pp. 226–245. ISSN: 1366-5812. DOI: 10.1080/00107514.2019.1667078. URL: http://dx.doi.org/10.1080/00107514.2019.1667078.

[40] Patrick M. Harrington, Erich J. Mueller, and Kater W. Murch. "Engineered dissipation for quantum information science". In: *Nature Rev. Phys.* 4.10 (2022), pp. 660–671. DOI: 10.1038/s42254-022-00494-8. arXiv: 2202.05280 [quant-ph].

[41] Matthew P.A. Fisher et al. "Random Quantum Circuits". In: *Annual Review of Condensed Matter Physics* 14.1 (Mar. 2023), pp. 335–379. ISSN: 1947-5462. DOI: 10.1146/annurev-conmatphys-031720-030658. URL: http://dx.doi.org/10.1146/annurev-conmatphys-031720-030658.

[42] Crystal Noel et al. "Measurement-induced quantum phases realized in a trapped-ion quantum computer". In: *Nature Physics* 18.7 (June 2022), pp. 760–764. ISSN: 1745-2481. DOI: 10.1038/s41567-022-01619-7. URL: http://dx.doi.org/10.1038/s41567-022-01619-7.

[43] Jin Ming Koh et al. "Measurement-induced entanglement phase transition on a superconducting quantum processor with mid-circuit readout". In: *Nature Physics* 19.9 (June 2023), pp. 1314–1319. ISSN: 1745-2481. DOI: 10.1038/s41567-023-02076-6. URL: http://dx.doi.org/10.1038/s41567-023-02076-6.

[44] Google AI and Collaborators. "Measurement-induced entanglement and teleportation on a noisy quantum processor". In: *Nature* 622.7983 (Oct. 2023), pp. 481–486. ISSN: 1476-4687. DOI: 10.1038/s41586-023-06505-7. URL: http://dx.doi.org/10.1038/s41586-023-06505-7.

[45] Michael Victor Berry. "Quantal phase factors accompanying adiabatic changes". In: *Proceedings of the Royal Society of London. A. Mathematical and Physical Sciences* 392.1802 (1984), pp. 45–57.

[46] Erik Sjöqvist. "Geometric phases in quantum information". In: *International Journal of Quantum Chemistry* 115.19 (May 2015), pp. 1311–1326. DOI: 10.1002/qua.24941. URL: https://doi.org/10.1002%2Fqua.24941.

[47] Shi-Liang Zhu and Paolo Zanardi. "Geometric quantum gates that are robust against stochastic control errors". In: *Phys. Rev. A* 72 (2 Aug. 2005), p. 020301. DOI: 10.1103/PhysRevA.72.020301. URL: https://link.aps.org/doi/10.1103/PhysRevA.72.020301.

[48] Chetan Nayak et al. "Non-Abelian anyons and topological quantum computation". In: *Rev. Mod. Phys.* 80 (3 Sept. 2008), pp. 1083–1159. DOI: 10.1103/RevModPhys.80.1083. URL: https://link.aps.org/doi/10.1103/RevModPhys.80.1083.

[49] Di Xiao, Ming-Che Chang, and Qian Niu. "Berry phase effects on electronic properties". In: *Rev. Mod. Phys.* 82 (3 July 2010), pp. 1959–2007. DOI: 10.1103/RevModPhys.82.1959. URL: https://link.aps.org/doi/10.1103/RevModPhys.82.1959.

[50] Já nos K. Asbóth, László Oroszlány, and András Pályi. *A Short Course on Topological Insulators*. Springer International Publishing, 2016. DOI: 10.1007/978-3-319-25607-8. URL: https://doi.org/10.1007%5C%2F978-3-319-25607-8.

[51] Joseph Samuel and Rajendra Bhandari. "General Setting for Berry's Phase". In: *Phys. Rev. Lett.* 60 (23 June 1988), pp. 2339–2342. DOI: 10.1103/PhysRevLett.60.2339. URL: https://link.aps.org/doi/10.1103/PhysRevLett.60.2339.

[52] M. V. Berry and S. Klein. "Geometric phases from stacks of crystal plates". In: *Journal of Modern Optics* 43.1 (1996), pp. 165–180. DOI: 10.1080/09500349608232731. eprint: https://www.tandfonline.com/doi/pdf/10.1080/09500349608232731. URL: https://www.tandfonline.com/doi/abs/10.1080/09500349608232731.

[53] Paul G. Kwiat and Raymond Y. Chiao. "Observation of a nonclassical Berry's phase for the photon". In: *Phys. Rev. Lett.* 66 (5 Feb. 1991), pp. 588–591. DOI: 10.1103/PhysRevLett.66.588. URL: https://link.aps.org/doi/10.1103/PhysRevLett.66.588.

[54] Valentin Gebhart. "Measurement-induced geometric phases". PhD thesis. Masterarbeit, Universität Freiburg, 2017.

[55] Ludmila Viotti et al. *Geometric phases along quantum trajectories*. 2023. arXiv: 2301.04222 [quant-ph].

[56] Kyrylo Snizhko et al. "Weak-measurement-induced phases and dephasing: Broken symmetry of the geometric phase". In: *Physical Review Research* 3.4 (Oct. 2021). DOI: 10.1103/physrevresearch.3.043045. URL: https://doi.org/10.1103%2Fphysrevresearch.3.043045.

[57] Kyrylo Snizhko et al. "Weak-Measurement-Induced Asymmetric Dephasing: Manifestation of Intrinsic Measurement Chirality". In: *Physical Review*

Letters 127.17 (Oct. 2021). DOI: 10.1103/physrevlett.127.170401. URL: https://doi.org/10.1103%2Fphysrevlett.127.170401.

[58] A. A. Wood et al. "Interplay between geometric and dynamic phases in a single-spin system". In: *Phys. Rev. B* 102 (12 Sept. 2020), p. 125428. DOI: 10.1103/PhysRevB.102.125428. URL: https://link.aps.org/doi/10.1103/PhysRevB.102.125428.

[59] Manuel F. Ferrer-Garcia et al. "Topological transitions of the generalized Pancharatnam-Berry phase". In: *Science Advances* 9.47 (2023), eadg6810. DOI: 10.1126/sciadv.adg6810. eprint: https://www.science.org/doi/pdf/10.1126/sciadv.adg6810. URL: https://www.science.org/doi/abs/10.1126/sciadv.adg6810.

[60] Manuel F. Ferrer-Garcia et al. *Topological transitions of the generalized Pancharatnam-Berry phase*. 2022. arXiv: 2211.08519 [quant-ph].

[61] Yunzhao Wang et al. "Observing a topological transition in weak-measurement-induced geometric phases". In: *Phys. Rev. Res.* 4 (2 June 2022), p. 023179. DOI: 10.1103/PhysRevResearch.4.023179. URL: https://link.aps.org/doi/10.1103/PhysRevResearch.4.023179.

[62] Bei Zeng et al. *Quantum Information Meets Quantum Matter – From Quantum Entanglement to Topological Phase in Many-Body Systems*. 2018. arXiv: 1508.02595 [cond-mat.str-el].

[63] P. W. Anderson. "Absence of Diffusion in Certain Random Lattices". In: *Phys. Rev.* 109 (5 Mar. 1958), pp. 1492–1505. DOI: 10.1103/PhysRev.109.1492. URL: https://link.aps.org/doi/10.1103/PhysRev.109.1492.

[64] Boris L. Altshuler et al. "Quasiparticle Lifetime in a Finite System: A Nonperturbative Approach". In: *Phys. Rev. Lett.* 78 (14 Apr. 1997), pp. 2803–2806. DOI: 10.1103/PhysRevLett.78.2803. URL: https://link.aps.org/doi/10.1103/PhysRevLett.78.2803.

[65] D.M. Basko, I.L. Aleiner, and B.L. Altshuler. "Metal–insulator transition in a weakly interacting many-electron system with localized single-particle states". In: *Annals of Physics* 321.5 (2006), pp. 1126–1205. ISSN: 0003-4916. DOI: https://doi.org/10.1016/j.aop.2005.11.014. URL: https://www.sciencedirect.com/science/article/pii/S0003491605002630.

[66] D.A. Abanin et al. "Distinguishing localization from chaos: Challenges in finite-size systems". In: *Annals of Physics* 427 (2021), p. 168415. ISSN: 0003-4916. DOI: https://doi.org/10.1016/j.aop.2021.168415. URL: https://www.sciencedirect.com/science/article/pii/S000349162100021X.

[67] Dmitry A. Abanin et al. "Colloquium: Many-body localization, thermalization, and entanglement". In: *Rev. Mod. Phys.* 91 (2 May 2019), p. 021001. DOI: 10.1103/RevModPhys.91.021001. URL: https://link.aps.org/doi/10.1103/RevModPhys.91.021001.

[68] Alexei Kitaev and John Preskill. "Topological Entanglement Entropy". In: *Phys. Rev. Lett.* 96 (11 Mar. 2006), p. 110404. DOI: 10.1103/PhysRevLett.96.110404. URL: https://link.aps.org/doi/10.1103/PhysRevLett.96.110404.

[69] Don N. Page. "Average entropy of a subsystem". In: *Physical Review Letters* 71.9 (Aug. 1993), pp. 1291–1294. ISSN: 0031-9007. DOI: 10.1103/physrevlett.71.1291. URL: http://dx.doi.org/10.1103/PhysRevLett.71.1291.

[70] Yaodong Li, Xiao Chen, and Matthew P. A. Fisher. "Quantum Zeno effect and the many-body entanglement transition". In: *Phys. Rev. B* 98 (20 Nov. 2018), p. 205136. DOI: 10.1103/PhysRevB.98.205136. URL: https://link.aps.org/doi/10.1103/PhysRevB.98.205136.

[71] Amos Chan et al. "Unitary-projective entanglement dynamics". In: *Phys. Rev. B* 99 (22 June 2019), p. 224307. DOI: 10.1103/PhysRevB.99.224307. URL: https://link.aps.org/doi/10.1103/PhysRevB.99.224307.

[72] Brian Skinner, Jonathan Ruhman, and Adam Nahum. "Measurement-Induced Phase Transitions in the Dynamics of Entanglement". In: *Phys. Rev. X* 9 (3 July 2019), p. 031009. DOI: 10.1103/PhysRevX.9.031009. URL: https://link.aps.org/doi/10.1103/PhysRevX.9.031009.

[73] Adam Nahum et al. "Quantum Entanglement Growth under Random Unitary Dynamics". In: *Phys. Rev. X* 7 (3 July 2017), p. 031016. DOI: 10.1103/PhysRevX.7.031016. URL: https://link.aps.org/doi/10.1103/PhysRevX.7.031016.

[74] M. Szyniszewski, A. Romito, and H. Schomerus. "Entanglement transition from variable-strength weak measurements". In: *Phys. Rev. B* 100 (6 Aug. 2019), p. 064204. DOI: 10.1103/PhysRevB.100.064204. URL: https://link.aps.org/doi/10.1103/PhysRevB.100.064204.

[75] Sebastian Deffner and Eric Lutz. "Nonequilibrium Entropy Production for Open Quantum Systems". In: *Phys. Rev. Lett.* 107 (14 Sept. 2011), p. 140404. DOI: 10.1103/PhysRevLett.107.140404. URL: https://link.aps.org/doi/10.1103/PhysRevLett.107.140404.

[76] Massimiliano Esposito, Upendra Harbola, and Shaul Mukamel. "Nonequilibrium fluctuations, fluctuation theorems, and counting statistics in quantum systems". In: *Rev. Mod. Phys.* 81 (4 Dec. 2009), pp. 1665–1702. DOI: 10.1103/RevModPhys.81.1665. URL: https://link.aps.org/doi/10.1103/RevModPhys.81.1665.

[77] Michele Campisi, Peter Hänggi, and Peter Talkner. "Colloquium: Quantum fluctuation relations: Foundations and applications". In: *Rev. Mod. Phys.* 83 (3 July 2011), pp. 771–791. DOI: 10.1103/RevModPhys.83.771. URL: https://link.aps.org/doi/10.1103/RevModPhys.83.771.

[78] Carlos Bustamante, Jan Liphardt, and Felix Ritort. "The Nonequilibrium Thermodynamics of Small Systems". In: *Physics Today* 58.7 (July 2005), pp. 43–48. ISSN: 0031-9228. DOI: 10.1063/1.2012462. eprint: https://

pubs.aip.org/physicstoday/article-pdf/58/7/43/16729192/43_1_online.pdf. URL: https://doi.org/10.1063/1.2012462.

[79] Antoine Bérut et al. "Experimental verification of Landauer's principle linking information and thermodynamics". In: *Nature* 483 (2012), pp. 187–189. URL: https://api.semanticscholar.org/CorpusID:9415026.

[80] Johannes Roßnagel et al. "A single-atom heat engine". In: *Science* 352.6283 (2016), pp. 325–329. DOI: 10.1126/science.aad6320. eprint: https://www.science.org/doi/pdf/10.1126/science.aad6320. URL: https://www.science.org/doi/abs/10.1126/science.aad6320.

[81] Gonzalo Manzano and Roberta Zambrini. "Quantum thermodynamics under continuous monitoring: A general framework". In: *AVS Quantum Science* 4.2 (May 2022), p. 025302. ISSN: 2639-0213. DOI: 10.1116/5.0079886. eprint: https://pubs.aip.org/avs/aqs/article-pdf/doi/10.1116/5.0079886/19803548/025302_1_online.pdf. URL: https://doi.org/10.1116/5.0079886.

[82] Jordan M. Horowitz. "Quantum-trajectory approach to the stochastic thermodynamics of a forced harmonic oscillator". In: *Phys. Rev. E* 85 (3 Mar. 2012), p. 031110. DOI: 10.1103/PhysRevE.85.031110. URL: https://link.aps.org/doi/10.1103/PhysRevE.85.031110.

[83] F. W. J. Hekking and J. P. Pekola. "Quantum Jump Approach for Work and Dissipation in a Two-Level System". In: *Phys. Rev. Lett.* 111 (9 Aug. 2013), p. 093602. DOI: 10.1103/PhysRevLett.111.093602. URL: https://link.aps.org/doi/10.1103/PhysRevLett.111.093602.

[84] P. Kammerlander and J. Anders. "Coherence and measurement in quantum thermodynamics". In: *Scientific Reports* 6.1 (Feb. 2016). ISSN: 2045-2322. DOI: 10.1038/srep22174. URL: http://dx.doi.org/10.1038/srep22174.

[85] Jader P. Santos et al. "The role of quantum coherence in non-equilibrium entropy production". In: *npj Quantum Information* 5.1 (Mar. 2019). ISSN: 2056-6387. DOI: 10.1038/s41534-019-0138-y. URL: http://dx.doi.org/10.1038/s41534-019-0138-y.

[86] G. Francica, J. Goold, and F. Plastina. "Role of coherence in the nonequilibrium thermodynamics of quantum systems". In: *Phys. Rev. E* 99 (4 Apr. 2019), p. 042105. DOI: 10.1103/PhysRevE.99.042105. URL: https://link.aps.org/doi/10.1103/PhysRevE.99.042105.

[87] Jonathan Oppenheim et al. "Thermodynamical Approach to Quantifying Quantum Correlations". In: *Phys. Rev. Lett.* 89 (18 Oct. 2002), p. 180402. DOI: 10.1103/PhysRevLett.89.180402. URL: https://link.aps.org/doi/10.1103/PhysRevLett.89.180402.

[88] Karen V. Hovhannisyan et al. "Entanglement Generation is Not Necessary for Optimal Work Extraction". In: *Phys. Rev. Lett.* 111 (24 Dec. 2013), p. 240401. DOI: 10.1103/PhysRevLett.111.240401. URL: https://link.aps.org/doi/10.1103/PhysRevLett.111.240401.

[89] Jordan M Horowitz and Juan M R Parrondo. "Entropy production along nonequilibrium quantum jump trajectories". In: *New Journal of Physics* 15.8 (Aug. 2013), p. 085028. ISSN: 1367-2630. DOI: 10.1088/1367-2630/15/8/085028. URL: http://dx.doi.org/10.1088/1367-2630/15/8/085028.

[90] Jordan M. Horowitz and Takahiro Sagawa. "Equivalent Definitions of the Quantum Nonadiabatic Entropy Production". In: *Journal of Statistical Physics* 156.1 (Apr. 2014), pp. 55–65. ISSN: 1572-9613. DOI: 10.1007/s10955-014-0991-1. URL: http://dx.doi.org/10.1007/s10955-014-0991-1.

[91] Gentaro Watanabe et al. "Quantum fluctuation theorems and generalized measurements during the force protocol". In: *Phys. Rev. E* 89 (3 Mar. 2014),

p. 032114. DOI: 10.1103/PhysRevE.89.032114. URL: https://link.aps.org/doi/10.1103/PhysRevE.89.032114.

[92] Michele Campisi, Peter Talkner, and Peter Hänggi. "Fluctuation Theorems for Continuously Monitored Quantum Fluxes". In: *Phys. Rev. Lett.* 105 (14 Sept. 2010), p. 140601. DOI: 10.1103/PhysRevLett.105.140601. URL: https://link.aps.org/doi/10.1103/PhysRevLett.105.140601.

[93] Michele Campisi, Peter Talkner, and Peter Hänggi. "Influence of measurements on the statistics of work performed on a quantum system". In: *Phys. Rev. E* 83 (4 Apr. 2011), p. 041114. DOI: 10.1103/PhysRevE.83.041114. URL: https://link.aps.org/doi/10.1103/PhysRevE.83.041114.

[94] Tameem Albash et al. "Fluctuation theorems for quantum processes". In: *Phys. Rev. E* 88 (3 Sept. 2013), p. 032146. DOI: 10.1103/PhysRevE.88.032146. URL: https://link.aps.org/doi/10.1103/PhysRevE.88.032146.

[95] Alexey E. Rastegin and Karol Życzkowski. "Jarzynski equality for quantum stochastic maps". In: *Phys. Rev. E* 89 (1 Jan. 2014), p. 012127. DOI: 10.1103/PhysRevE.89.012127. URL: https://link.aps.org/doi/10.1103/PhysRevE.89.012127.

[96] R. Dorner et al. "Extracting Quantum Work Statistics and Fluctuation Theorems by Single-Qubit Interferometry". In: *Phys. Rev. Lett.* 110 (23 June 2013), p. 230601. DOI: 10.1103/PhysRevLett.110.230601. URL: https://link.aps.org/doi/10.1103/PhysRevLett.110.230601.

[97] L. Mazzola, G. De Chiara, and M. Paternostro. "Measuring the Characteristic Function of the Work Distribution". In: *Phys. Rev. Lett.* 110 (23 June 2013), p. 230602. DOI: 10.1103/PhysRevLett.110.230602. URL: https://link.aps.org/doi/10.1103/PhysRevLett.110.230602.

[98] Augusto J. Roncaglia, Federico Cerisola, and Juan Pablo Paz. "Work Measurement as a Generalized Quantum Measurement". In: *Phys. Rev. Lett.*

113 (25 Dec. 2014), p. 250601. DOI: 10.1103/PhysRevLett.113.250601. URL: https://link.aps.org/doi/10.1103/PhysRevLett.113.250601.

[99] Tiago B. Batalhão et al. "Experimental Reconstruction of Work Distribution and Study of Fluctuation Relations in a Closed Quantum System". In: *Phys. Rev. Lett.* 113 (14 Oct. 2014), p. 140601. DOI: 10.1103/PhysRevLett.113.140601. URL: https://link.aps.org/doi/10.1103/PhysRevLett.113.140601.

[100] Shuoming An et al. "Experimental test of the quantum Jarzynski equality with a trapped-ion system". In: *Nature Physics* 11.2 (Dec. 2014), pp. 193–199. ISSN: 1745-2481. DOI: 10.1038/nphys3197. URL: http://dx.doi.org/10.1038/nphys3197.

[101] Gonzalo Manzano, Jordan M. Horowitz, and Juan M. R. Parrondo. "Nonequilibrium potential and fluctuation theorems for quantum maps". In: *Phys. Rev. E* 92 (3 Sept. 2015), p. 032129. DOI: 10.1103/PhysRevE.92.032129. URL: https://link.aps.org/doi/10.1103/PhysRevE.92.032129.

[102] Gonzalo Manzano, Jordan M. Horowitz, and Juan M. R. Parrondo. "Quantum Fluctuation Theorems for Arbitrary Environments: Adiabatic and Nonadiabatic Entropy Production". In: *Phys. Rev. X* 8 (3 Aug. 2018), p. 031037. DOI: 10.1103/PhysRevX.8.031037. URL: https://link.aps.org/doi/10.1103/PhysRevX.8.031037.

[103] Kurt Jacobs and Daniel A Steck. "Engineering quantum states, nonlinear measurements and anomalous diffusion by imaging". In: *New Journal of Physics* 13.1 (Jan. 2011), p. 013016. DOI: 10.1088/1367-2630/13/1/013016. URL: https://dx.doi.org/10.1088/1367-2630/13/1/013016.

[104] Andrew N. Jordan and Markus Büttiker. "Continuous Quantum Measurement with Independent Detector Cross Correlations". In: *Phys. Rev. Lett.* 95 (22 Nov. 2005), p. 220401. DOI: 10.1103/PhysRevLett.95.220401. URL: https://link.aps.org/doi/10.1103/PhysRevLett.95.220401.

[105] Y. Levinson. "Dephasing in a quantum dot due to coupling with a quantum point contact". In: *Europhysics Letters* 39.3 (July 1997), p. 299. DOI: 10.1209/epl/i1997-00351-x. URL: https://dx.doi.org/10.1209/epl/i1997-00351-x.

[106] Alexander N. Korotkov. "Continuous quantum measurement of a double dot". In: *Phys. Rev. B* 60 (8 Aug. 1999), pp. 5737–5742. DOI: 10.1103/PhysRevB.60.5737. URL: https://link.aps.org/doi/10.1103/PhysRevB.60.5737.

[107] S Ashhab, J Q You, and Franco Nori. "Information about the state of a charge qubit gained by a weakly coupled quantum point contact". In: *Physica Scripta* 2009.T137 (Dec. 2009), p. 014005. DOI: 10.1088/0031-8949/2009/T137/014005. URL: https://dx.doi.org/10.1088/0031-8949/2009/T137/014005.

[108] Areeya Chantasri. "Stochastic path integral formalism for continuous quantum measurement". PhD thesis. University of Rochester, 2016.

[109] John Preskill. *Lecture Notes for Ph219/CS219:Quantum Information Chapter 3*. http://theory.caltech.edu/~preskill/ph219/chap3_15.pdf. [Online; accessed March-2024]. 2018.

[110] Daniel Manzano. "A short introduction to the Lindblad master equation". In: *AIP Advances* 10.2 (Feb. 2020), p. 025106. ISSN: 2158-3226. DOI: 10.1063/1.5115323. eprint: https://pubs.aip.org/aip/adv/article-pdf/doi/10.1063/1.5115323/12881278/025106_1_online.pdf. URL: https://doi.org/10.1063/1.5115323.

[111] D. Chruscinski and A. Jamiolkowski. *Geometric Phases in Classical and Quantum Mechanics*. Progress in Mathematical Physics. Birkhäuser Boston, 2012. ISBN: 9780817681760. URL: https://books.google.co.uk/books?id=JVHlBwAAQBAJ.

[112] S. Pancharatnam. "Generalized theory of interference and its applications". In: *Proceedings of the Indian Academy of Sciences - Section A* 44 (1956), pp. 398–417. URL: https://api.semanticscholar.org/CorpusID:118711938.

[113] J H Hannay. "Angle variable holonomy in adiabatic excursion of an integrable Hamiltonian". In: *Journal of Physics A: Mathematical and General* 18.2 (Feb. 1985), p. 221. DOI: 10.1088/0305-4470/18/2/011. URL: https://dx.doi.org/10.1088/0305-4470/18/2/011.

[114] Akira Tomita and Raymond Y. Chiao. "Observation of Berry's Topological Phase by Use of an Optical Fiber". In: *Phys. Rev. Lett.* 57 (8 Aug. 1986), pp. 937–940. DOI: 10.1103/PhysRevLett.57.937. URL: https://link.aps.org/doi/10.1103/PhysRevLett.57.937.

[115] Barry Simon. "Holonomy, the Quantum Adiabatic Theorem, and Berry's Phase". In: *Phys. Rev. Lett.* 51 (24 Dec. 1983), pp. 2167–2170. DOI: 10.1103/PhysRevLett.51.2167. URL: https://link.aps.org/doi/10.1103/PhysRevLett.51.2167.

[116] Chetan Nayak et al. "Non-Abelian anyons and topological quantum computation". In: *Rev. Mod. Phys.* 80 (3 Sept. 2008), pp. 1083–1159. DOI: 10.1103/RevModPhys.80.1083. URL: https://link.aps.org/doi/10.1103/RevModPhys.80.1083.

[117] Shi-Liang Zhu and Paolo Zanardi. "Geometric quantum gates that are robust against stochastic control errors". In: *Phys. Rev. A* 72 (2 Aug. 2005), p. 020301. DOI: 10.1103/PhysRevA.72.020301. URL: https://link.aps.org/doi/10.1103/PhysRevA.72.020301.

[118] B. Zwiebach. *Quantum Physics III Chapter 6: Adiabatic Approximation.* https://ocw.mit.edu/courses/8-06-quantum-physics-iii-spring-2018/95ffb7405e75bec4f75564318e173ce0_MIT8_06S18ch6.pdf. [Online; accessed March-2024]. 2017.

[119] Marcos Atala et al. “Direct measurement of the Zak phase in topological Bloch bands”. In: *Nature Physics* 9.12 (Nov. 2013), pp. 795–800. DOI: 10.1038/nphys2790. URL: https://doi.org/10.10382%5C%Fnphys2790.

[120] Michael Schüler et al. “Local Berry curvature signatures in dichroic angle-resolved photoelectron spectroscopy from two-dimensional materials”. In: *Science Advances* 6.9 (2020), eaay2730. DOI: 10.1126/sciadv.aay2730. eprint: https://www.science.org/doi/pdf/10.1126/sciadv.aay2730. URL: https://www.science.org/doi/abs/10.1126/sciadv.aay2730.

[121] Y. Aharonov and J. Anandan. “Phase change during a cyclic quantum evolution”. In: *Phys. Rev. Lett.* 58 (16 Apr. 1987), pp. 1593–1596. DOI: 10.1103/PhysRevLett.58.1593. URL: https://link.aps.org/doi/10.1103/PhysRevLett.58.1593.

[122] Young-Wook Cho et al. “Emergence of the geometric phase from quantum measurement back-action”. In: *Nature Physics* 15.7 (Apr. 2019), pp. 665–670. DOI: 10.1038/s41567-019-0482-z.

[123] Arno Bohm et al. “Classification theorem for principal fibre bundles, Berry’s phase, and exact cyclic evolution”. In: *Journal of Geometry and Physics* 12.1 (1993), pp. 13–28. ISSN: 0393-0440. DOI: https://doi.org/10.1016/0393-0440(93)90085-S. URL: https://www.sciencedirect.com/science/article/pii/039304409390085S.

[124] Armin Uhlmann. “Parallel transport and “quantum holonomy” along density operators”. In: *Reports on Mathematical Physics* 24.2 (1986), pp. 229–240. ISSN: 0034-4877. DOI: https://doi.org/10.1016/0034-4877(86)90055-8. URL: https://www.sciencedirect.com/science/article/pii/0034487786900558.

[125] Armin Uhlmann. “On Berry phases along mixtures of states”. In: *Annalen der Physik* 501.1 (1989), pp. 63–69.

[126] Armin Uhlmann. "A gauge field governing parallel transport along mixed states". In: *letters in mathematical physics* 21 (1991), pp. 229–236.

[127] Erik Sjöqvist et al. "Geometric Phases for Mixed States in Interferometry". In: *Phys. Rev. Lett.* 85 (14 Oct. 2000), pp. 2845–2849. DOI: 10.1103/PhysRevLett.85.2845. URL: https://link.aps.org/doi/10.1103/PhysRevLett.85.2845.

[128] A. Carollo et al. "Geometric Phase in Open Systems". In: *Phys. Rev. Lett.* 90 (16 Apr. 2003), p. 160402. DOI: 10.1103/PhysRevLett.90.160402. URL: https://link.aps.org/doi/10.1103/PhysRevLett.90.160402.

[129] Marie Ericsson et al. "Generalization of the geometric phase to completely positive maps". In: *Phys. Rev. A* 67 (2 Feb. 2003), p. 020101. DOI: 10.1103/PhysRevA.67.020101. URL: https://link.aps.org/doi/10.1103/PhysRevA.67.020101.

[130] Kyrylo Snizhko et al. "Weak-measurement-induced phases and dephasing: Broken symmetry of the geometric phase". In: *Phys. Rev. Res.* 3 (4 Oct. 2021), p. 043045. DOI: 10.1103/PhysRevResearch.3.043045. URL: https://link.aps.org/doi/10.1103/PhysRevResearch.3.043045.

[131] Kyrylo Snizhko et al. "Weak-Measurement-Induced Asymmetric Dephasing: Manifestation of Intrinsic Measurement Chirality". In: *Phys. Rev. Lett.* 127 (17 Oct. 2021), p. 170401. DOI: 10.1103/PhysRevLett.127.170401. URL: https://link.aps.org/doi/10.1103/PhysRevLett.127.170401.

[132] Graham Kells, Dganit Meidan, and Alessandro Romito. "Topological transitions in weakly monitored free fermions". In: *SciPost Phys.* 14 (2023), p. 031. DOI: 10.21468/SciPostPhys.14.3.031. URL: https://scipost.org/10.21468/SciPostPhys.14.3.031.

[133] Sthitadhi Roy et al. "Measurement-induced steering of quantum systems". In: *Phys. Rev. Res.* 2 (3 Sept. 2020), p. 033347. DOI: 10.1103/PhysRevResearch.

2.033347. URL: https://link.aps.org/doi/10.1103/PhysRevResearch.2.033347.

[134] Nicolai Lang and Hans Peter Büchler. "Entanglement transition in the projective transverse field Ising model". In: *Phys. Rev. B* 102 (9 Sept. 2020), p. 094204. DOI: 10.1103/PhysRevB.102.094204. URL: https://link.aps.org/doi/10.1103/PhysRevB.102.094204.

[135] Ali Lavasani, Yahya Alavirad, and Maissam Barkeshli. "Measurement-induced topological entanglement transitions in symmetric random quantum circuits". In: *Nature Physics* 17.3 (Jan. 2021), pp. 342–347. ISSN: 1745-2481. DOI: 10.1038/s41567-020-01112-z. URL: http://dx.doi.org/10.1038/s41567-020-01112-z.

[136] Yunzhao Wang et al. "Dissipative preparation and stabilization of many-body quantum states in a superconducting qutrit array". In: *Physical Review A* 108.1 (July 2023). ISSN: 2469-9934. DOI: 10.1103/physreva.108.013712. URL: http://dx.doi.org/10.1103/PhysRevA.108.013712.

[137] Tathagata Karmakar, Philippe Lewalle, and Andrew N. Jordan. "Stochastic Path-Integral Analysis of the Continuously Monitored Quantum Harmonic Oscillator". In: *PRX Quantum* 3 (1 Feb. 2022), p. 010327. DOI: 10.1103/PRXQuantum.3.010327. URL: https://link.aps.org/doi/10.1103/PRXQuantum.3.010327.

[138] Michael B. Mensky. *Continuously Measured Systems,Path Integrals and Information*. 2000. arXiv: quant-ph/0007089 [quant-ph].

[139] P. C. Martin, E. D. Siggia, and H. A. Rose. "Statistical Dynamics of Classical Systems". In: *Phys. Rev. A* 8 (1 July 1973), pp. 423–437. DOI: 10.1103/PhysRevA.8.423. URL: https://link.aps.org/doi/10.1103/PhysRevA.8.423.

[140] L. Onsager and S. Machlup. "Fluctuations and Irreversible Processes". In: *Phys. Rev.* 91 (6 Sept. 1953), pp. 1505–1512. DOI: 10.1103/PhysRev.91.1505. URL: https://link.aps.org/doi/10.1103/PhysRev.91.1505.

[141] C.W. Gardiner. *Handbook of Stochastic Methods for Physics, Chemistry, and the Natural Sciences*. Springer complexity. Springer, 2004. ISBN: 9783540208822. URL: https://books.google.co.uk/books?id=wLm7QgAACAAJ.

[142] L. Onsager and S. Machlup. "Fluctuations and Irreversible Processes". In: *Phys. Rev.* 91 (6 Sept. 1953), pp. 1505–1512. DOI: 10.1103/PhysRev.91.1505. URL: https://link.aps.org/doi/10.1103/PhysRev.91.1505.

[143] Daniel G. Barci, Zochil González Arenas, and Miguel Vera Moreno. "Path integral approach to nonequilibrium potentials in multiplicative Langevin dynamics". In: *Europhysics Letters* 113.1 (Feb. 2016), p. 10009. DOI: 10.1209/0295-5075/113/10009. URL: https://dx.doi.org/10.1209/0295-5075/113/10009.

[144] C. Van den Broeck, J. M. R. Parrondo, and R. Toral. "Noise-Induced Nonequilibrium Phase Transition". In: *Phys. Rev. Lett.* 73 (25 Dec. 1994), pp. 3395–3398. DOI: 10.1103/PhysRevLett.73.3395. URL: https://link.aps.org/doi/10.1103/PhysRevLett.73.3395.

[145] Luca Gammaitoni et al. "Stochastic resonance". In: *Rev. Mod. Phys.* 70 (1 Jan. 1998), pp. 223–287. DOI: 10.1103/RevModPhys.70.223. URL: https://link.aps.org/doi/10.1103/RevModPhys.70.223.

[146] H.S. Wio, S. Bouzat, and B. von Haeften. "Stochastic resonance in spatially extended systems: the role of far from equilibrium potentials". In: *Physica A: Statistical Mechanics and its Applications* 306 (2002). Invited Papers from the 21th IUPAP International Conference on St atistical Physics, pp. 140–156. ISSN: 0378-4371. DOI: https://doi.org/10.1016/S0378-4371(02)00493-4. URL: https://www.sciencedirect.com/science/article/pii/S0378437102004934.

[147] Alexander Altland and Ben D. Simons. *Condensed Matter Field Theory*. 2nd ed. Cambridge University Press, 2010. DOI: 10.1017/CBO9780511789984.

[148] *An introduction to the Martin-Siggia-Rose formalism*. https://inordinatum.wordpress.com/2012/09/27/a-quick-introduction-to-the-martin-siggia-rose-formalism/. Accessed: 31/03/2014.

[149] Herbert B. Callen and Theodore A. Welton. "Irreversibility and Generalized Noise". In: *Phys. Rev.* 83 (1 July 1951), pp. 34–40. DOI: 10.1103/PhysRev.83.34. URL: https://link.aps.org/doi/10.1103/PhysRev.83.34.

[150] M. Toda et al. *Statistical Physics II: Nonequilibrium Statistical Mechanics*. Springer Series in Solid-State Sciences. Springer Berlin Heidelberg, 2012. ISBN: 9783642582448. URL: https://books.google.co.uk/books?id=cF3wCAAAQBAJ.

[151] Gavin Earl Crooks. "Excursions in statistical dynamics". PhD thesis. University of California, Berkeley, Jan. 1999.

[152] C. Jarzynski. "Nonequilibrium Equality for Free Energy Differences". In: *Phys. Rev. Lett.* 78 (14 Apr. 1997), pp. 2690–2693. DOI: 10.1103/PhysRevLett.78.2690. URL: https://link.aps.org/doi/10.1103/PhysRevLett.78.2690.

[153] Markus Rademacher et al. "Nonequilibrium Control of Thermal and Mechanical Changes in a Levitated System". In: *Phys. Rev. Lett.* 128 (7 Feb. 2022), p. 070601. DOI: 10.1103/PhysRevLett.128.070601. URL: https://link.aps.org/doi/10.1103/PhysRevLett.128.070601.

[154] Sebastian Deffner and Eric Lutz. "Nonequilibrium Entropy Production for Open Quantum Systems". In: *Phys. Rev. Lett.* 107 (14 Sept. 2011), p. 140404. DOI: 10.1103/PhysRevLett.107.140404. URL: https://link.aps.org/doi/10.1103/PhysRevLett.107.140404.

[155] Michele Campisi, Peter Talkner, and Peter Hänggi. "Fluctuation Theorems for Continuously Monitored Quantum Fluxes". In: *Phys. Rev. Lett.* 105 (14 Sept. 2010), p. 140601. DOI: 10.1103/PhysRevLett.105.140601. URL: https://link.aps.org/doi/10.1103/PhysRevLett.105.140601.

[156] Michele Campisi, Peter Hänggi, and Peter Talkner. "Colloquium: Quantum fluctuation relations: Foundations and applications". In: *Rev. Mod. Phys.* 83 (3 July 2011), pp. 771–791. DOI: 10.1103/RevModPhys.83.771. URL: https://link.aps.org/doi/10.1103/RevModPhys.83.771.

[157] H.J. Rothe and K.D. Rothe. *Classical and Quantum Dynamics of Constrained Hamiltonian Systems*. World Scientific lecture notes in physics. World Scientific, 2010. ISBN: 9789814299657. URL: https://books.google.co.uk/books?id=CAJ_uwNYiGEC.

[158] Miguel V. Moreno, Daniel G. Barci, and Zochil González Arenas. "Conditional probabilities in multiplicative noise processes". In: *Phys. Rev. E* 99 (3 Mar. 2019), p. 032125. DOI: 10.1103/PhysRevE.99.032125. URL: https://link.aps.org/doi/10.1103/PhysRevE.99.032125.

[159] Klaus Kirsten and Alan J McKane. "Functional determinants for general Sturm–Liouville problems". In: *Journal of Physics A: Mathematical and General* 37.16 (Apr. 2004), pp. 4649–4670. DOI: 10.1088/0305-4470/37/16/014. URL: https://doi.org/10.1088%2F0305-4470%2F37%2F16%2F014.

[160] Pierre Rouchon and Jason F. Ralph. "Efficient quantum filtering for quantum feedback control". In: *Phys. Rev. A* 91 (1 Jan. 2015), p. 012118. DOI: 10.1103/PhysRevA.91.012118. URL: https://link.aps.org/doi/10.1103/PhysRevA.91.012118.

[161] Yuxiao Jiang et al. "Optimality of feedback control for qubit purification under inefficient measurement". In: *Phys. Rev. A* 102 (2 Aug. 2020), p. 022612. DOI: 10.1103/PhysRevA.102.022612. URL: https://link.aps.org/doi/10.1103/PhysRevA.102.022612.

[162] Rusko Ruskov and Alexander N. Korotkov. "Entanglement of solid-state qubits by measurement". In: *Phys. Rev. B* 67 (24 June 2003), p. 241305. DOI: 10.1103/PhysRevB.67.241305. URL: https://link.aps.org/doi/10.1103/PhysRevB.67.241305.

[163] D Moehring et al. "Entanglement of single-atom quantum bits at a distance". In: *Nature* 449 (Oct. 2007), pp. 68–71. DOI: 10.1038/nature06118.

[164] Chantal L. Hutchison et al. "Quantum trajectory equation for multiple qubits in circuit QED: Generating entanglement by measurementThis paper was presented at the Theory CANADA 4 conference, held at Centre de recherches mathématiques, Montréal, Québec, Canada on 4–7 June 2008." In: *Canadian Journal of Physics* 87.3 (Mar. 2009), pp. 225–231. ISSN: 1208-6045. DOI: 10.1139/p08-140. URL: http://dx.doi.org/10.1139/P08-140.

[165] Kevin Lalumière, J. M. Gambetta, and Alexandre Blais. "Tunable joint measurements in the dispersive regime of cavity QED". In: *Physical Review A* 81.4 (Apr. 2010). ISSN: 1094-1622. DOI: 10.1103/physreva.81.040301. URL: http://dx.doi.org/10.1103/PhysRevA.81.040301.

[166] H. Bernien et al. "Heralded entanglement between solid-state qubits separated by three metres". In: *Nature* 497.7447 (Apr. 2013), pp. 86–90. ISSN: 1476-4687. DOI: 10.1038/nature12016. URL: http://dx.doi.org/10.1038/nature12016.

[167] Eduardo Mascarenhas et al. "Physically realizable entanglement by local continuous measurements". In: *Physical Review A* 83.2 (Feb. 2011). ISSN: 1094-1622. DOI: 10.1103/physreva.83.022311. URL: http://dx.doi.org/10.1103/PhysRevA.83.022311.

[168] T Kalsi, A Romito, and H Schomerus. "Three-fold way of entanglement dynamics in monitored quantum circuits". In: *Journal of Physics A: Mathematical and Theoretical* 55.26 (June 2022), p. 264009. ISSN: 1751-8121. DOI:

10.1088/1751-8121/ac71e8. URL: http://dx.doi.org/10.1088/1751-8121/ac71e8.

[169] T. Boorman et al. "Diagnostics of entanglement dynamics in noisy and disordered spin chains via the measurement-induced steady-state entanglement transition". In: *Phys. Rev. B* 105 (14 Apr. 2022), p. 144202. DOI: 10.1103/PhysRevB.105.144202. URL: https://link.aps.org/doi/10.1103/PhysRevB.105.144202.

[170] Henning Schomerus. "Noisy monitored quantum dynamics of ergodic multi-qubit systems". In: *Journal of Physics A: Mathematical and Theoretical* 55.21 (May 2022), p. 214001. ISSN: 1751-8121. DOI: 10.1088/1751-8121/ac6320. URL: http://dx.doi.org/10.1088/1751-8121/ac6320.

[171] K. Murch and X. Linpeng. private communication. 2023.

[172] R. Barends et al. "Coherent Josephson Qubit Suitable for Scalable Quantum Integrated Circuits". In: *Phys. Rev. Lett.* 111 (8 Aug. 2013), p. 080502. DOI: 10.1103/PhysRevLett.111.080502. URL: https://link.aps.org/doi/10.1103/PhysRevLett.111.080502.